Uncertainty Budgeting Methods for Conceptual Aircraft Design

by

Max Maria Jacques Opgenoord

B.Sc. Aerospace Engineering, Delft University of Technology (2014)

Submitted to the Department of Aeronautics and Astronautics
in partial fulfillment of the requirements for the degree of

Master of Science in Aeronautics and Astronautics

at the

MASSACHUSETTS INSTITUTE OF TECHNOLOGY

February 2016

Author .....
Department of Aeronautics and Astronautics
January 27, 2016

Certified by .....
Karen E. Willcox
Professor of Aeronautics and Astronautics
Thesis Supervisor

Accepted by .....
Paulo C. Lozano
Associate Professor of Aeronautics and Astronautics
Chair, Graduate Program Committee

Uncertainty Budgeting Methods for Conceptual Aircraft Design

by

Max Maria Jacques Opgenoord

Submitted to the Department of Aeronautics and Astronautics
on January 27, 2016, in partial fulfillment of the
requirements for the degree of
Master of Science in Aeronautics and Astronautics

Abstract

Quantification and management of uncertainty are critical in the design of engineering systems, especially in the early stages of conceptual design. This thesis presents an approach to defining budgets on the acceptable levels of uncertainty in design quantities of interest, such as the allowable risk in not meeting a critical design constraint and the allowable deviation in a system performance metric. A sensitivity-based method analyzes the effects of design decisions on satisfying those budgets, and a multi-objective optimization formulation permits the designer to explore the tradespace of uncertainty reduction activities while also accounting for a cost budget. For models that are computationally costly to evaluate, a surrogate modeling approach based on high dimensional model representation achieves efficient computation of the sensitivities. Example problems in aircraft conceptual design illustrate the approach. The first example investigates the influence of uncertainty in the propulsion technology on the overall aircraft design, whereas the second problem looks at the influence of six different uncertain design parameters from three different disciplines within the aircraft design.

Secondly, the distributional sensitivity analysis (DSA) method is extended for better computational efficiency and wider applicability. Instead of assuming that all uncertainty in an input parameter can be reduced, DSA apportions output uncertainty as a function of the uncertainty reduction of a particular input parameter. This leads to more information on influences of uncertainty reduction, and to a more informative ranking of input parameters. In this thesis the ANOVA-HDMR framework is used for DSA to increase computational efficiency. Additionally, this approach allows for using DSA for more general distributions.

Thesis Supervisor: Karen E. Willcox
Title: Professor of Aeronautics and Astronautics

Acknowledgments

Firstly, I would like to thank Professor Karen Willcox. Little over a year ago, she welcomed me into her group and has given me lots of support since. She always makes time to meet – even when she is traveling all around the globe – and those meetings always yield a new insight. Moreover, I have thoroughly enjoyed working with her and she is one of the main reasons I decided to stick around for a PhD.

Additionally, I would like to thank Professor Mark Drela for allowing TASOPT to be used for this project, and Professor Douglas Allaire for the helpful discussions on Distributional Sensitivity Analysis.

I would also like to thank the members of the Aerospace Computational Design Laboratory (ACDL) for the productive and fun working enviroment. Specifically, I would like to thank Sergio for helping me get started on this project. To the members of the HyperCube: thank you for all the laughter and (sometimes) intellectual discussions. Thanks must also go the other second-years for the shared burden of classes and qualifying exams, and to the more senior students for helping us prepare for these exams. Outside of lab, thanks to my many friends around campus for making this a wonderful place. And to my friends back home: thank you for not forgetting about me and keeping in touch, going home is always a joy because of you.

Finally, I would not be writing this thesis if it was not for my family. Mom, Dad, you have been such a support throughout my life. I appreciate that especially in our situation, it is hard on you for me to be 5,668 kilometers away. The fact that you support me 100% in spite of that shows just how lucky I am to have you. I miss all of you guys a lot, but the Skype sessions with Mom and Dad, and Jill (and the rest of the Ernst-Opgenoord family) make up for a lot. I am sorry I won't be coming home just yet.

This work was supported in part by the NASA LEARN program through grant number NNX14AC73A, technical monitor Justin S. Gray, and by the United States Department of Energy, Office of Advanced Scientific Computing Research (ASCR), Applied Mathematics Program, awards DE-FG02-08ER2585 and DE-SC0009297, as part of the DiaMonD Multifaceted Mathematics Integrated Capability Center, program manager Steven Lee.

Table of Contents

Nomenclature

Greek Symbols

Symbol	Description
α_j, β_j, γ, θ_j	Weighting parameters for the objective function
α_r^i	Weighting coefficient for first-order component functions
β_{pq}^{ij}	Weighting coefficient for second-order component functions
η_{film}	Turbine cooling heat transfer efficiency, $[-]$
η_i	Average main effect sensitivity index
η_{fan}	Fan efficiency, $[-]$
$\eta_{\text{pol}_{lc}}$	High pressure compressor efficiency, $[-]$
$\eta_{\text{pol}_{ht}}$	High pressure turbine efficiency, $[-]$
$\eta_{\text{pol}_{lc}}$	Low pressure compressor efficiency, $[-]$
$\eta_{\text{pol}_{lt}}$	Low pressure turbine efficiency, $[-]$
λ_i	Factor of updated input variance over original input variance
$\boldsymbol{\mu}$	Vector containing the mean of each input variable
μ_Y	Mean of QoI
ν_j	Parameter of a probability distribution
π_D	Fan pressure ratio, $[-]$
$\rho_{\text{fus,bend}}$	Fuselage bending-material density, $[kg/m^3]$
$\rho_{\text{fus,skin}}$	Fuselage pressure-skin density, $[kg/m^3]$
ρ_{mat}	Material density for D8.6, $[kg/m^3]$
$\rho_{\text{wt,cap}}$	Wing and tail spar cap material density, $[kg/m^3]$
$\rho_{\text{wt,web}}$	Wing and tail skin material density, $[kg/m^3]$

$\boldsymbol{\sigma}$	Vector containing the standard deviation of each input variable
$\sigma_{\text{fus,bend}}$	Maximum allowable fuselage shell bending stress, $[Psi]$
$\sigma_{\text{fus,skin}}$	Maximum allowable fuselage skin pressurization stress, $[Psi]$
$\sigma_{\text{wt,cap}}$	Maximum allowable wing and tail spar cap stress, $[Psi]$
σ_Y	Standard deviation of QoI
$\sigma_{Y,b}$	Budget on the standard deviation of the QoI
$\tau_{\text{wt,web}}$	Maximum allowable wing and tail spar web shear stress, $[Psi]$
φ_i	Basis functions
ξ	Running parameter for basis functions
ζ_i	Variance-based sensitivity index function

Roman Symbols

Symbol	Description
a, b, c	Parameters of a probability distribution
C	Cost of changing the distributions of the input variables
C_b	Budget on the cost of changes in the input distributions
C_L	Cruise aircraft lift coefficient, $[-]$
$C_{L_{\perp,\max}}$	Maximum lift coefficient perpendicular to the chord of the wing $(= C_{L,\max}/\cos(\Lambda)^2)$, $[-]$
C_b	Budget on cost of changing the distributions of the input variables
$\mathbf{e}_j$	Unit vector
$E_{\text{wt,cap}}$	Young's modulus wing and tail spar cap, $[Psi]$
$\mathcal{F}$	Objective function for optimization problem
f	Probability density function
f_{BLI_f}	Fuselage boundary layer ingestion fraction, $[-]$
$f_{f_{\text{excr}}}$	Fuselage excrescence drag factor, $[-]$
$f_{\sigma,\text{mat}}$	Material yield stress multiplier, $[-]$
$f_{t_{\text{excr}}}$	Tail excrescence drag factor, $[-]$

$f_{w_{\text{excr}}}$	Wing excrescence drag factor, [−]
$f_{S,\text{eng}}$	Secondary engine components weight fraction, [−]
$f_{S,\text{wing}}$	Secondary wing components weight fraction, [−]
$f_Y(r)$	Value of the probability density function of y at $y = r$
$\mathcal{G}$	Nonlinear constraint for optimization problem
g	Engineering system representation, prescribing the relation between the input variables and the QoI
g_0, g_i, g_{ij}, ...	Component functions of HDMR surrogate
h	Step size for differencing, or integrand
I	Generic integral
K^n	Input space mapped to the unit hypercube
L	Order of the cut-HDMR expansion
M	Mach number, [−]
$MTOW$	Maximum Takeoff Weight, [lb]
N	Number of samples
n	Number of input variables
N_{dist}	Number of samples over distributions
N_{lift}	Vertical load factor for wing bending, [−]
N_q	Number of quadrature points in one dimension
OPR_D	Overall pressure ratio, [−]
P	Risk of QoI exceeding r
P_0	Risk of QoI exceeding r for nominal input variable distributions
P_b	Budget on the risk of the QoI
P_b	Budget on risk of QoI exceeding r
$\hat{p}$	Risk of QoI y exceeding the value r
P'	Updated risk for changes in the distributions of the input variables
S_i, S_{ij}, ...	Sensitivity indices

St_h	Turbine cooling Stanton number, $[-]$
t_{film}	Turbine cooling film effectiveness factor, $[-]$
T_{metal}	Turbine metal temperature, $[K]$
$(T_{t4})_{\text{CR}}$	Cruise turbine inlet total temperature, $[K]$
$(T_{t4})_{\text{TO}}$	Takeoff turbine inlet total temperature, $[K]$
V_i, V_{ij}, ...	Variance of component functions of HDMR
$\mathbf{x}$, x_i, x_j	Input variables
y	Quantity of interest (QoI)
$\mathbf{z}$	Anchor point for cut-HDMR

List of Abbreviations

AIAA American Institute of Aeronautics and Astronautics. 22

ANOVA Analysis of Variance. 27, 33, 37, 38, 40–42, 44, 46, 54, 59–62, 91

ATC Analytical Target Cascading. 22

DSA Distributional Sensitivity Analysis. 3, 8, 16, 22, 29–32, 43, 45, 46, 58, 66–69, 91

FAA Federal Aviation Administration. 70

FAST Fourier Amplitude Sensitivity Test. 21

GSA Global Sensitivity Analysis. 8, 21, 26, 28, 30, 46, 50, 51, 66, 68, 83

HDMR High Dimensional Model Representation. 26, 27, 33, 37, 38, 40–42, 44, 46, 54, 57–62, 86, 91

K-L Kullback-Leibler. 21

LEARN Leading Edge Aeronautics Research for NASA. 5

MC Monte Carlo. 86

MMA Method of Moving Asymptotes. 56

NASA National Aeronautics and Space Administration. 5

PCE Polynomial Chaos Expansion. 94

PDF Probability Density Function. 26, 52

QoI Quantity of Interest. 16, 20, 21, 25–30, 42, 50–53, 56, 59, 61, 65–69, 72–74, 76, 78–84, 88, 91–93, 102, 103

TASOPT Transport Aircraft Sizing and OPTimization tool. 5, 16, 17, 65, 72, 74, 81–83, 86, 88, 102

List of Figures

List of Tables

Chapter 1

Introduction

We present a sensitivity-based methodology to support decision-making in the design of multidisciplinary engineering systems, with a focus on the challenge of quantifying and managing uncertainty. We consider the early stages of the design phase, where quantification of uncertainty permits designers to identify critical areas of design risk and to allocate resources accordingly. Uncertainties abound in engineering design and decision: technical uncertainties due to novel configurations and new technologies, programmatic uncertainties in cost and schedule, design requirements and/or operating conditions that may evolve over time, and uncertainties introduced due to the use of simplified models. As an example consider the design process of a recent commercial airliner, the Boeing 787, of which a timelime of the design process is shown in Fig. 1-1. We see that the engine partners were selected in 2004, more than a year afer the start of design, and that their first test was in 2006. Therefore, at the start of the design there was a large uncertainty in the engine performance. Additionally, there was the uncertainty in the composite technology, because that technology also still needed to be developed.

Such uncertainties pose a serious risk to the critical decisions made in engineering design, especially when considering novel systems for which experience and historical data are lacking. Despite a growing recognition of the importance of accounting for uncertainties, systematic methods to quantify and manage uncertainty remain a significant challenge, especially for systems that comprise many interacting subcomponents and/or disciplines.

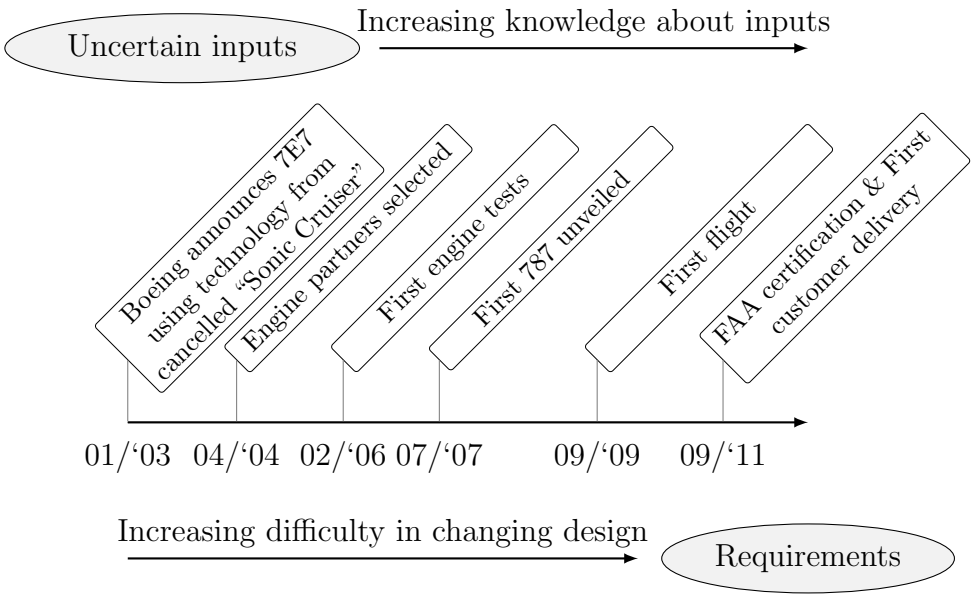

Figure 1-1: *Timeline of design process of Boeing 787, from Ref. 1.*

Past work has addressed the challenge of forward propagation of uncertainty: Given uncertain parameters and uncertain system inputs, what is the corresponding uncertainty in the outcome? Uncertain outcomes are typically characterized by uncertainty associated with the design quantities of interest (QoI).[5–7] The literature categorizes uncertainty as epistemic, owing to insufficient or imperfect knowledge, or aleatory, which arises from natural randomness and is therefore irreducible.[6,8–10] Other work has distinguished among several types of uncertainty, including the many sources associated with the use of computer-based simulation models in system design.[11] In this thesis, we use probabilistic models to represent uncertainty in design parameters and (QoI).[6,12–14] Other ways of characterizing uncertainty include using a probability box to capture the imprecision in the available uncertainty information.[15] Regardless of the method chosen to represent uncertainty, forward propagation of uncertainty typically involves repeated model evaluations to conduct the needed sampling; thus, a great deal of recent work has focused on methods to reduce computational expense, including the use of less-expensive surrogate models to approximate system response.[16–21]

Sensitivity analysis targets the inverse question: What are the uncertain parameters and inputs that contribute the most to output variability, and how would re-

ducing uncertainty in these parameters lead to reduction in output uncertainty? In the context of engineering system design, sensitivity analysis permits better understanding of the effects of uncertainty in order to make well-informed decisions aimed at uncertainty reduction.[12,22] Existing sensitivity analysis approaches typically use variance as a measure of uncertainty. The process of apportioning output variance across model factors in a global sensitivity analysis (GSA) can be carried out by both a Fourier Amplitude Sensitivity Test (FAST) method, and the Sobol' method.[23–27] The FAST method is based on Fourier transforms, while the Sobol' method utilizes Monte Carlo simulation. In addition to variance-based sensitivity analysis, work has also been done in the development of methods for global and regional sensitivity analysis using information entropy as a measure of uncertainty. One such method uses the Kullback-Leibler (K-L) divergence, or relative entropy, to quantify the distance between two probability distributions.[28] These distributions correspond to estimates of the (QoI) before and after some model parameter has been fixed at a particular value (e.g., its mean value). The K-L divergence between the two distributions then serves to quantify the impact of the factor that has been fixed: the larger the value of the K-L divergence, the more substantial the contribution of that parameter to uncertainty in the (QoI).

In addressing design under uncertainty, robustness—which according to Knoll and Vogel is "the property of systems that enables them to survive unforeseen or unusual circumstances"[29]—and reliability—which describes a system's "probability of success in satisfying some performance criterion"[5]—are typically treated separately. The origins of robust design stem back to the pioneering work of Taguchi, with the aim of reducing the sensitivity of products and processes to various noise factors, such as manufacturing variability, environmental conditions, and degradation over time.[30–32] In Ref. 33, an integrated framework for optimization under uncertainty is developed that accounts for both design objective robustness and probabilistic design constraints.

This thesis develops a broadly applicable sensitivity-based methodology that, given a model of the sources of uncertainty, provides systematic guidance to a decision-

maker in identifying and selecting uncertainty reduction options and design choices. Our goal is to allocate the resources of cost, schedule and risk, while also identifying opportunities to tailor the design so as to minimize uncertainty in key areas while retaining flexibility in others. Underlying our proposed approach is the view that uncertainty is a currency: a designer can tolerate a particular level of uncertainty, typically characterized by specified acceptable levels (i.e., budgets) of risk, reliability and/or robustness. The key challenge then becomes how to "spend" the uncertainty—where to focus uncertainty reduction efforts so as not to waste valuable resources reducing uncertainty in parameters that contribute little to output uncertainty, but instead to target the most sensitive parameters and manage resources in a systematic way. This modeling of the design process is consistent with decomposition-based formulations of the design problem, such as analytical target cascading (ATC), where the system is modeled using hierarchical levels and design targets are cascaded from upper levels to lower levels.[34–36]

Thesis Contributions

This work builds on the mathematical framework of Ref. 37, which views the system design problem as a stochastic estimation process as shown in Figure 1-2. The material presented here advances that work by formalizing the idea of uncertainty budgeting, in particular by formulating and solving a multi-objective optimization problem that seeks optimal strategies to manage the uncertainty and design risk. A second contribution of this thesis is to introduce a tailored surrogate modeling approach that permits analysis of complex system models. A major part of this uncertainty budgeting methodology has been presented at the AIAA Scitech meeting in January 2016.[38]

Furthermore, this thesis presents a more efficient approach to distributional sensitivity analysis (DSA), which also extends its use to more general distributions. Whereas in global sensitivity analysis one assumes that all the uncertainty in input variables can be reduced, with distributional sensitivity analysis one investigates what

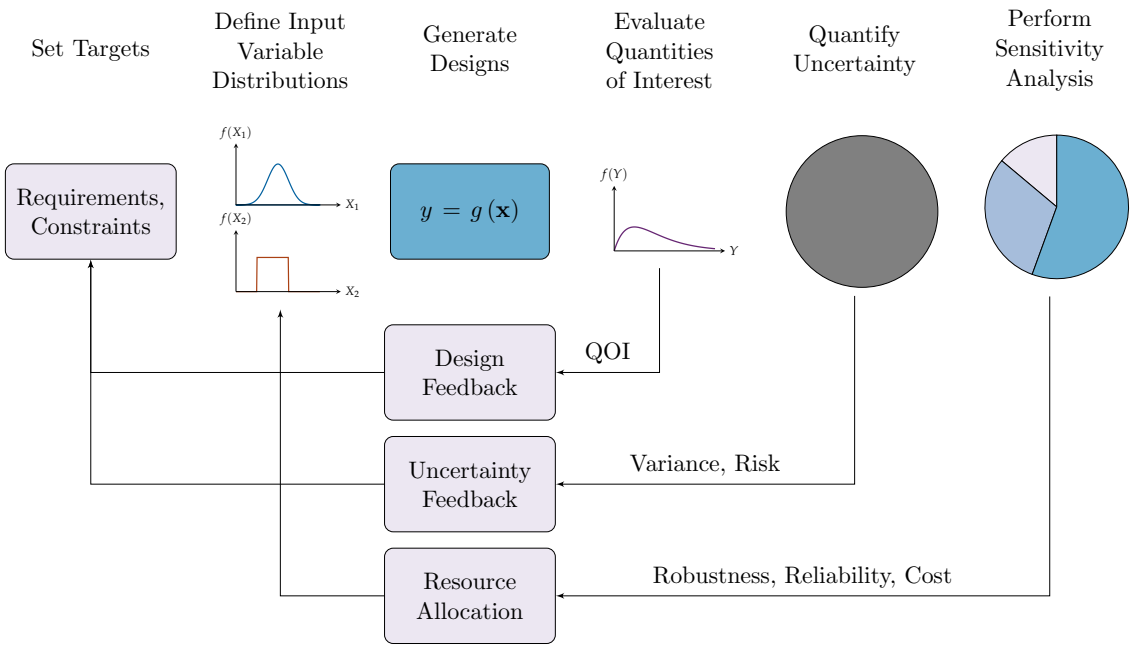

Figure 1-2: *Modeling the system design as a stochastic estimation process with feedback. Figure adapted from Ref. 2.*

happens if we reduce only part of the uncertainty in the inputs. This allows for more informed decision-making. We apply this approach to a complex engineering system, specifically an aircraft design problem.

Thesis Outline

This thesis is organized as follows. Chapter 2 provides a description of the problem setup and background on the sensitivity analysis methods. Chapter 3 explains the new methodology for distributional sensitivity analysis. Chapter 4 describes the uncertainty budgeting methodology, formulates the resource allocation optimization problem and presents a surrogate modeling approach that can be used to reduce the computational expense of solving the uncertainty budgeting optimization problem. Chapter 5 demonstrates the uncertainty budgeting approach by presenting illustrative examples in conceptual aircraft design. Finally, Chapter 6 concludes this thesis.

Chapter 2

Problem Setup and Background

This chapter defines the overall problem setup in Section 2.1, and introduces background on high dimensional model representation (HDMR) and analysis of variance (ANOVA) in Section 2.2.

2.1 Problem setup

In the initial stages of designing a complex system, the key inputs for that design are still uncertain. In aircraft design, for instance, engine technology has a major influence on the design, but may not be fixed at the start of the design phase because of possible future advances.[39] However, the designers still have requirements for the system, and the risk of not meeting those requirements must be quantified and mitigated. Furthermore, key QoI describing the performance and cost of the design are also uncertain during early design stages. This uncertainty must be managed to acceptable levels as the design process evolves. In this work, we formalize the view that uncertainty is a currency: a designer can tolerate a particular level of uncertainty; the decision then becomes how to "spend" the uncertainty. To formulate this mathematically, we define *cost budgets* and *uncertainty budgets*. The uncertainty budget allocates quantitative limits on the acceptable risk in not meeting design requirements and on the acceptable variability in the design QoI (i.e., it specifies the desired reliability and robustness of the design). The cost budget allocates quantitative limits on the resources that can be expended on uncertainty reduction (e.g., money, time,

computational resources).

We consider a general system, represented as

$$y = g(\mathbf{x}),$$

where y is the system QoI, $\mathbf{x}$ are the system input variables, and g is the mapping from input $\mathbf{x}$ to QoI y. Throughout this thesis this system mapping is considered as a general black box – it could be, for example, a computational model or an experiment; however, it is assumed that there is freedom in choosing the input values (i.e., the function $g(\mathbf{x})$ can be evaluated for input $\mathbf{x}$). In the following we develop the methodology for a single scalar QoI, although the approach is straightforward to apply to the case of multiple QoI.

We represent the uncertainty in the input variables probabilistically, that is, we consider $\mathbf{x}$ to be a random variable and we describe each component of $\mathbf{x}$ using a probability density function (PDF). The QoI y is then also a random variable. The PDFs for each input variable are specified by the designer and could be determined from historical data, expert opinion, etc. The PDF of y is estimated using Monte Carlo simulation to propagate uncertainty through the system. We then set budgets on allowable cost and uncertainty. In this work we consider a budget on the allowable standard deviation of the QoI, a budget on the allowable probability of not meeting design requirements, and a budget on the allowable cost of the changes in the input variables. Every design change has an associated cost—whether it be a cost associated with a change in the mean values of the input variables, or a cost associated with a reduction in input uncertainty. The problem therefore becomes a constrained optimization problem to find the best resource allocation strategy that satisfies both cost and uncertainty budgets. This is described mathematically in Chapter 4. Our approach to formulating and solving this problem uses a global sensitivity analysis (GSA), built on the theory of high dimensional model representation (HDMR). The next subsection gives background on HDMR and GSA.

2.2 High Dimensional Model Representation (HDMR) and Global Sensitivity Analysis (GSA)

HDMR is an analysis tool used in representing the relationship between inputs and outputs in a general model.[3,40,41] In this method, the function $g(\mathbf{x})$ is expanded into independent component subfunctions in terms of the input variables,

$$\begin{aligned} g(\mathbf{x}) = g_0 + \sum_{i=1}^{n} g_i(x_i) + \sum_{1\le i<j\le n} g_{ij}(x_i, x_j) + \dots \\ + \sum_{1\le i_1<\dots<i_l\le n} g_{i_1 i_2 \dots i_l}(x_{i_1}, x_{i_2}, \dots, x_{i_l}) + \dots \\ + g_{12\dots n}(x_1, x_2, \dots, x_n). \end{aligned} \tag{2.1}$$

Here, g_0 represents the mean response of $g(\mathbf{x})$ over the input space, while the component subfunction $g_i(x_i)$ captures the contribution of the ith input variable alone. We use the notation x_i to denote the ith input variable and we consider the case of n input variables, $\mathbf{x} = [x_1, \dots, x_n]^\top$. The component subfunction $g_{ij}(x_i, x_j)$ represents the correlated contribution of the ith and jth input variable to $g(\mathbf{x})$, and so on.

The decomposition as written in Eq. (2.1) is not unique.[8] It can however be uniquely defined by imposing the vanishing condition,[25,42,43] which states that the integral of an HDMR component function with respect to any of its own variables is zero:[44]

$$\int f_s(x_s)\, g_{i_1 i_2 \dots i_k}(x_{i_1}, x_{i_2}, \dots, x_{i_k})\, \mathrm{d}x_s = 0 \quad \forall s \in \{i_1, i_2, \dots, i_k\}, \tag{2.2}$$

where $f_s(x_s)$ is the probability density function of the sth input variable. The HDMR representation with constraint (2.2) is called the ANOVA-HDMR; as described in the following, the resulting functional decomposition of $g(\mathbf{x})$ provides a quantitative basis on which to assess how the various inputs contribute to QoI uncertainty.[45,46]

Because of the orthogonality constraints in Eq. (2.2), the variance of the QoI can

be expressed as

$$V(y) = \sum_i V_i + \sum_{1 \le i < j \le n} V_{ij} + \ldots + V_{12\ldots n}, \tag{2.3}$$

where V_i is the portion of the QoI variance associated with the subfunction g_i,

$$V_i = V(g_i(x_i)) = V[\mathbb{E}(y|x_i)], \tag{2.4}$$

and V_{ij} is the portion of the QoI variance associated with the subfunction g_{ij},

$$V_{ij} = V(g_{ij}(x_i, x_j)) = V[\mathbb{E}(y|x_i, x_j)] - V[\mathbb{E}(y|x_i)] - V[\mathbb{E}(y|x_j)]. \tag{2.5}$$

Similar expressions can be built up for V_{ijk} and further. Dividing Eq. (2.3) by the total variance, the decomposition of sensitivity indices is obtained,

$$\sum_i S_i + \sum_{1 \le i < j \le n} S_{ij} + \ldots + S_{12\ldots n} = 1, \tag{2.6}$$

where $S_i = V_i/V$, $S_{ij} = V_{ij}/V$, and so on for the higher-order terms. The main effect sensitivity index S_i represents the normalized expected reduction in total variance if the variance of the ith input variable were reduced to zero. Computing these sensitivity indices is termed a global sensitivity analysis (GSA).[45]

Chapter 3

Distributional Sensitivity Analysis

When performing global sensitivity analysis, the designer only has to specify the initial distribution and then gets information on the expected uncertainty reduction in the quantity of interest (QoI) when an input parameter is fixed to its true value. For distributional sensitivity analysis that assumption is relaxed to better inform engineering decisions.

This chapter firstly introduces DSA formally in Section 3.1 and explains the different approaches towards sampling over different distributions in Section 3.2. Finally, the surrogate-modeling technique is explained in Section 3.3.

3.1 DSA: A new factor priorization method

Performing a global sensitivity analysis allows for factor priorization; ranking the input variables based on how much uncertainty in y would be reduced if that variable was fixed to its true value.[45] Unfortunately, it is typically not possible to reduce all uncertainty in a variable,[47] which would also take up a lot of resources. It would therefore make more sense to consider the uncertainty reduction in an input parameter as a random variable. This is the approach Allaire and Willcox[48] take in their distributional sensitivity analysis method. The result of this method is not only an *average main effect sensitivity index* but also a function which tells the designer how

much uncertainty of y is reduced if the uncertainty in the input parameter is reduced a particular amount. That means we can also treat the uncertainty reduction in y as a continuous variable as opposed to a discrete variable for GSA.

As an example we show notional results for the two approaches in Fig. 3-1. We are aiming to reduce the uncertainty of y by 50%. Using GSA, we find that the uncertainty in X_2 is responsible for 50% of the uncertainty in y and therefore we try to reduce all uncertainty in X_2. With DSA, we can instead quantify the influence on the QoI when the uncertainty in both input variables is partially reduced, and choose our uncertainty reduction strategy accordingly. In practice, one expects it to be more feasible and more cost effective to partially reduce uncertainties in multiple variables, rather than to assume that all uncertainty can be eliminated in one particular variable.

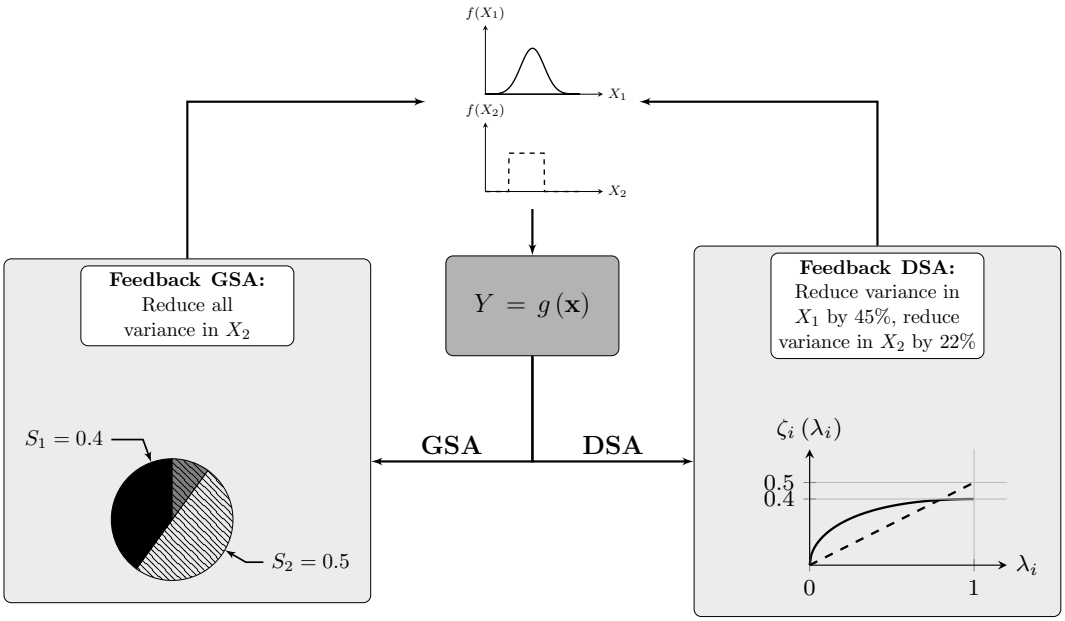

Figure 3-1: *Comparison of design process using global sensitivity analysis and distributional sensitivity analysis.*

In global sensitivity analysis, the factor prioritization is performed by ranking the input variables based on how much uncertainty in Y is reduced by fixing a particular input to its true value in the input space. This ranking is based solely on the main effect sensitivity indices in Eq. (2.6). Such a factor prioritization strategy relies on the assumption that in fact all uncertainty of a particular input variable can be reduced.

Distributional sensitivity analysis by Allaire and Willcox[48] relaxes this assumption by treating the amount of variance reduction in a particular input variable as a random variable instead of assuming it can be reduced completely to zero. They assume that for a given amount of variance reduction in the input variable X_i they can define a family of reasonable distributions and calculate an average change in the variance of Y over this family. In the design setting this is particularly useful, because reducing the uncertainty in an input parameter to zero is in general very hard.

In DSA we consider a variance-based sensitivity index function ζ_i. When reducing the variance of X_i by a percentage $100\,(1-\lambda_i)\,\%$, this variance-based sensitivity index function ζ_i is defined as

$$\zeta_i\left(\lambda_i\right) = \frac{\operatorname{var}\left(Y^0\right) S_i^0 - \mathbb{E}\left[\operatorname{var}\left(Y'\right) S_i' \mid \Lambda_i = \lambda_i\right]}{\operatorname{var}\left(Y^0\right)}. \tag{3.1}$$

Here $\operatorname{var}\left(Y'\right)$ is the new variance of Y for the new random variable X_i', the distribution of which was found by doing further research on that input variable. Furthermore, S_i' is the new main effect sensitivity index associated with the new random variable X_i'. $\lambda_i = \operatorname{var}\left(X_i'\right)/\operatorname{var}\left(X_i\right)$ is the ratio of the remaining variance of X_i to the variance of the original distribution. Lastly, $\operatorname{var}\left(Y^0\right)$ and S_i^0 are the variance of Y and the main effect sensitivity index of X_i for the original input distribution of X_i, respectively.

Since it is not known how we can reduce the uncertainty in the input variables, we take the expected value of the reduction in variance of Y over all reasonable distributions. $\mathbb{E}\left[\operatorname{var}\left(Y'\right) S_i' \mid \Lambda_i = \lambda_i\right]$ is the expected value of the product of the updated sensitivity indices and the updated variance of Y, taken over all reasonable distributions. Those reasonable distributions are further defined in Chapter 3 for different distribution families.

However, it is unknown how much uncertainty can be reduced before doing further research, therefore the parameter λ_i is considered a uniform random variable Λ_i on $[0,1]$. Further research could indicate that the uncertainty of the input variable increases, but that would mean the original input distribution was flawed. Therefore $\lambda_i > 1$ is not considered in this work. Other distributions for λ could be considered,

for instance to bias λ towards smaller reduction in uncertainties. This work could easily accomodate that, but it is not included in this thesis because its implementation is problem dependent.

For factor prioritization, we consider the expected value of $\zeta_i(\lambda_i)$ to obtain the *average main effect sensitivity index* (η), as

$$\eta_i = \mathbb{E}_{\Lambda_i}\left[\zeta_i(\Lambda_i)\right]. \tag{3.2}$$

This parameter can then be used to rank input variables based on the average amount variance of Y that can be reduced by doing further research on a particular input variable.

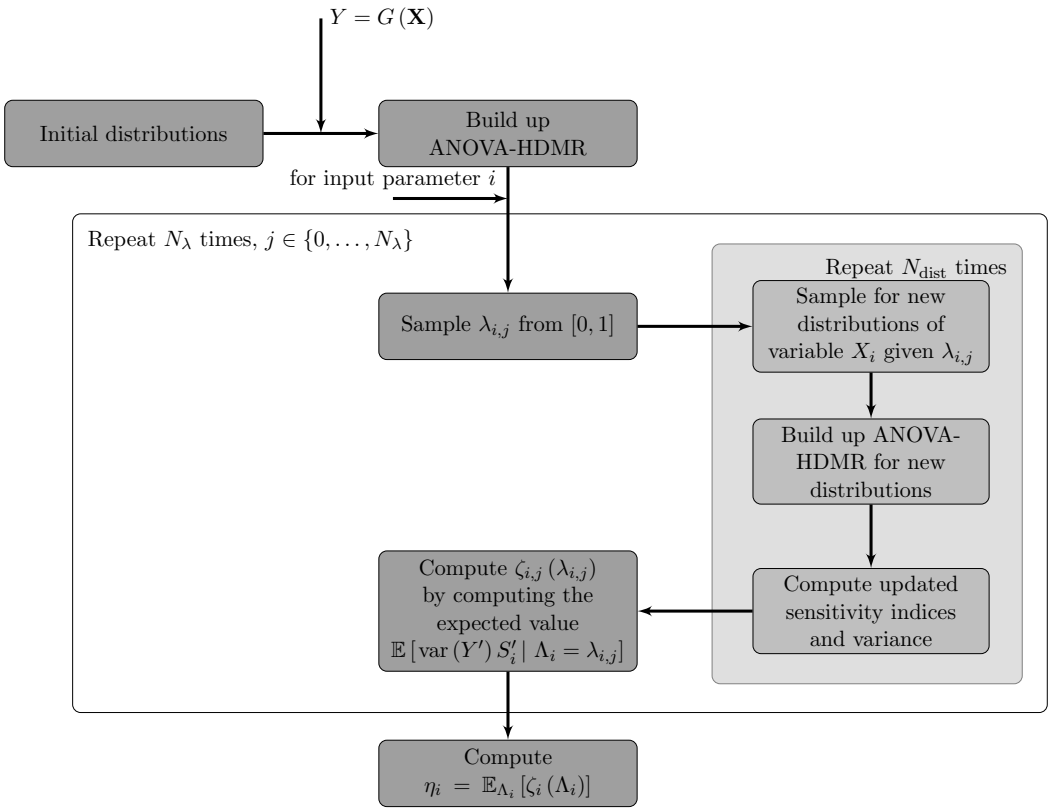

Figure 3-2: *Flow chart for distributional sensitivity analysis*

The overall DSA approach is shown in Fig. 3-2, where N_λ is the number of samples we use to compute η_i and N_{dist} is the number of times we draw a new distribution for a given λ_i. In order for DSA to be useful in an engineering setting, accuracy

and computationally efficiency are key. The rest of this chapter therefore focuses on defining the reasonable distributions we need to sample over in order to obtain ζ_i and on a surrogate modeling technique based on the ANOVA-HDMR which is used throughout this work.

3.2 Sampling over different distributions

We consider three different distributions: the uniform, normal and triangular distribution. The uniform distribution is usually used when not a great deal of information is available about the input parameter, apart from its range. The normal distribution can be considered for error modeling, e.g. model error in a simulation code. When more information is available about the problem, a triangular distribution may be used. Therefore, all three of them are useful in the engineering setting and hence the method is explained in detail for these three distributions. The general method however is extensible to other distributions. The methodologies for sampling from these distributions is adapted from the work from Allaire and Willcox.[48]

3.2.1 Uniform distribution

The sampling algorithm for the uniform distribution has been developed by Allaire and Willcox.[48] The variance of an arbitrary uniform distribution $\mathcal{U}[a, b]$ is given as $\mathrm{var}(X) = (b-a)^2/12$. Considering the original distribution as $\mathcal{U} = [a^0, b^0]$ and an updated distribution as $\mathcal{U} = [a', b']$, λ_i would then be given by $\lambda_i = [(b'-a')/(b^0-a^0)]^2$. Therefore, all updated distribution for a given λ_i have the same width, as $\lambda_i^{1/2}(b^0-a^0)$. In order to compute $\mathbb{E}[\mathrm{var}(Y')\, S_i' \mid \Lambda_i = \lambda_i]$ we sample over different distributions using Algorithm 3-1.

However, instead of just sampling over new distributions for every λ_i, we can also compute $\mathbb{E}[\mathrm{var}(Y')\, S_i' \mid \Lambda_i = \lambda_i)]$ using Gauss-Legendre quadrature. That is if we assume that $\mathrm{var}(Y')\, S_i'$ can be accurately represented by a polynomial. The reason that we can now solve this integral with Gauss-quadrature is because we can exactly specify what we want the mean and the standard deviation of the new distribution to

Algorithm 3-1: *Computing the variance-based sensitivity index function for a uniform distribution using sampling, from Ref. 48.*

Sample λ_i from a uniform distribution on the interval $[0, 1]$
for $j \leftarrow 1, N_{\text{dist}}$ **do**
    Sample b' from a uniform distribution on the interval $\left[a^0 + \sqrt{\lambda_i}\left(b^0 - a^0\right), b^0\right]$
    Let $a' = b' - \sqrt{\lambda_i}\left(b^0 - a^0\right)$
    Compute $\text{var}\left(Y'\right)_j$ and $S'_{i,j}$ for the distribution $\mathcal{U}\left[a', b'\right]$
end for
Compute $\mathbb{E}\left[\text{var}\left(Y'\right) S'_i \mid \Lambda_i = \lambda_i\right] = \frac{1}{N_{\text{dist}}} \sum_j \text{var}\left(Y'\right)_j S'_{i,j}$
Compute variance-based sensitivity index function using Eq. (3.1) for λ_i.

be. This is not possible with a sampling-based method, because one is dependent on the original samples and may therefore not get the exact mean and variance. To solve for the expected value, we rewrite it as an integral over μ', the mean of the updated distribution,

$$\mathbb{E}\left[\text{var}\left(Y'\right) S'_i \mid \Lambda_i = \lambda_i\right] = \left.\frac{\int \text{var}\left(Y'\right) S'_i \mathrm{d}\mu'}{\int \mathrm{d}\mu'}\right|_{\Lambda_i = \lambda_i}. \tag{3.3}$$

A method for computing the variance-based sensitivity index function ζ_i using Gauss-Legendre quadrature is given in Algorithm 3-2.

Algorithm 3-2: *Computing the variance-based sensitivity index function for a uniform distribution using Gauss-Legendre quadrature.*

Sample λ_i from a uniform distribution on the interval $[0, 1]$
Let lower bound for the mean μ_l be $a^0 + \frac{1}{2}\sqrt{\lambda_i}\left(b^0 - a^0\right)$ and the upper bound μ_u be $b^0 - \frac{1}{2}\sqrt{\lambda_i}\left(b^0 - a^0\right)$
for $j \leftarrow 1$ **to** N_q **do**
    Let μ_j be Gauss-Legendre quadrature node on the interval $[\mu_l, \mu_u]$
    Let $a' = \mu_j - \frac{1}{2}\sqrt{\lambda_i}\left(b^0 - a^0\right)$ and $b' = \mu_j + \frac{1}{2}\sqrt{\lambda_i}\left(b^0 - a^0\right)$
    Compute $\text{var}\left(Y'\right)_j$ and $S'_{i,j}$ for the distribution $\mathcal{U}\left[a', b'\right]$
end for
Compute $\mathbb{E}\left[\text{var}\left(Y'\right) S'_i \mid \Lambda_i = \lambda_i\right] = \sum_j w_j \text{var}\left(Y'\right)_j S'_{i,j} / \left(\mu_u - \mu_l\right)$, where w_j are the Gauss-Legendre quadrature weights on the domain $[\mu_l, \mu_u]$
Compute variance-based sensitivity index function using Eq. (3.1) for λ_i

3.2.2 Normal distribution

The procedure for computing the variance-based sensitivity ζ_i for a normal distribution is similar to that for a uniform distribution, because the distribution is also char-

acterized by only two parameters. Let the original distribution be given by $\mathcal{N}(\mu_0, \sigma_0^2)$ and the updated distribution by $\mathcal{N}\left(\mu', \sigma'^2\right)$, where σ'^2 is $\lambda_i {\sigma_0}^2$. A method for computing ζ_i by sampling over possible distributions is given in Algorithm 3-3. Here, we consider the case where we allow the mean of the distribution to change, in contrast to the work of Allaire and Willcox,[48] because here we do not have the problem of sample impoverishment towards the tail of the distribution. Considering the support of the normal distribution is infinite, we need to bound the mean of the updated distribution to sample over it. We therefore only allow the mean of the updated mean to vary within the interval $\mu' \in [\mu'_l, \mu'_u]$, where μ'_l is the minimum allowable mean and μ'_u is the maximum allowable mean of the updated distributions. Here we choose μ'_l and μ'_u such that $\mu'_l - \sigma' = \mu_0 - \sigma_0$ and $\mu'_u + \sigma' = \mu_0 + \sigma_0$. This is also illustrated in Fig. 3-3.

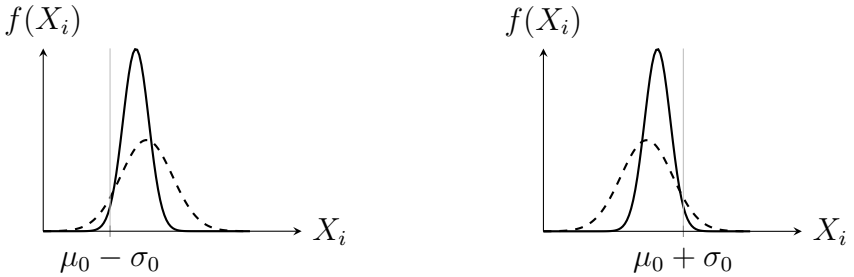

(a) Updated distribution with lowest allowable mean

(b) Updated distribution with highest allowable mean

Figure 3-3: *Illustration of updated distributions for sampling over reasonable distributions for DSA with a normal distribution. In this example* $\lambda_i = 0.5$.

Algorithm 3-3: *Computing the variance-based sensitivity index function for a normal distribution using sampling.*

1: Sample λ_i from a uniform distribution on the interval $[0, 1]$
2: **for** $j \leftarrow 1$ **to** N_{dist} **do**
3: Sample μ' from a uniform distribution on the interval $\left[\mu_0 - \left(1 - \sqrt{\lambda_i}\right)\sigma_0, \mu_0 + \left(1 - \sqrt{\lambda_i}\right)\sigma_0\right]$
4: Compute $\text{var}\left(Y'\right)_j$ and $S'_{i,j}$ for the distribution $\mathcal{N}\left[\mu', \lambda_i \sigma_0^2\right]$
5: **end for**
6: Compute $\mathbb{E}\left[\text{var}\left(Y'\right) S'_i \mid \Lambda_i = \lambda_i\right] = \frac{1}{N_{\text{dist}}} \sum_j \text{var}\left(Y'\right)_j S'_{i,j}$
7: Compute variance-based sensitivity index function using Eq. (3.1) for λ_i

---

Again, we can also solve for $\mathbb{E}\left[\text{var}\left(Y'\right) S'_i \mid \Lambda_i = \lambda_i\right]$ using Gauss-Legendre quadra-

ture, instead of sampling over the distributions. The algorithm for that procedure is shown in Algorithm 3-4.

Algorithm 3-4: *Computing the variance-based sensitivity index function for a normal distribution using Gauss-Legendre quadrature.*

1: Sample λ_i from a uniform distribution on the interval $[0, 1]$
2: Let lower bound for the mean μ_l be $\mu_0 - \left(1 - \sqrt{\lambda_i}\right)\sigma_0$ and the upper bound $\mu_0 + \left(1 - \sqrt{\lambda_i}\right)\sigma_0$
3: **for** $j \leftarrow 1$ **to** N_q **do**
4: Let μ_j be Gauss-Legendre quadrature node on the interval $[\mu_l, \mu_u]$
5: Compute $\mathrm{var}\left(Y'\right)_j$ and $S'_{i,j}$ for the distribution $\mathcal{N}\left[\mu_j, \lambda_i \sigma_0^2\right]$
6: **end for**
7: Compute $\mathbb{E}\left[\mathrm{var}\left(Y'\right) S'_i \mid \Lambda_i = \lambda_i\right] = \sum_j w_j \mathrm{var}\left(Y'\right)_j S'_{i,j} / \left(\mu_u - \mu_l\right)$, where w_j are the Gauss-Legendre quadrature weights on the domain $[\mu_l, \mu_u]$
8: Compute variance-based sensitivity index function using Eq. (3.1) for λ_i

3.2.3 Triangular distribution

The triangular distribution has three parameters, which makes the sampling more complicated than the sampling procedure for the normal and uniform distributions. We present two different ways of sampling and it depends on the problem at hand which strategy makes most sense. Let $\mathcal{T}\left(a^0, b^0, c^0\right)$ be the original input distribution and $\mathcal{T}\left(a', b', c'\right)$ the updated distribution. For a triangular distribution $\mathcal{T}\left(a, b, c\right)$ the variance is $\left(a^2 + b^2 + c^2 - ab - ac - bc\right)/18$. Therefore λ_i is given by

$$\lambda_i = \frac{a'^2 + b'^2 + c'^2 - a'b' - a'c' - b'c'}{a^{0^2} + b^{0^2} + c^{0^2} - a^0 b^0 - a^0 c^0 - b^0 c^0}. \tag{3.4}$$

The first strategy considers distributions whose shape does not change. That is, if all distributions were mapped to the $[0, 1]$ domain, they would overlay one another. The maximum allowable shift in mean is then constrained by the fact that the support of the updated distribution should be within the support of the original distribution, i.e. $a' \geq a^0$ and $b' \leq b^0$. This strategy is illustrated in Figures 3.4(a) and 3.4(b) and the algorithm for it is shown in Algorithm 3-5.

In the second strategy, proposed by Allaire,[49] the most likely value of the distribution is kept fixed and we sample distributions around that. The algorithm for

Algorithm 3-5: *Computing the variance-based sensitivity index function for a triangular distribution using Gauss-Legendre quadrature where the shape of the distribution is kept constant.*

1: Sample λ_i from a uniform distribution on the interval $[0, 1]$
2: Let lower bound for a' be $a'_l = a^0$ and the upper bound
$a'_u = a^0 + \left(1 - \sqrt{\lambda_i}\right)(b^0 - a^0)$
3: **for** $j \leftarrow 1$ **to** N_q **do**
4: Let a' be $x_j (a'_u - a'_l)/2 + (a'_l + a'_u)/2$, where x_j is the Gauss-Legendre quadrature node on the interval $[0, 1]$
5: Compute $\mathrm{var}(Y')_j$ and $S'_{i,j}$ for the distribution $\mathcal{T}[a', b', c']$
6: **end for**
7: Compute $\mathbb{E}[\mathrm{var}(Y') S'_i \mid \Lambda_i = \lambda_i] = \sum_j w_j \mathrm{var}(Y')_j S'_{i,j}$, where w_j are the Gauss-Legendre quadrature weights on the domain $[0, 1]$
8: Compute variance-based sensitivity index function using Eq. (3.1) for λ_i

sampling from the distributions does differ from Ref. 49. Thus, we consider $c^0 = c'$. At the same time, the support of the updated distribution has to be within the support of the original distribution, i.e. $a' \geq a^0$ and $b' \leq b^0$. The algorithm for computing the variance-based sensitivity index function using this strategy is shown in Algorithm 3-6.

3.3 HDMR-based surrogate

The methodologies outlined in Sections 3.2.1 to 3.2.3 work for any variance-based sensitivity analysis. However, computing the sensitivity indices for every new distribution using the full model $g(\mathbf{x})$ is prohibitively expensive. That is the reason why in Ref. 48 the original MC samples from the global sensitivity analysis are reused by means of rejection sampling. We instead use the ANOVA-HDMR both to reduce the initial cost of performing the global sensitivity analysis and to evaluate distributions where rejection sampling is inaccurate. One such example is the triangular distribution: when the most likely value of the updated distribution is almost at the tail of the original distribution, there are very few samples one can use to compute the sensitivity indices.

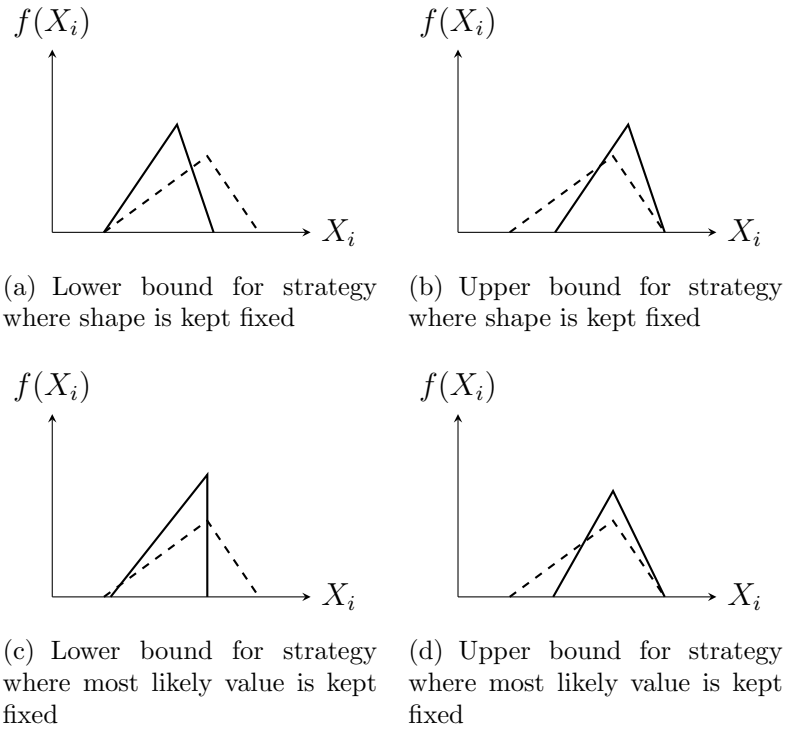

(a) Lower bound for strategy where shape is kept fixed

(b) Upper bound for strategy where shape is kept fixed

(c) Lower bound for strategy where most likely value is kept fixed

(d) Upper bound for strategy where most likely value is kept fixed

Figure 3-4: *Different strategies for sampling over reasonable distributions for DSA with triangular distributions. In this example* $\lambda_i = 0.5$.

Building up the full ANOVA-HDMR as in Eq. (2.1) is often not necessary. For many systems and models, the third-order and higher terms are negligibly small.[3] That allows us to truncate the HDMR by neglecting these higher order terms, yielding the approximation[40]

$$g(\mathbf{x}) \approx g_0 + \sum_{j=1}^{n} g_i(x_i) + \sum_{1 \le i < j \le n} g_{ij}(x_i, x_j). \tag{3.5}$$

In the same way as in Ref. 44, an accurate and fast surrogate model can be built up by approximating the remaining component functions as expansions of an appropriate set of basis functions,

Algorithm 3-6: *Computing the variance-based sensitivity index function for a triangular distribution where the most likely value is kept constant.*

Sample λ_i from a uniform distribution on the interval $[0, 1]$
Solve for a_l' using Eq. (3.4) with $b' = c^0$ and $c' = c^0$
if $a_l' < a^0$ **then**
    $a_l' = a^0$
end if
Solve for b_u' using Eq. (3.4) with $a' = c^0$ and $c' = c^0$
if $b_u' > b^0$ **then**
    Solve for a_u' using Eq. (3.4) with $b' = b^0$ and $c' = c^0$
else
    $a_u' = c^0$
end if
for $j \leftarrow 1$ **to** N_{dist} **do**
    Sample a' from a uniform distribution on the interval $[a_l', a_u']$ and set $c' = c^0$
    Solve for a' using Eq. (3.4)
    Compute $\text{var}\left(Y'\right)_j$ and $S_{i,j}'$ for the distribution $\mathcal{T}\left[a', b', c'\right]$
end for
Compute $\mathbb{E}\left[\text{var}\left(Y'\right) S_i' \mid \Lambda_i = \lambda_i\right] = \frac{1}{N_{\text{dist}}} \sum_j \text{var}\left(Y'\right)_j S_{i,j}'$
Compute variance-based sensitivity index function using Eq. (3.1) for λ_i

$$g_i\left(x_i\right) \approx \sum_{r=1}^{\ell} \alpha_r^i \varphi_r\left(x_i\right) \tag{3.6}$$

$$g_{ij}\left(x_i, x_j\right) \approx \sum_{p=1}^{\ell} \sum_{q=1}^{\ell} \beta_{pq}^{ij} \varphi_{pq}\left(x_i, x_j\right) \tag{3.7}$$

where $g_i\left(x_i\right)$ is expanded into ℓ basis functions $\varphi_1, \ldots, \varphi_\ell$ and α_r^i is the coefficient for the rth basis function, corresponding to the ith input variable. In the same way, β_{pq}^{ij} is the coefficient corresponding to the pqth basis function and the ijth second-order component function. Here, we take $\varphi_{pq}\left(x_i, x_j\right)$ to be $\varphi_p(x_i)\varphi_q(x_j)$.

In this work, we choose orthonormal polynomials as basis functions. The choice for orthonormal basis functions makes for evaluating the coefficients of the component

functions as[44]

$$\alpha_r^i = \int_{K^n} g(\mathbf{x})\, \varphi_r(x_i)\, f_{\mathbf{x}}(\mathbf{x})\, \mathrm{d}\mathbf{x} \tag{3.8}$$

$$\beta_{pq}^{ij} = \int_{K^n} g(\mathbf{x})\, \varphi_p(x_i)\, \varphi_q(x_j)\, f_{\mathbf{x}}(\mathbf{x})\, \mathrm{d}\mathbf{x}. \tag{3.9}$$

Because we need orthonormal basis functions with respect to the distribution, different basis functions are needed for every distribution considered. It is well known that *normalized shifted Legendre polynomials* on the domain $[0, 1]$ are orthonormal with respect to the uniform distribution on that domain. Note that this requires us to rescale the input variables to the unit hypercube as well. The integrals in Equations (4.11) and (4.12) are then efficiently solved using Gauss-Legendre quadrature.

For the normal distribution the normalized probabilists' Hermite-polynomials are used, which requires us to map the input variables to all have $\mathcal{N}(0, 1)$ distribution. In this case, we solve the integrals for every α_r^i and β_{pq}^{ij} in Equations (4.11) and (4.12) efficiently using (probabilists') Gauss-Hermite quadrature.

In building up the ANOVA-HDMR for the triangular distributions, one has to deal with the discontinuous derivative of the probability density function. This complicates finding the correct basis functions. Furthermore, the basis functions now also depend on the shape of the probability density function directly. This in contrast to the uniform and normal distribution, where we map $\mathcal{U}(a, b)$ to $\mathcal{U}(0, 1)$ and $\mathcal{N}(\mu, \sigma^2)$ to $\mathcal{N}(0, 1)$, respectively. Here, we map $\mathcal{T}(a, b, c)$ to $\mathcal{T}(0, 1, \mu)$, which means that the basis functions depend on μ and therefore depend directly on the shape of the probability density function. The first three basis functions for the triangular distributions are derived by Wang et al.[42] Finding higher-order basis functions is cumbersome, therefore only up to third-order basis functions for the triangular distributions are considered in this thesis.

In solving the integrals for every α_r^i and β_{pq}^{ij} in Equations (4.11) and (4.12) special care has to be taken to include the discontinuous derivative of the probability density function. Solving these integrals using Gauss-Legendre quadrature would not work, because the integrand is not even close to a smooth polynomial in the domain.

Therefore, we split the integrand up in the two linear parts of the probability density function and solve them separately using Gauss-Legendre quadrature. For example in 1D,

$$I = \int_0^1 \mathcal{G}(\xi) f_\xi(\xi) \, \mathrm{d}\xi \tag{3.10}$$

$$\text{where } f_\xi = \begin{cases} \frac{2}{\mu}\xi & \text{for } 0 \leq \xi \leq \mu \\ \frac{2}{1-\mu}(1-\xi) & \text{for } \mu \leq \xi \leq 1 \end{cases} \tag{3.11}$$

where $\mathcal{G}(\xi)$ is some polynomial function on $[0, 1]$ and I is the value of the integral we want to compute. We then split the integral as

$$I = \int_0^\mu \mathcal{G}(\xi) \frac{2}{\mu}\xi \mathrm{d}\xi + \int_\mu^1 \mathcal{G}(\xi) \frac{2}{1-\mu}(1-\xi) \, \mathrm{d}\xi \tag{3.12}$$

where both parts can be accurately computed using Gauss-Legendre quadrature.

In higher dimensions the domain needs to be split up in more parts, as can be seen in the 2D example in Fig. 3-5. Thus, for the same order of polynomial for the integrand, we need twice as many quadrature points in every dimension.
Using the component functions of the ANOVA-HDMR, g_i and g_{ij}, the sensitivity indices S_i and S_{ij} are found by computing V_i and V_{ij} as

$$V_i = \int_{K^n} g_i^2(\mathbf{x}) f_{\mathbf{x}'}(\mathbf{x}') \, \mathrm{d}\mathbf{x} \tag{3.13}$$

$$V_{ij} = \int_{K^n} g_{ij}^2(\mathbf{x}) f_{\mathbf{x}'}(\mathbf{x}') \, \mathrm{d}\mathbf{x}. \tag{3.14}$$

The total variance is then found by

$$V(Y) = \sum_i V_i + \sum_{1 \leq i < j \leq n} V_{ij}. \tag{3.15}$$

Finally, the sensitivity indices are computed as

$$S_i = \frac{V_i}{V(Y)}, \quad S_{ij} = \frac{V_{ij}}{V(Y)}. \tag{3.16}$$

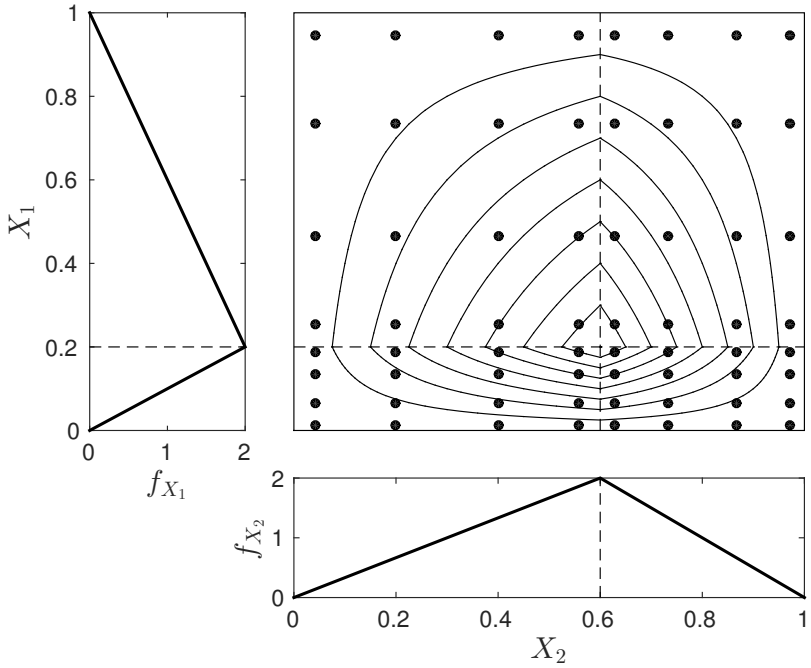

Figure 3-5: *Example of how the input space is split up for 2 inputs. The black dots are the quadrature points and the contour is* $f_{\mathbf{x}}(\mathbf{x})$.

Following the strategy outlined in Fig. 3-2, we build up the ANOVA-HDMR for the original input distributions and then reuse that surrogate to find the new standard deviation of the QoI for updated input distributions. For every change in distribution of the input variables, we therefore need to build up a new ANOVA-HDMR for the new distribution.

We build up a new ANOVA-HDMR by finding the coefficients $\alpha_r^{\prime i}$ and $\beta_{pq}^{\prime ij}$ for the new component functions as

$$\alpha_r^{\prime i} = \int_{K^n} g(\mathbf{x}) \, \varphi_r'(x_i) \, f_{\mathbf{x}'}(\mathbf{x}) \, \mathrm{d}\mathbf{x} \tag{3.17}$$

$$\beta_{pq}^{\prime ij} = \int_{K^n} g(\mathbf{x}) \, \varphi_p'(x_i) \, \varphi_q'(x_j) \, f_{\mathbf{x}'}(\mathbf{x}) \, \mathrm{d}\mathbf{x}. \tag{3.18}$$

Here $f_{\mathbf{x}'}(\mathbf{x})$ is the updated joint probability density. Note that this integral is still solved on the original domain. Therefore the basis functions need to be altered such that they are still orthonormal with respect to the updated distribution.

Using the component functions for the updated ANOVA-HDMR, the updated

sensitivity indices are then found in the same way as discussed in Section 2.2 only now using $g'_{AH}(\mathbf{x}')$ and $f_{\mathbf{x}'}(\mathbf{x}')$.

3.4 Results for analytical functions

In this section, a distributional sensitivity analysis is performed on several test functions using the methods described in this thesis. For the uniform and normal distribution we use the same test functions as used in the work of Allaire and Willcox.[48]

3.4.1 Ishigami function with uniform distribution

For the uniform distribution we use the Ishigami function as test function, given by

$$Y = \sin X_1 + a \sin^2 X_2 + b X_3^4 \sin X_1 \tag{3.19}$$

with $a = 5$ and $b = 0.1$, as used in.[50] Here the X_i's are considered to be independent and uniformly distributed on $\mathcal{U}[-\pi, \pi]$. The main effect sensitivity indices for this function and these distributions are $S_1 = 0.40$, $S_2 = 0.29$ and $S_3 = 0.00$ and the only non-zero interaction term is $S_{1,3} = 0.31$. These were computed using the analytical expressions in Ref. 45. Looking merely at these main effect sensitivity indices might lead to the conclusion that research efforts should be focused towards reducing uncertainty in X_1.

The DSA results paint a different picture, as shown in Fig. 3.6(a). Note that here only X_1 and X_2 are considered, because there is no associated main effect with X_3. The behavior of the effect of future research on the uncertainty of Y is highly nonlinear. In fact, an average 25% reduction of the variance in X_1 actually increases the variance of Y. Therefore, for a variance reduction of less than 50%, it is better to focus research efforts towards uncertainty reduction in X_2.

Taking a uniform distribution for the possible reduction in uncertainty, i.e. $\lambda_i \sim \mathcal{U}[0, 1]$, allows for computing the average main effect sensitivity indices. These are compared to the main effect sensitivity indices in Fig. 3.6(b). Here, $\eta_1 = 0.07$ and

$\eta_2 = 0.04$. The ranking in itself is therefore unchanged, but these results reveal that neither factor is expected to reduce the variance of Y substantially.

These results were generated using an ANOVA-HDMR consisting of up to 8th-order basis functions and using 9 quadrature points in one dimension. With three input variables, we therefore need a total of 729 function evaluations of Eq. (3.19). This is a substantial reduction in the number of function evaluations required, as the sampling approach in Ref. 48 needed 4,096 function evaluations.

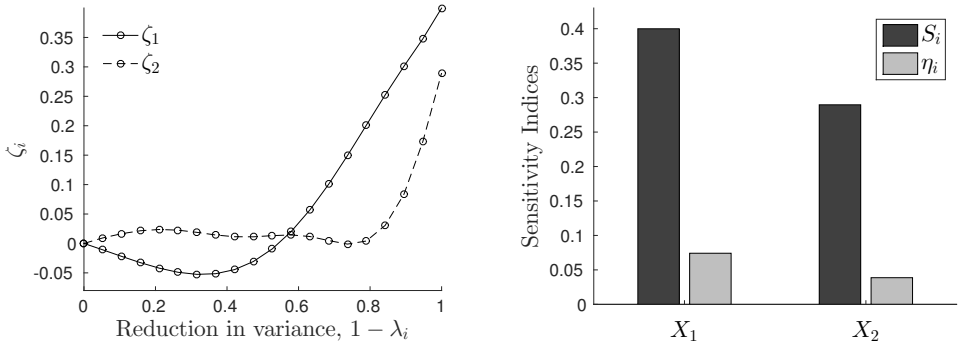

(a) Variance-based sensitivity index functions for X_1 and X_2 with $\lambda_i = 0.0, 0.05, \ldots, 1.0$.

(b) Comparison between main-effect sensitivity indices S_i and average main effect sensitivity indices η_i.

Figure 3-6: *Distributional sensitivity analysis results for the Ishigami function with uniform distributions.*

3.4.2 Additive function with normal distribution

To illustrate the method using a normal distribution, we consider an additive function

$$Y = 100X_1 + 4\exp(X_2) + 350\sin X_3 \tag{3.20}$$

with $X_i \sim \mathcal{N}(0, 4)$. To build up the ANOVA-HDMR, up to 8th-order basis functions and 10 quadrature points in one dimension are used. For three input parameters, that means a total of 1,000 function evaluations are required to build up the ANOVA-HDMR, again a substantial reduction from the 65,536 used in Ref. 48. The main effect sensitivity indices are found to be $S_1 = 0.27$, $S_2 = 0.31$ and $S_3 = 0.41$. Factor

priorization would then lead to the conclusion that the research focus should be on uncertainty reduction in X_3.

The distributional sensitivity analysis results in Fig. 3.7(a), however, show that it might be more worthwhile to invest in uncertainty reduction in X_2. This is also indicated by the average main effect sensitivity indices in Fig. 3.7(b), again found by considering $\lambda_i \sim \mathcal{U}[0,1]$. Those indicate that the ranking for factor priorization should be factor 2, factor 1 and then factor 3, instead of the ranking factor 3, factor 2, factor 1 found by global sensitivity analysis.

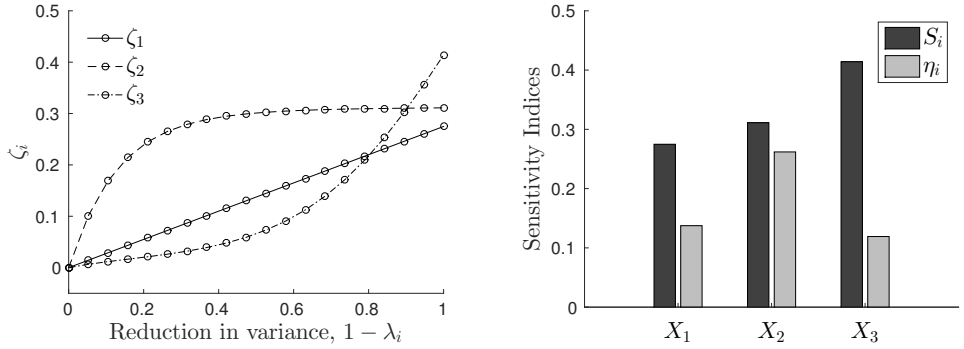

(a) Variance-based sensitivity index functions for X_1, X_2 and X_3 with $\lambda_i = 0.0, 0.05, \ldots, 1.0$.

(b) Comparison between main-effect sensitivity indices S_i and average main effect sensitivity indices η_i.

Figure 3-7: *Distributional sensitivity analysis results for the additive function with normal distributions.*

3.4.3 Test function with triangular distribution

In this work we also consider triangular distributions. The sampling-based DSA method can be used for triangular distributions as well, but has a problem with sample impoverishment towards the tail of the distributions. If an updated distribution has a most likely value close to the tail of the original distribution, that might result in a new set of samples of only a very small part of the original samples, which impairs the accuracy dramatically. In the method considered in this work, such problems do not arise.

The test function for the triangular distributions used here is

$$Y = X_1 + aX_2^3 + bX_3^3 X_1 \tag{3.21}$$

with $a = 0.2$, $b = 0.1$ and $X_i \sim \mathcal{T}(-\pi, \pi, 0)$. The main effect sensitivity indices are then $S_1 = 0.46$, $S_2 = 0.38$ and $S_3 = 0.00$. The only nonzero interaction is $S_{1,3}$ at 0.16. The used ANOVA-HDMR was built up using up to 3rd-order basis functions and 4 quadrature points in one dimension. For a three-dimensional problem that requires 512 function evaluations, due to the domain decomposition shown in Fig. 3-5. Using those parameters, the ANOVA-HDMR recovers the function exactly, because the error is below machine precision. This is expected, because Eq. (3.21) also only contains up to third-order polynomials.

As mentioned in Section 3.2.3, we consider two different approaches to sample over reasonable distributions in the distributional sensitivity analysis. These approaches are compared to one another in Fig. 3-8. The approaches generally have the same behavior, and as mentioned before it depends mostly on the problem at hand which approach makes most sense. The average main effect sensitivity indices, again found with $\lambda_i \sim \mathcal{U}(0, 1)$, also have almost the same value. In both cases, DSA reveals that it would make most sense to focus research efforts towards X_2 instead of X_1, which is suggested by GSA.

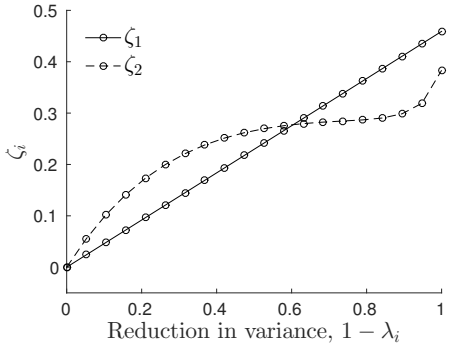

(a) Variance-based sensitivity index functions for X_1 and X_2 for a *constant shape* with $\lambda_i = 0.0, 0.05, \ldots, 1.0$.

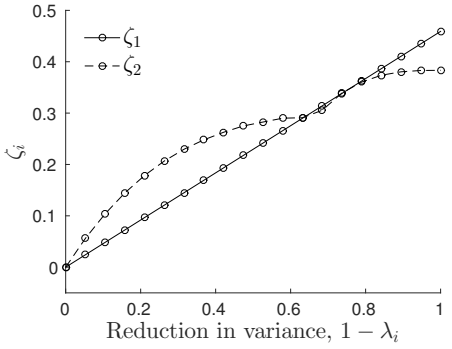

(b) Variance-based sensitivity index functions for X_1 and X_2 for a *constant most likely value* with $\lambda_i = 0.0, 0.05, \ldots, 1.0$.

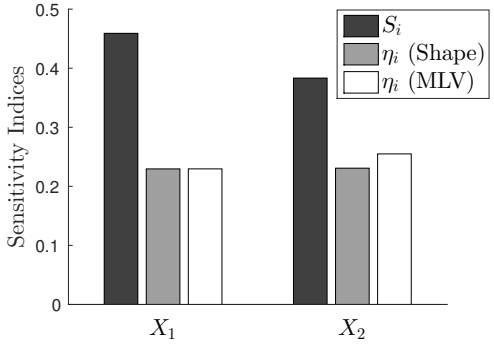

(c) Comparison between main-effect sensitivity indices S_i and average main effect sensitivity indices η_i. "Shape" indicates the result for when the shape is kept constant in sampling over distributions and "MLV" indicates the result for when the most likely value is kept constant in the sampling process.

Figure 3-8: *Distributional sensitivity analysis results for the test function with triangular distributions.*

Chapter 4

Uncertainty Budgeting Methodology

In this chapter we turn to the decision-making that targets management of uncertainties in design. This chapter leverages the sensitivity analysis methods of the previous chapters and formulates an optimization approach for managing uncertainty budgets in system design.

The overall uncertainty quantification method is illustrated in Figure 4-1. The initial problem setup is explained in Section 4.1. Section 4.2 formulates a multi-objective optimization problem to solve the resource allocation problem and discusses the chosen solution method. In order to make the problem computationally tractable we need a surrogate model which is discussed in Section 4.3.

4.1 Problem formulation

In the design of complex systems, key inputs to that design are often uncertain. The question of which of those inputs has the largest influence on the performance of the system has been addressed in Chapter 3. In this chapter, we focus on where we need to reduce the uncertainty to meet the performance targets for that complex system. Specifically, we formulate a methodology to meet risk, uncertainty and cost budgets on such a system.

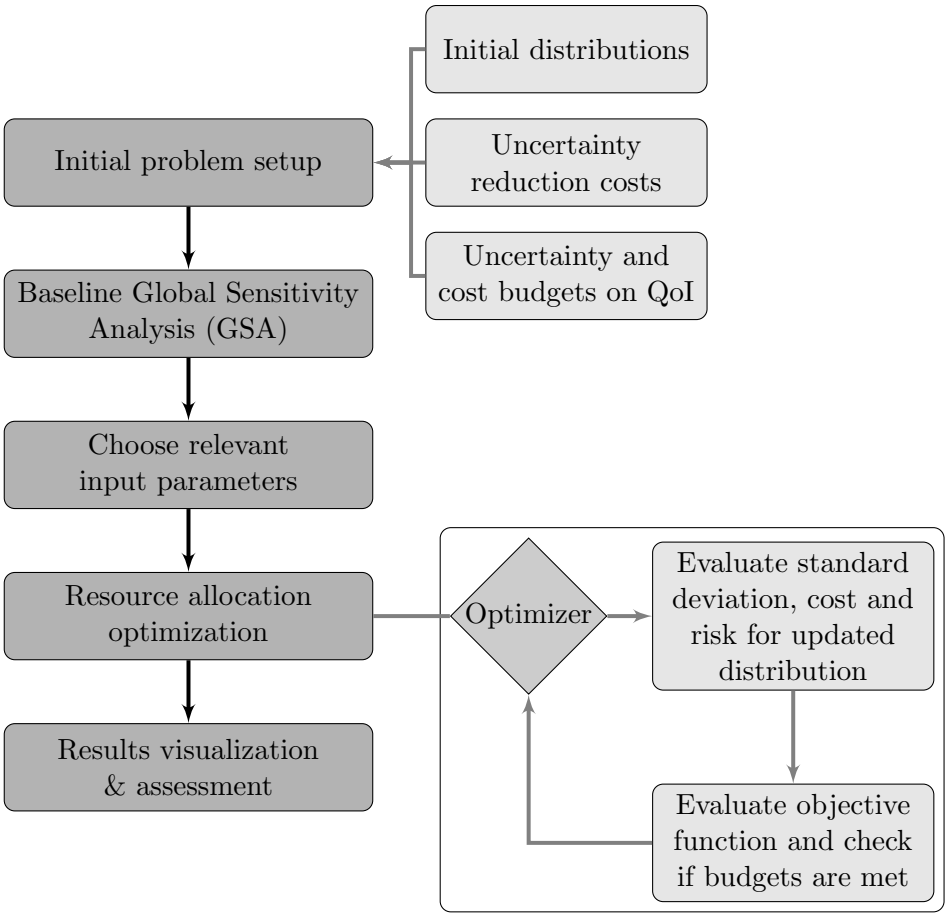

Figure 4-1: *Flow chart showing the uncertainty budgeting methodology.*

As shown in Figure 4-1, the inputs to our methodology are the initial distributions describing uncertainty in each of the system inputs, a model of the costs of uncertainty reduction activities, and cost and uncertainty budgets. The initial uncertainty distribution for each input variable can be constructed from expert elicitation and/or historical data. In this part of the work, only uniform distributions are considered; therefore in our setting, for each input variable the designer has two degrees of freedom: the mean of the input variable and the standard deviation of the input variable. Thus, with n input variables, the problem has a total of $2n$ degrees of freedom in changing the input variable distributions. Figure 4-2 illustrates the degrees of freedom in changing a single uniform input distribution. The extension to other distribution types is straightforward, although the resulting parametrization of changes in uncertainty may have more degrees of freedom per input variable.

For the QoI, three budgets are considered: a budget on risk, P_b, a budget on standard deviation, $\sigma_{Y,b}$, and a budget on the cost of changing the input variables' distributions, C_b. We define the risk as the probability that the QoI fails to meet a requirement, so that the risk budget constraint becomes $\mathbb{P}(y > y_{\text{crit}}) \leq P_b$, where $\mathbb{P}$ denotes probability, y_{crit} is a critical value that the QoI must not exceed, and P_b is the designer-specified budget on the allowable risk probability.

We also require the specification of a model for the cost of changing the distribution of each input variable. We consider both the cost of changing the mean input value (i.e., a change in the nominal design with no accompanying change in uncertainty) and the cost of reducing the input variable's uncertainty (i.e., changing the range of the uniform distribution). A change in input variable mean could, for instance, imply a redesign to a less aggressive design in order to reduce variance in the QoI and thus improve design robustness, or a redesign to a higher-performing design in order to decrease risk of not meeting system requirements. The costs of these changes should include the actual redesign activities as well as any costs that might be incurred to advance technologies that underly the new design point. Reducing uncertainty of an input variable would typically be achieved by additional research and development effort, and/or by experiments, again with associated costs.

Given these initial distributions, a baseline QoI estimates the contributions of each uncertain input to the QoI variance as described in Section 2.2. The GSA results can then be used to screen for the input parameters with the highest influence on the QoI. If a parameter has a low total sensitivity index, then its effect on QoI variance will be small and it is better to exclude that parameter from the optimization. This will speed up the optimization by reducing the number of degrees of freedom, and will also remove low-sensitivity (flat) regions in the design space that would otherwise hamper the optimization convergence.

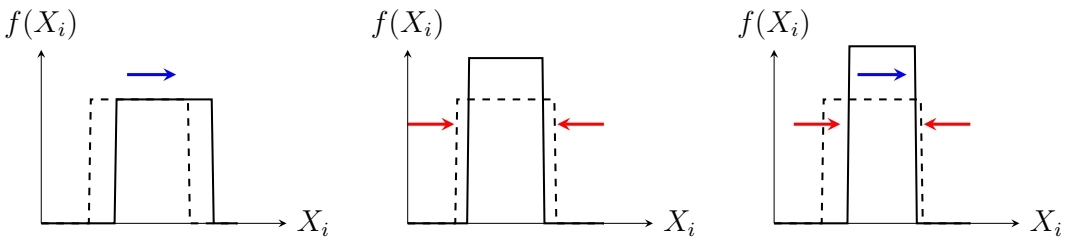

(a) Shift in mean

(b) Reduction in uncertainty

(c) Shift in mean together with a reduction in uncertainty

Figure 4-2: *Illustration of design freedom in changing the parameters of a uniform distribution.*

4.2 Resource allocation optimization

Our methodology next formulates the optimal resource allocation strategy as a constrained optimization problem, where the optimization degrees of freedom are the parameters describing the input variable PDFs (in our case, the mean and standard deviation for each input variable). The optimal resource allocation must meet the budgets on cost and uncertainty. It is likely that there are multiple feasible input PDFs that meet those constraints. Our approach is to visualize the tradespace of feasible options, and to identify an optimal strategy by forming an objective function that expresses designer preferences on cost, standard deviation and risk. This optimization problem is written as

$$\begin{aligned}
\underset{\boldsymbol{\mu},\boldsymbol{\sigma}}{\text{minimize}} \quad & \mathcal{F}(\boldsymbol{\mu},\boldsymbol{\sigma}) &&= \alpha\frac{P(\boldsymbol{\mu},\boldsymbol{\sigma})}{P_b} + \beta\frac{\sigma_Y(\boldsymbol{\mu},\boldsymbol{\sigma})}{\sigma_{Y,b}} + \gamma\frac{C(\boldsymbol{\mu},\boldsymbol{\sigma})}{C_b} \\
\text{subject to} \quad & \mathcal{G}_P(\boldsymbol{\mu},\boldsymbol{\sigma}) &&= P(\boldsymbol{\mu},\boldsymbol{\sigma}) - P_b \leq 0 \\
& \mathcal{G}_\sigma(\boldsymbol{\mu},\boldsymbol{\sigma}) &&= \sigma_Y(\boldsymbol{\mu},\boldsymbol{\sigma}) - \sigma_{Y,b} \leq 0 \\
& \mathcal{G}_C(\boldsymbol{\mu},\boldsymbol{\sigma}) &&= C(\boldsymbol{\mu},\boldsymbol{\sigma}) - C_b \leq 0
\end{aligned} \tag{4.1}$$

where the designer selects the weighting factors α, β and γ assigned to the risk, standard deviation, and cost, respectively. Here C is the cost associated with changing the input distributions, P is the risk (probability of failing to meet a design requirement), and σ_Y is the standard deviation of the QoI. Each of these three quantities is shown

as a function of $\boldsymbol{\mu}$, the vector containing the means of the n input distributions, and $\boldsymbol{\sigma}$, the vector containing the standard deviations of the n input distributions. The terms in the objective function are normalized by the cost, risk and standard deviation budgets, C_b, P_b and $\sigma_{Y,b}$, respectively. Throughout this work, this optimization problem is solved using a gradient-based optimizer.

Figure 4-3 depicts the process of solving the optimization problem. Given updated input variable distributions specified by $\boldsymbol{\mu}$ and $\boldsymbol{\sigma}$, we must estimate the QoI standard deviation, risk and cost to evaluate the objective function $\mathcal{F}(\boldsymbol{\mu}, \boldsymbol{\sigma})$ and constraints $\mathcal{G}_P(\boldsymbol{\mu}, \boldsymbol{\sigma})$, $\mathcal{G}_\sigma(\boldsymbol{\mu}, \boldsymbol{\sigma})$, $\mathcal{G}_C(\boldsymbol{\mu}, \boldsymbol{\sigma})$.

In order to solve the optimization problem, the updated standard deviation and risk must be estimated for changes in the input distribution (as provided by the optimizer). For the standard deviation, this requires estimating

$$\begin{aligned} {\sigma'_Y}^2 &= \int \left(g\left(\mathbf{x}\right) - g'_0\right)^2 f'_{\mathbf{x}}\left(\mathbf{x}\right) \mathrm{d}\mathbf{x} \\ \text{where} \quad g'_0 &= \int g\left(\mathbf{x}\right) f'_{\mathbf{x}}\left(\mathbf{x}\right) \mathrm{d}\mathbf{x}, \end{aligned} \tag{4.2}$$

where $f'_{\mathbf{x}}\left(\mathbf{x}\right)$ is the updated joint probability distribution for the inputs $\mathbf{x}$ and ${\sigma'_Y}^2$ is the corresponding updated QoI variance. These integrals can be evaluated using quadrature methods. This process is also illustrated in Figure 4-4. In that example $X_1, X_2 \sim \mathcal{U}\left[-1, 1\right]$, whereas the updated distributions are $X'_1 \sim \mathcal{U}\left[0, 0.5\right]$ and $X'_2 \sim \mathcal{U}\left[-1, 0.5\right]$. That means that the integral for the standard deviation (Eq. (4.2)) needs to be computed for $g(\mathbf{x})$ on the domain $[0, 0.5] \times [-1, 0.5]$, as illustrated by the hatched area in Figure 4-4.

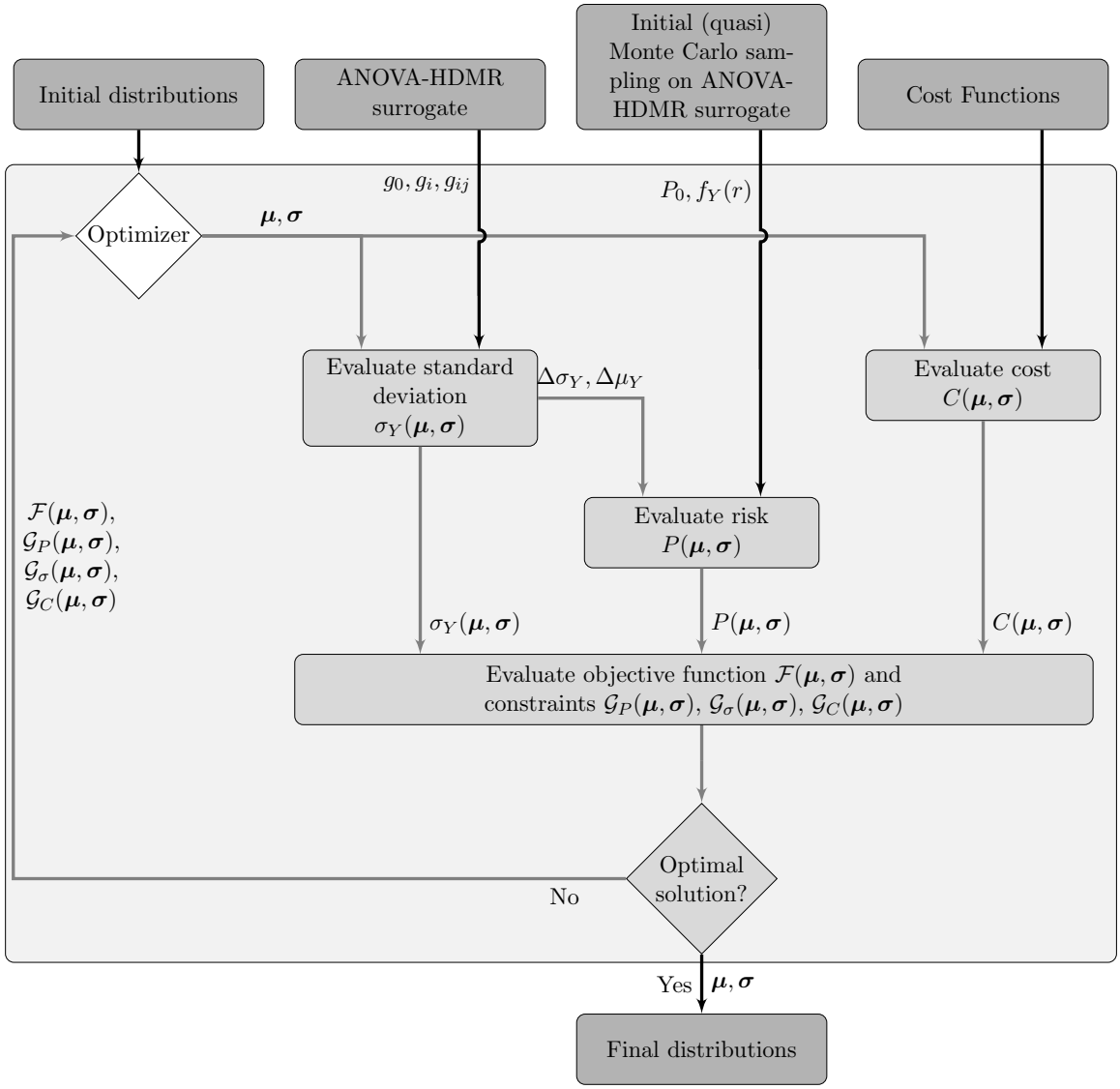

Figure 4-3: *Flow chart for the resource allocation optimization.*

The risk can be estimated via Monte Carlo simulation, using the unbiased estimator $\hat{p}$:

$$P\left(Y > r\right) \approx \hat{p} = \frac{1}{N_s} \sum_{i=1}^{N_s} \mathbb{I}\left(Y_i\right), \tag{4.3}$$

$$\text{with } \mathbb{I}\left(Y_i\right) = \begin{cases} 1, & \text{if} \quad Y_i > r \\ 0, & \text{if} \quad Y_i \leq r \end{cases}$$

where N_s is the total number of Monte Carlo samples. One could use importance sampling for the Monte Carlo estimator if the probabilities become very small,[51] but that is not used in this work, because our budgets are usually on the order of a few per cent and we can use many Monte Carlo samples because the surrogate is cheap.

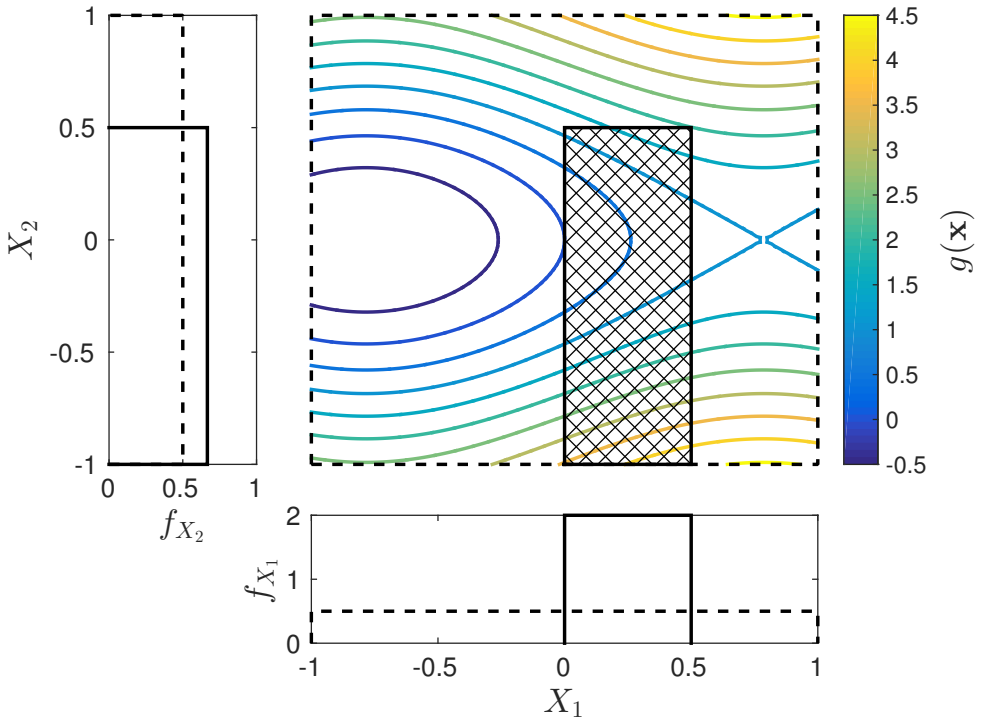

Figure 4-4: *Illustration of the new domain for the updated standard deviation and risk. The dashed lines indicate the original PDFs and bounds of the domain. The hatched area is the new region of interest for computing the new values of the standard deviation and risk.*

This optimization problem is solved using either `MATLAB`'s optimization toolbox or `NLopt`[a].[52] For this problem, we can derive the gradients analytically with respect to the mean and standard deviation of the input parameters – i.e., we need to compute $\partial\sigma_Y/\partial\sigma_i$, $\partial\sigma_Y/\partial\mu_i$, $\partial\mu_Y/\partial\sigma_i$ and $\partial\mu_Y/\partial\mu_i$. The derivation for those gradients is shown in Appendix A. The expression for these quantities is repeated in Equations (4.4) to (4.7).

[a] `NLopt` is a nonlinear optimization library by Steven G. Johnnson, available at `http://ab-initio.mit.edu/wiki/index.php/NLopt`.

$$\frac{\partial \mu_Y}{\partial \mu_i} = \int g\left(\mathbf{x}^+\right) f\left(\mathbf{x}^+\right) \mathrm{d}\mathbf{x}^i - \int g\left(\mathbf{x}^-\right) f\left(\mathbf{x}^-\right) \mathrm{d}\mathbf{x}^i \tag{4.4}$$

$$\frac{\partial \mu_Y}{\partial \sigma_i} = -\frac{\mu_Y}{\sigma_i} + \frac{1}{2\sigma_i}\left[\int g\left(\mathbf{x}^+\right) f\left(\mathbf{x}^+\right) \mathrm{d}\mathbf{x}^i + \int g\left(\mathbf{x}^-\right) f\left(\mathbf{x}^-\right) \mathrm{d}\mathbf{x}^i\right] \tag{4.5}$$

$$\frac{\partial \sigma_Y}{\partial \mu_i} = \frac{1}{2\sqrt{\sigma_Y}}\left[\int \left(g\left(\mathbf{x}^+\right) - g_0\right)^2 f\left(\mathbf{x}^+\right) \mathrm{d}\mathbf{x}^i - \int \left(g\left(\mathbf{x}^-\right) - g_0\right)^2 f\left(\mathbf{x}^-\right) \mathrm{d}\mathbf{x}^i\right] \tag{4.6}$$

$$\begin{aligned}\frac{\partial \sigma_Y}{\partial \sigma_i} = \frac{1}{2\sqrt{\sigma_Y}}\Bigg[-\frac{\sigma_Y}{\sigma_i} + \frac{1}{2\sigma_i}\int \left(g\left(\mathbf{x}^+\right) - g_0\right)^2 f\left(\mathbf{x}^+\right) \mathrm{d}\mathbf{x}^i \ldots \\ + \frac{1}{2\sigma_i}\int \left(g\left(\mathbf{x}^-\right) - g_0\right)^2 f\left(\mathbf{x}^-\right) \mathrm{d}\mathbf{x}^i\Bigg]\end{aligned} \tag{4.7}$$

Thus, if the problem is n-dimensional, we need to evaluate $2n$ different $(n-1)$-dimensional integrals to find the gradient with respect to the mean of every input parameter and then $2n$ different $(n-1)$-dimensional integrals to find the gradient with respect to the standard deviation of every input parameter. In other words, we need the evaluate the mean and standard deviation of the QoI on each face of the n-dimensional hypercube. An example for this procedure with a three dimensional case is shown in Fig. 4-5.

We use either the interior-point method within `MATLAB`'s `fmincon` or the Method of Moving Asymptotes (MMA)[53] within `NLopt`, where the former is more robust but the latter's solution converges better to an optimum. Because the optimizer then could get stuck in a local minimum, we usually run the optimization from different initial conditions and compare those. Note that such a method does not guarantee we find a global minimum.

The uncertainty budgeting methodology presented in this section applies to general models – it requires only the ability to query the model output for specified input values. However, the sampling required to evaluate the QoI standard deviation and risk over many potential input distributions will in general require many model evaluations; that is, solving the optimization problem (4.1) may be expensive. To alleviate the computational cost of these model evaluations, one may use a surrogate model to

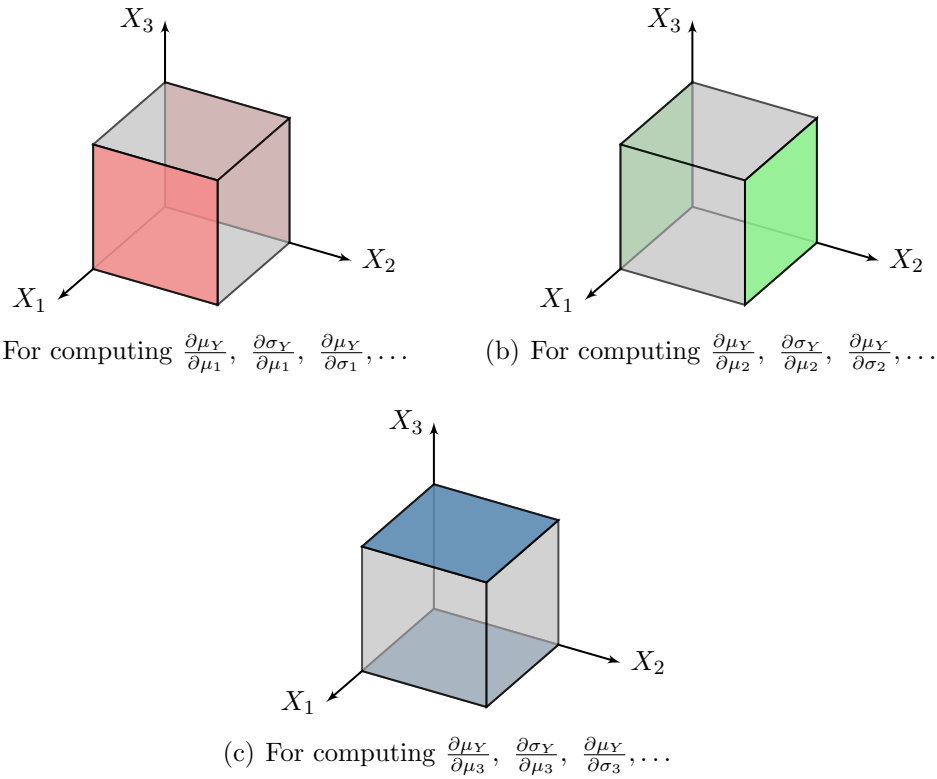

(a) For computing $\frac{\partial \mu_Y}{\partial \mu_1}$, $\frac{\partial \sigma_Y}{\partial \mu_1}$, $\frac{\partial \mu_Y}{\partial \sigma_1}$, ...

(b) For computing $\frac{\partial \mu_Y}{\partial \mu_2}$, $\frac{\partial \sigma_Y}{\partial \mu_2}$, $\frac{\partial \mu_Y}{\partial \sigma_2}$, ...

(c) For computing $\frac{\partial \mu_Y}{\partial \mu_3}$, $\frac{\partial \sigma_Y}{\partial \mu_3}$, $\frac{\partial \mu_Y}{\partial \sigma_3}$, ...

Figure 4-5: *Illustration of how to compute the integrals necessary for the gradient evaluation of a problem with three uniformly distributed input variables. The colored faces indicate on what face we need to solve the integrals for the gradient computation.*

estimate the objective functions and constraints. While any surrogate model could be used, as described in the next section, HDMR and local sensitivity analysis permit derivation of surrogate models that are tailored to the task at hand.

4.3 Surrogate modeling

This section presents a surrogate modeling approach that can be used to reduce the computational expense of solving the uncertainty budgeting optimization problem. Section 4.3.1 describes a surrogate model based on HDMR, used to estimate the updated standard deviation. Section 4.3.2 extends that HDMR framework to achieve higher computational efficiency for higher dimensional problems. Section 4.3.3 describes a local approximation that provides a surrogate risk estimate, these are also used in Section 4.3.4 for the gradient evaluation.

4.3.1 HDMR-based surrogate

For many systems, it is the case that main (single-variable) effects and two-way interactions dominate the input–output relationship. In such cases, third-order and higher-order terms in the HDMR can be neglected without incurring a large error, permitting an accurate surrogate to be derived via truncation of the HDMR.[3,40] This leads to the approximation

$$g(\mathbf{x}) \approx g_0 + \sum_{j=1}^{n} g_i(x_i) + \sum_{1 \le i < j \le n} g_{ij}(x_i, x_j). \tag{4.8}$$

Thus we use the same surrogate model as for the DSA work in Section 3.3. For completeness we go through the procedure here briefly again. Following Ref. 44, one can then build a surrogate model by representing the component functions using expansions of an appropriate set of basis functions:

$$g_i(x_i) \approx \sum_{r=1}^{\ell} \alpha_r^i \varphi_r(x_i), \tag{4.9}$$

$$g_{ij}(x_i, x_j) \approx \sum_{p=1}^{\ell} \sum_{q=1}^{\ell} \beta_{pq}^{ij} \varphi_{pq}(x_i, x_j), \tag{4.10}$$

where g_i is represented by ℓ basis functions $\varphi_1, \ldots, \varphi_\ell$, and α_r^i is the coefficient corresponding to the rth basis function. Similarly, g_{ij} is represented by the basis functions φ_{pq} with corresponding coefficients β_{pq}^{ij}. In this work, we use $\varphi_{pq}(x_i, x_j) = \varphi_p(x_i)\,\varphi_q(x_j)$ and we use the same number of basis functions, ℓ, for all input variables, but this need not be the case. We employ orthonormal polynomials as basis functions, so that the coefficients defining the surrogate model are found as[42]

$$\alpha_r^i = \int g(\mathbf{x})\,\varphi_r(x_i)\,f_{\mathbf{x}}(\mathbf{x})\,\mathrm{d}\mathbf{x} \qquad \forall\, r \quad \in \{1, \ldots, \ell\}, \tag{4.11}$$

$$\beta_{pq}^{ij} = \int g(\mathbf{x})\,\varphi_p(x_i)\,\varphi_q(x_j)\,f_{\mathbf{x}}(\mathbf{x})\,\mathrm{d}\mathbf{x} \quad \forall\, \{p, q\} \in \{1, \ldots, \ell\}. \tag{4.12}$$

To construct the HDMR-based surrogate model requires finding all α_r^i and β_{pq}^{ij} by

evaluating the integrals in Equations (4.11) and (4.12). We evaluate these integrals using Gauss-Legendre quadrature. For a low number of inputs (e.g., less than five) and a relatively smooth response, the behavior of the QoI can typically be characterized over the input space using on the order of tens or hundreds of samples. However, as the number of inputs increases, one would most likely be better off using (quasi) Monte Carlo sampling to resolve the integrals, as in the RS-HDMR method.[44,54] Regardless of the method of integration, the same set of samples can be re-used to find all α_r^i and β_{pq}^{ij}. For instance, if Gauss-Legendre quadrature is used, the function $g(\mathbf{x})$ is evaluated $(N_q)^n$ times, with N_q being the number of quadrature points in each dimension. We then use that set of samples to evaluate each α_r^i and each β_{pq}^{ij}. We choose basis functions that are appropriate for the specified input PDFs; for example, for uniform distributions, we employ shifted Legendre polynomials on the domain $[0, 1]$.

4.3.2 Extension to higher dimensions: cut-HDMR

The surrogate model from Section 4.3.1 works well for problems for a low number of input parameters. For higher dimensions however, the integrals in Equations (4.11) and (4.12) need to be solved on the full domain. This requires building up a full tensor product of Gauss quadrature points to cover the whole multidimensional domain. For example, for a problem with 7 input parameters and using a 5-point quadrature rule, computing the coefficients for our surrogate model requires 78,125 evaluations of our expensive function. The *curse of dimensionality* is therefore a significant problem in that approach.

However, even in the approach of Section 4.3.1 we already make an assumption about the structure of the problem: we discard all higher-order terms in $g(\mathbf{x})$. Those are discarded because it makes for a less complicated surrogate model, but it does not change the number of function calls. Why would we not exploit that from the beginning in order to reduce the number of function calls to build up the surrogate in the first place? That is the approach taken by the *cut-HDMR*. Instead of building up the ANOVA-HDMR directly from $g(\mathbf{x})$ we first build up the cut-HDMR and only then

build up the ANOVA-HDMR, as illustrated in Figure 4-6. The cut-HDMR of $g(\mathbf{x})$ is an expression of that function as a superposition of lines, planes and hyperplanes through the cut center in the domain, denoted as $\mathbf{z}$.[40] The value of this center is often irrelevant if the expansion is taken out until convergence. In this work, we use the centroid of the parameter space as the cut center, because that is expected to work well for uniform distributions.[55]

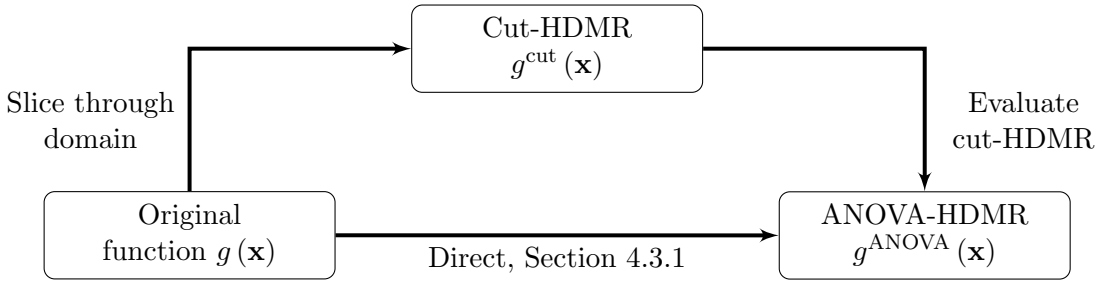

Figure 4-6: *Illustration of direct ANOVA-HDMR approach versus cut-HDMR approach. Figure adapted from Ref. 3.*

The first step in building up the ANOVA-HDMR through the cut-HDMR is to build the component functions for the cut-HDMR. These are given as[40]

$$\begin{aligned} g_0^{\text{cut}} &= g(\mathbf{z}) \\ g_i^{\text{cut}}(x_i) &= g^i(x_i) - g_0^{\text{cut}} \\ g_{ij}^{\text{cut}}(x_i, x_j) &= g^{ij}(x_i, x_j) - g_j^{\text{cut}}(x_j) - g_i^{\text{cut}}(x_i) - g_0^{\text{cut}} \\ &\vdots \\ \rightarrow g(\mathbf{x}) &= g_0^{\text{cut}} + \sum_i g_i^{\text{cut}}(x_i) + \dots \end{aligned} \tag{4.13}$$

where $g^i(x_i)$ is the complete function with all of its input variables, except for x_i set to $\mathbf{z}$, i.e. $g^i(x_i)$ is $g(z_1, \dots, z_{i-1}, x_i, z_{i+1}, \dots, z_n)$. The higher order functions follow the same notation.

In the same way as in Section 4.3.1, we also discard higher order terms in Eq. (4.13) and truncate after order L. That means we can evaluate the complete function $g(\mathbf{x})$ as a summation over component functions of at most L input variables. If we then use the cut-HDMR to find the coefficients for the component functions of the ANOVA-

HDMR using Equations (4.11) and (4.12), we can evaluate those by summing over integrals of at most L dimensions. The total number of function evaluations for N input parameters with an N_q quadrature rule is therefore $\binom{N}{L} N_q$, compared to $(N_q)^N$ for the direct ANOVA-HDMR. That is the reason we use the cut-HDMR approach throughout this work for both building the initial surrogate and for evaluating the standard deviation for changes in the distribution.

4.3.3 Local sensitivity surrogate for risk estimation

For the risk estimation, one can use the HDMR-based surrogate derived in Section 4.3.1; however, performing Monte Carlo sampling for every change in the input distributions may still be expensive, especially if the risk budget is a small probability value (since estimating a low probability to within acceptable error typically requires many more Monte Carlo samples than estimating the standard deviation). In order to obtain the risk of the QoI more efficiently, one can additionally employ local sensitivity estimates for risk as in Ref. 37. Firstly, we evaluate the risk for the baseline input distributions *once* using Monte Carlo sampling on the surrogate model, and we evaluate the surrogate risk estimator $\hat{p}$ defined in (4.3), where note now that the QoI y is estimated using the surrogate model rather than the original model g. We denote this baseline risk estimate by P_0. Local sensitivity estimates then provide an approximation for the change in risk due to a change in the mean of the QoI, $\Delta\mu_Y$, as

$$\Delta P_\mu \approx -\Delta\mu_Y f_Y(r), \tag{4.14}$$

and for the change in risk due to a change in the standard deviation of the QoI, $\Delta\sigma_Y$, as

$$\Delta P_\sigma \approx \frac{\Delta\sigma_Y}{\sigma_Y}(\mu_Y - r) f_Y(r). \tag{4.15}$$

The risk associated with the updated distribution, P', can then be found cheaply using the approximation

$$P' = P_0 - \Delta\mu_Y f_Y(r) + \frac{\Delta\sigma_Y}{\sigma_Y}(\mu_Y - r) f_Y(r). \tag{4.16}$$

This local approximation will become inaccurate for large changes in mean or standard deviation. In particular, for certain combinations of parameters, using Eq. (4.16) can result in negative risk. In that case, we either set the risk to zero or we invoke a full Monte Carlo estimation of the risk.

Using the surrogate models presented in this section introduces errors into the estimation of the standard deviation and risk, and consequently into the solution of the optimization problem. The described surrogate strategies are based on assumptions that have been empirically validated for a wide range of problems in the literature, but for a general model, the magnitude of these modeling errors will be unknown. It is important to note, however, that the surrogate models are used to accelerate the optimization process, but after running the optimization, all solutions of interest are evaluated *a posteriori* using the full model. In this way, we leverage the surrogate models to make the approach computationally tractable (avoiding repeated Monte Carlo simulations inside the optimization loop) and to find potentially interesting areas of the decision space, but we evaluate and investigate potential uncertainty reduction options using our highest fidelity models.

4.3.4 Gradient evaluation using surrogate

Evaluating the gradients of our problem requires us to evaluate Equations (4.4) to (4.7) using the surrogate. If one uses the direct ANOVA-HDMR approach, one can simply evaluate that surrogate on the faces of the hypercube and evaluate the integrals for the gradient using quadrature. For each gradient evaluation with an N_q-point quadrature rule we then need $2N_q^{n-1}$ function evaluations for these exact gradients versus N_q^n for finite differencing, an obvious win.

If the cut-HDMR approach is employed, extra steps are needed. Recall that the idea behind using the cut-HDMR is to reduce all integrals to superpositions of at most L-dimensional integrals. We therefore build up a new cut-HDMR and ANOVA-HDMR on each face of the hypercube, allowing us efficiently evaluate both the integrals for μ_Y and σ_Y using the same ANOVA-HDMR. In that case, one gradient evaluation takes $2\binom{n-1}{L}N_q^L$ for the exact gradients versus $\binom{n}{L}N_q^L$ for finite differencing.

In this case, the exact gradients are cheaper only for lower dimensions and for higher values of L. However, using exact gradients is expected to speed up the optimization, and therefore to result in a lower overall cost. Note that with function evaluations we mean surrogate evaluations, not the expensive blackbox function.

Chapter 5

Uncertainty Budgeting in Aircraft Design

The uncertainty budgeting method of Chapter 4 is applied to several illustrative examples that consider conceptual design of a commercial jetliner. In the rest of this chapter we first define the problem setup in Section 5.1 and perform a global sensitivity analysis together with a distributional sensitivity analysis on that problem in Section 5.2. This highlights the advantages of using distributional sensitivity analysis, but also shows why it is better to perform the full uncertainty budgeting method. That method is used firstly on a smaller-scale problem where we consider the influence of uncertainty in the engine on the aircraft as a whole in Section 5.3. The lower number of inputs in that example makes for better visualization of the results and better explanation of the method. Finally, we apply the method to a problem with multiple disciplines within the aircraft design in Section 5.4 to investigate system-wide trade-offs.

5.1 Problem setup

The example aircraft is sized using the *Transport Aircraft Sizing and OPTimization tool (TASOPT)*. TASOPT comprises low-order physics-based aircraft sizing models with minimal reliance on empirical and historical data, which makes it appropriate to simulate the changes in design QoIs with respect to changes in input variables.[56]

The example problems consider a baseline aircraft based on the Boeing 737-800. We consider a sizing mission with a range of 2950 nautical miles, 180 passengers, and a cruise altitude of 35,000 ft.

We choose all parameters from Ref. 4 to be uncertain as a first pass[a], with the exception of E_{strut}, σ_{strut} and ρ_{strut} because this configuration has no strut. The parameters of all distributions are repeated in Appendix B. To get a sense of how uncertain the aircraft design is with these uncertain inputs, we show the aircraft layout for all values at the minimum of their distribution and at the maximum of their distribution in Fig. 5-2. Furthermore, we show histograms of three QoI's – $MTOW$, $PFEI$ and L/D – in Fig. 5.1(a). $PFEI$ is the fuel energy consumption per payload-range.[57] These results show the aircraft design to be quite uncertain, and therefore justify a design strategy to account for that uncertainty in design decisions.

5.2 GSA and DSA results for all parameters

When there are uncertainties in a design, common practice is to perform a global sensitivity analysis to identify those parameters that contribute most to the uncertainty in the QoI's. The results from such a GSA are outlined in Fig. 5-3 for all uncertain parameters considered before from Ref. 4. These results for instance clearly indicate that for all quantities of interest, T_{metal}, $(T_{t4})_{CR}$, OPR_D, $\sigma_{\text{fus,bend}}$, $\sigma_{\text{wt,cap}}$ and C_L contribute most to the uncertainty of the QoI's.

Using the GSA we have indicated the most critical uncertain parameters in the design. However, if those GSA results are used in a design setting, one quickly runs into trouble. For instance, do we need to reduce the uncertainty completely in all of those parameters, and if not, by how much should the uncertainty in each of the design parameters be reduced? It may in fact not be possible to reduce the uncertainty in the design parameters completely[48] and it may also not make sense to do so in the conceptual design.

[a]Note that we did change the distribution of $\sigma_{\text{wt,cap}}$ from $\mathcal{U}[28500, 31500]$ Psi to $\mathcal{U}[29500, 30500]$ Psi, otherwise the sensitivity index for that parameter for $MTOW$ was $> 80\%$. This was deemed unrealistic.

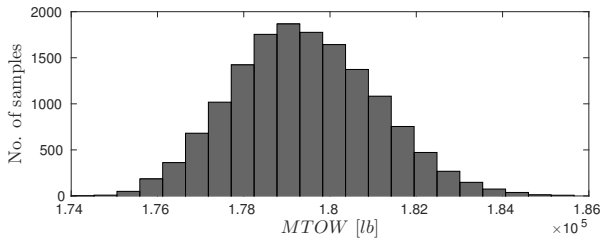

(a) $MTOW$

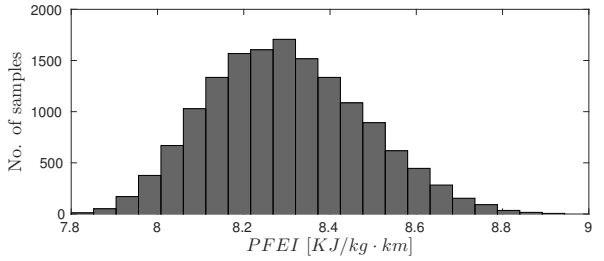

(b) $PFEI$

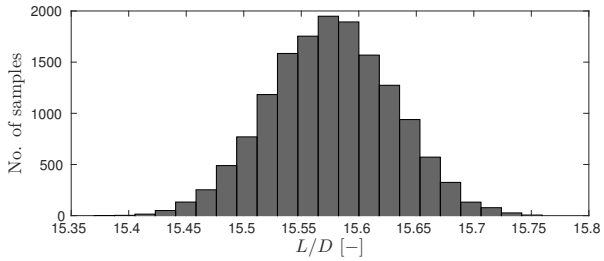

(c) L/D

Figure 5-1: *Histograms for all uncertain parameters using 15,000 Monte Carlo samples.*

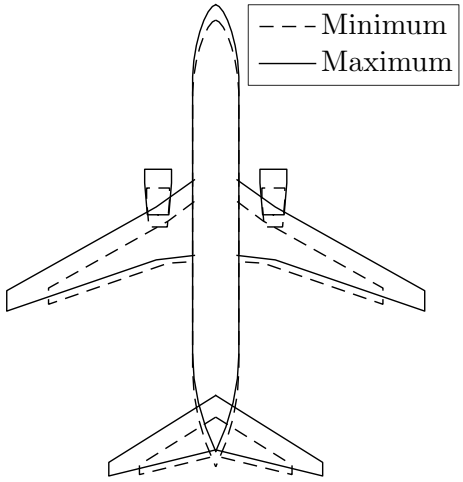

Figure 5-2: *Aircraft layout for uncertain parameters at their maximum (solid) and minimum (dashed) values.*

Distributional sensitivity analysis (DSA) is better suited to answer such questions. As mentioned in previous chapters, in DSA one finds both a more informative sensitivity index which accounts for the fact that not all uncertainty may be reduced, and a variance-based sensitivity index function which informs the designer on the influence of a partial uncertainty reduction in an input parameter on a QoI. The average main effect sensitivity indices from DSA are shown in Fig. 5-4, while the variance-based sensitivity index functions are shown only for the most important input parameters in Fig. 5-5.

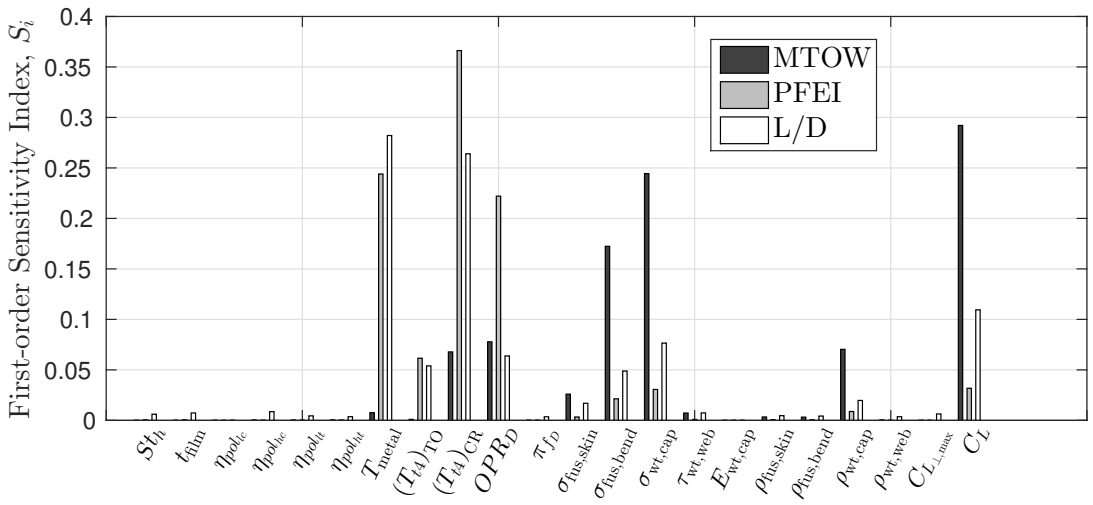

Figure 5-3: *Sensitivity indices of all uncertain design input parameters according to the distributions for the Boeing 737-800 in Ref. 4.*

We see that the ranking between GSA and DSA – shown in Figures 5-3 and 5-4, respectively – does not change for the most important input parameters, which is due to the fact that the variance-based sensitivity index functions in Fig. 5-5 are almost linear. However, rather than obtaining just the ranking in the input parameters, we are now able to quantify how much the uncertainty in each design variable should reduce in order for the uncertainty in the QoI's to reduce using those variance-based sensitivity index functions. Combined with cost models for changes in the input distributions and requirements on risk, uncertainty and cost, we are then able to find new input distributions which meet those requirements, using these variance-based sensitivity index functions. This is the approach taken in Ref. 37.

There are however two main issues when we apply this approach to a complex engineering problem. Firstly, we have only used first-order sensitivity indices in constructing the variance-based sensitivity index functions. In cases where the problem has a significant problem term – as we will see in Section 5.3 – this approach would not capture that; in fact if all uncertainty in the input parameters would be reduced, the QoI uncertainty would incorrectly be nonzero. Secondly, the variance-based sensitivity index functions lump any contribution from the mean of the input parameters into one single function by sampling over reasonable distributions. While that is use-

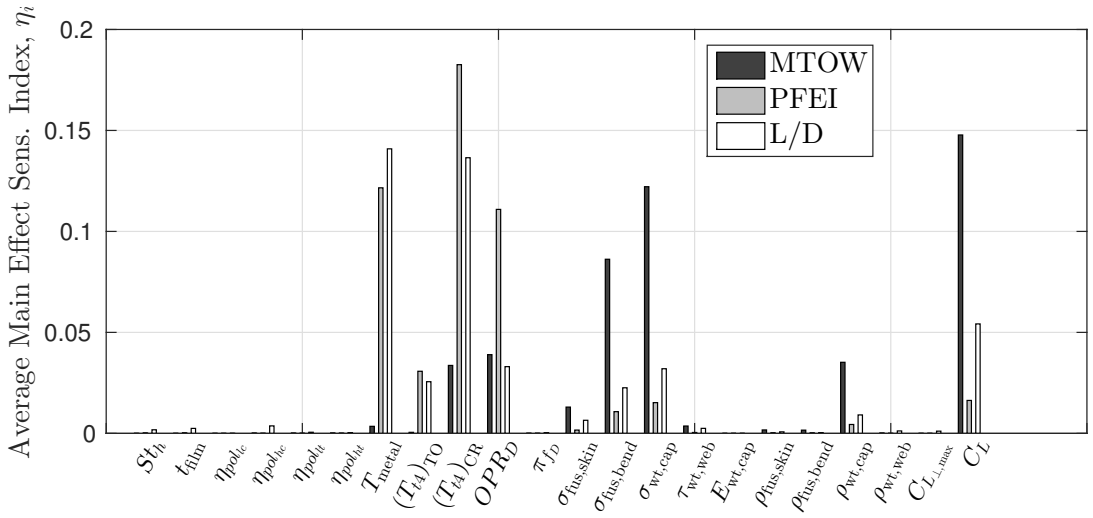

Figure 5-4: *Average main effect sensitivity indices from DSA of all uncertain design input parameters according to the distributions for the Boeing 737-800 in Ref. 4.*

ful to obtain a meaningful ranking, in trying to find new input distributions we need to keep that (potentially nonlinear) coupling between mean and standard deviation. For these reasons, for our problem the uncertainty budgeting method from Chapter 4 is more suitable. DSA is however still useful by providing a better initial ranking for the input parameters, and for sensitivity analysis in general.

5.3 Engine uncertainty with two uncertain inputs

The first illustrative example of the full uncertainty budgeting method considers the effects of uncertainty in engine technologies on early conceptual aircraft design decisions. The aircraft Maximum Take-off Weight ($MTOW$) is used as the QoI y; this is a quantity that represents many aspects of the overall vehicle design. The uncertainties in propulsion technology are represented by taking the uncertain input variables to be $\mathbf{x} = [T_{\text{metal}}, (T_{t4})_{\text{CR}}]^\top$, where T_{metal} is the maximum allowable temperature of the metal in the turbine blades, and $(T_{t4})_{\text{CR}}$ is the total temperature at the inlet of the turbine at cruise conditions. $(T_{t4})_{\text{CR}}$ is directly related to the thermal efficiency of the engine and is at the same time restricted by T_{metal}. Therefore, it is expected that uncertainty in these two variables will have a large influence on the fuel efficiency and thereby the maximum takeoff weight of the aircraft. It is also expected that there is

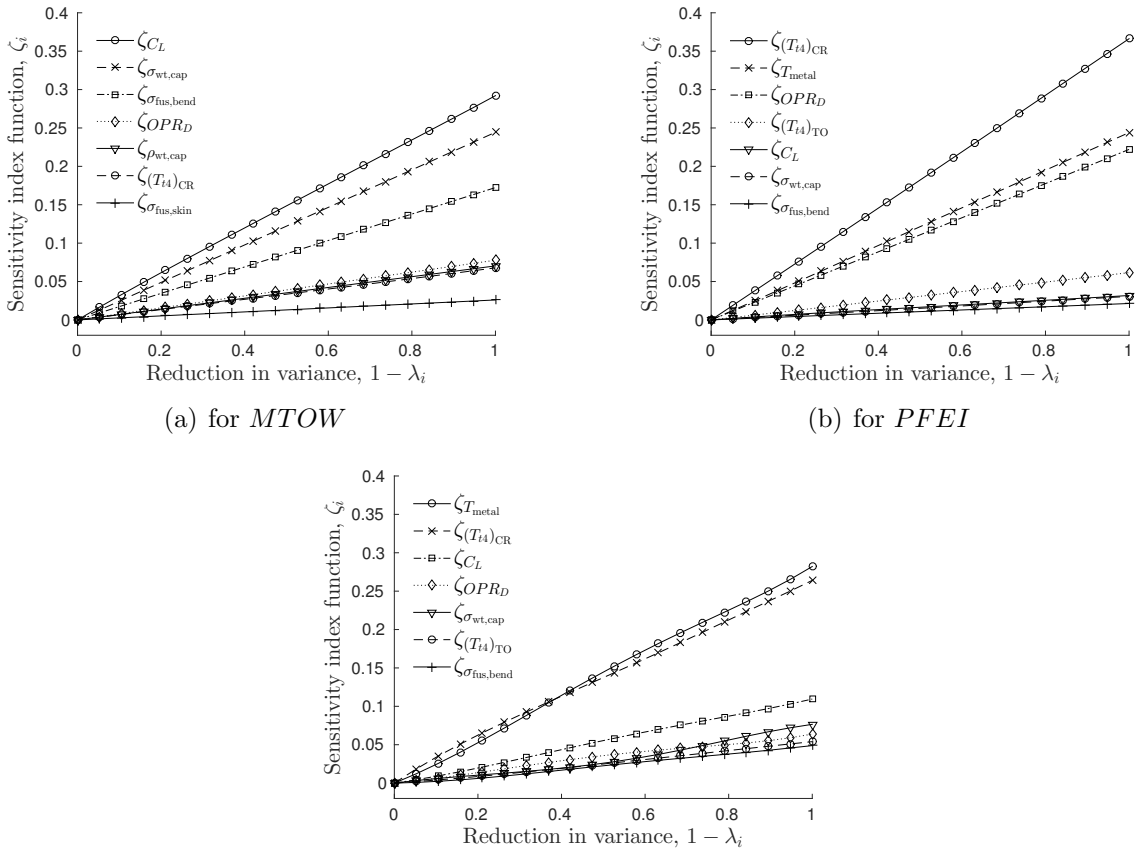

(a) for $MTOW$

(b) for $PFEI$

(c) for L/D

Figure 5-5: *Variance-based sensitivity index functions for the seven most important input parameters for the Boeing 737-800.*

an interaction between the two variables.

The corresponding distributions for T_{metal} and $(T_{t4})_{\text{CR}}$ are estimated using a combination of information from Federal Aviation Administration (FAA) databases and expert elicitation from FAA consultants.[4] T_{metal} and $(T_{t4})_{\text{CR}}$ are modeled as uniform random variables such that $T_{\text{metal}} \sim U[1172, 1272]$ K and $(T_{t4})_{\text{CR}} \sim U[1541.5, 1641.5]$ K. The initial mean value of T_{metal} is therefore 1222 K with a standard deviation of 28.87 K, and the initial mean of $(T_{t4})_{\text{CR}}$ is 1591.5 K with a standard deviation of 28.87 K. With two input variables with uniform distributions, there are in total four degrees of freedom in changing the distributions of the input variables, since both the mean and standard deviation of each parameter can be altered.

Budgets are set on risk, standard deviation and cost. The risk budget is set such

that the probability of $MTOW$ exceeding 1.802×10^5 lb is at most 4%, while the standard deviation of $MTOW$ is required to be at most 450 lb. The cost of changing the distributions of the input variables must remain below 18 cost units. Thus, the budget constraints are written as

$$\mathbb{P}(MTOW > 1.802 \cdot 10^5 \ lb) \leq 4\% = P_b, \quad \sigma_Y \leq 450 \ lb = \sigma_b, \quad C \leq 18 = C_b. \quad (5.1)$$

The notional cost model for T_{metal} and $(T_{t4})_{\text{CR}}$ is shown in Figure 5-6. Note that the x-axis has been normalized by their maximum allowable changes due to the different scales of the two input variables. The cost model for changes in mean is asymmetric, because it requires more effort to increase the mean temperature, thus it is more expensive. For T_{metal}, an increase in mean value would, for instance, require using a new material for the turbine, which would be a major design overhaul and might even require developing a new alloy with better thermal properties.

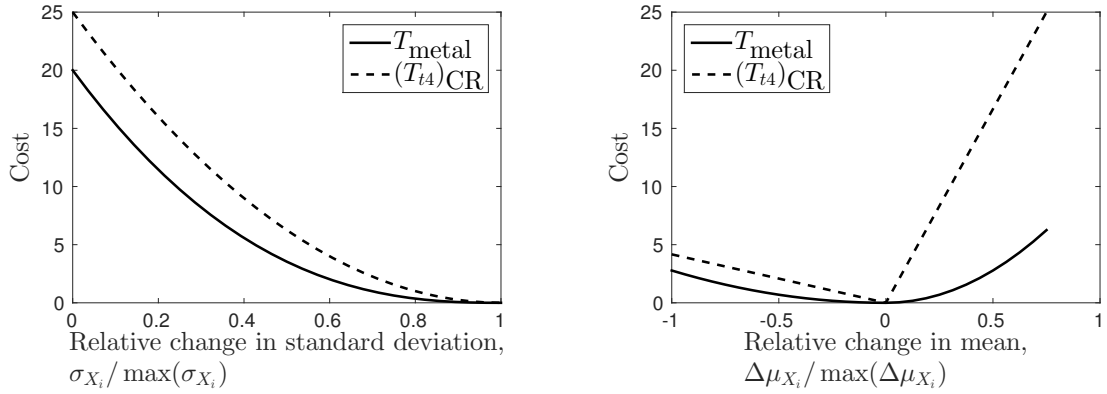

(a) for changes in the input standard deviation

(b) for changes in the input mean

Figure 5-6: *Notional cost model for T_{metal} and $(T_{t4})_{\text{CR}}$.*

5.3.1 Surrogate and sensitivity analysis

We construct an HDMR-based surrogate model using the method described in Chapter 4. This requires estimating the coefficients α_r^i and β_{pq}^{ij} by evaluating the integrals in Equations (4.11) and (4.12). Since the inputs T_{metal} and $(T_{t4})_{\text{CR}}$ are modeled using

uniform distributions, we employ shifted Legendre polynomials for the basis functions. The first three shifted Legendre polynomials are

$$\begin{aligned}
\varphi_1(\xi) &= \sqrt{3}(2\xi - 1), \\
\varphi_2(\xi) &= 6\sqrt{5}\left(\xi^2 - \xi + \frac{1}{6}\right), \\
\varphi_3(\xi) &= 20\sqrt{7}\left(\xi^3 - \frac{3}{2}\xi^2 + \frac{3}{5}\xi - \frac{1}{20}\right),
\end{aligned} \tag{5.2}$$

with $0 \leq \xi \leq 1$. Furthermore, because the number of inputs is low, the integrals in Equations (4.11) and (4.12) are solved efficiently using Gauss-Legendre quadrature, requiring a minimum number of TASOPT runs. In this case, only 49 TASOPT runs are required to build the surrogate model.

For purposes of illustration, we assess the convergence of the root mean squared error between the surrogate QoI estimate and the TASOPT QoI estimate for different numbers of quadrature points and orders of basis functions. We use the error definition from Sobol',[25] defined as

$$\begin{aligned}
\delta(g, \tilde{g}) &= \frac{1}{V}\int [g(\mathbf{x}) - \tilde{g}(\mathbf{x})]\,\mathrm{d}\mathbf{x} \\
\text{with } V &= \int [g(\mathbf{x}) - g_0]^2\,\mathrm{d}\mathbf{x}.
\end{aligned} \tag{5.3}$$

Here g is the actual function mapping input to QoI (here the TASOPT simulation), $\tilde{g}$ is the truncated ANOVA-HDMR surrogate model, and V is the variance associated with the actual QoI.

Figure 5-7 shows the convergence of the error $\delta(g, \tilde{g})$, where we solve the integral in Eq. (5.3) using quasi Monte Carlo sampling with 5000 samples. For this problem, a choice of $N_q = 7$ quadrature points in each dimension and fifth-order basis functions leads to a surrogate model with acceptably low error (below 10^{-5}). As mentioned above, this surrogate is constructed with just 49 TASOPT evaluations. To further illustrate the accuracy of the surrogate model, TASOPT is evaluated at 225 points in the interior in order to compare estimates of MTOW over the design space. Figure 5-8 shows the resulting contours of $MTOW$ estimated by TASOPT and by the surrogate

model.

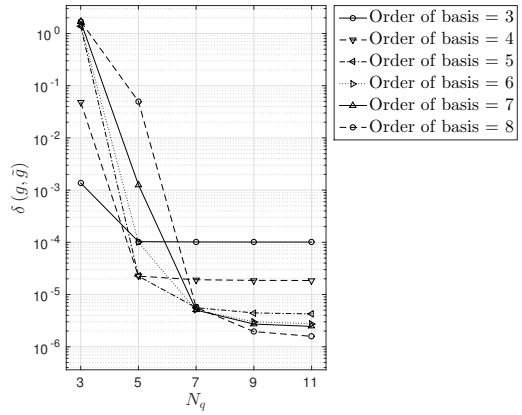

Figure 5-7: *Convergence of $\delta(g, \tilde{g})$ for different numbers of quadrature points and different orders of basis functions.*

Figure 5-9 shows the GSA results using the HDMR-based surrogate model. The results show that T_{metal} accounts for an expected 10% of the $MTOW$ variance, while $(T_{t4})_{\text{CR}}$ is responsible for 75%. $(T_{t4})_{\text{CR}}$ is directly related to the fuel efficiency of the engine; it is therefore expected that it contributes a larger portion of the uncertainty in the maximum take-off weight. Lastly, in line with expectations, a considerable interaction term between the two variables accounts for the remaining 15% of the variance in $MTOW$. Both input parameters have considerable influence on the uncertainty in the QoI and therefore both are included in the resource allocation optimization.

5.3.2 Design space visualization

Visualization of the design space can provide the designer with useful insight into the effects on QoI uncertainty and cost of changing the input distribution parameters. We explore the design space via a series of two-dimensional plots, as shown in the pairwise contour plot for risk in Figure 5.10(a) and for standard deviation in Figure 5.10(b). These slices are generated by evaluating the risk, cost, and standard deviation of the QoI in the same way as in Figure 4-3, only now for a specified $\boldsymbol{\mu}$ and $\boldsymbol{\sigma}$. We vary $\boldsymbol{\mu}$ and $\boldsymbol{\sigma}$ to generate a contour plot. We slice through the design space by varying two design parameters (e.g., the mean and standard deviation of one particular input

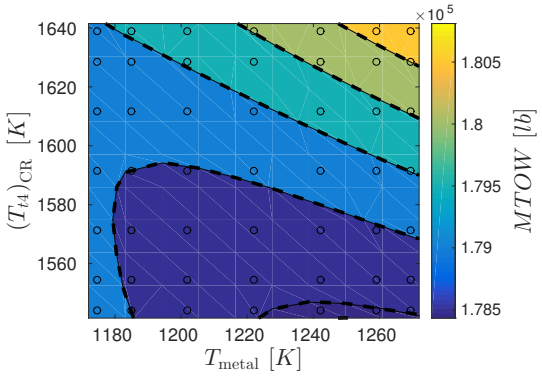

Figure 5-8: *MTOW estimated by surrogate model (solid lines) compared to TASOPT (dashed lines). The circles indicate the quadrature points used to create the surrogate model.*

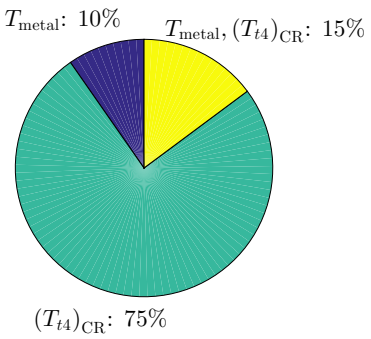

Figure 5-9: *Global sensitivity analysis results from the HDMR-based surrogate model.*

variable) and fixing the other design parameters at the mean value of their respective nominal distributions.

The general shape of these contours is consistent with expectations based on knowledge of the design problem: as the input standard deviation is reduced, the risk is reduced because the output distribution is more concentrated around the mean. However, the plots also show a large area where the risk is zero; therefore, it is expected that there are multiple ways to achieve a minimum-risk solution. Furthermore, Figure 5.10(b) shows that, for this problem, a reduction in input standard deviation has a larger effect on the QoI standard deviation than a shift in input mean.

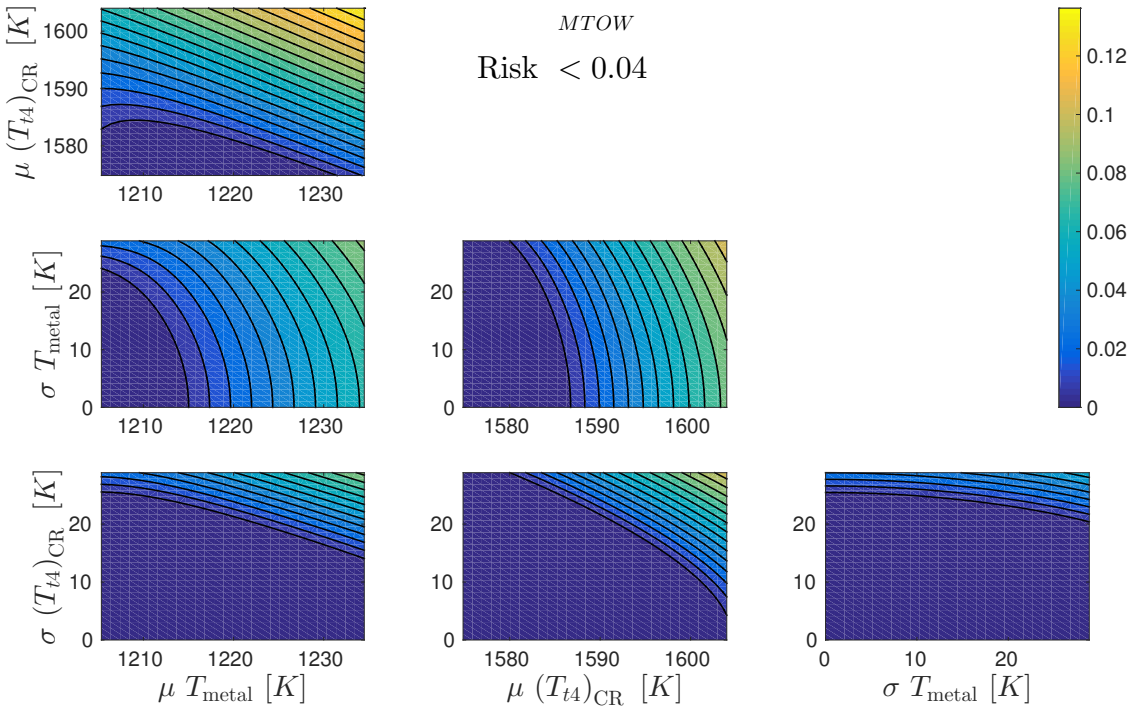

(a) Risk

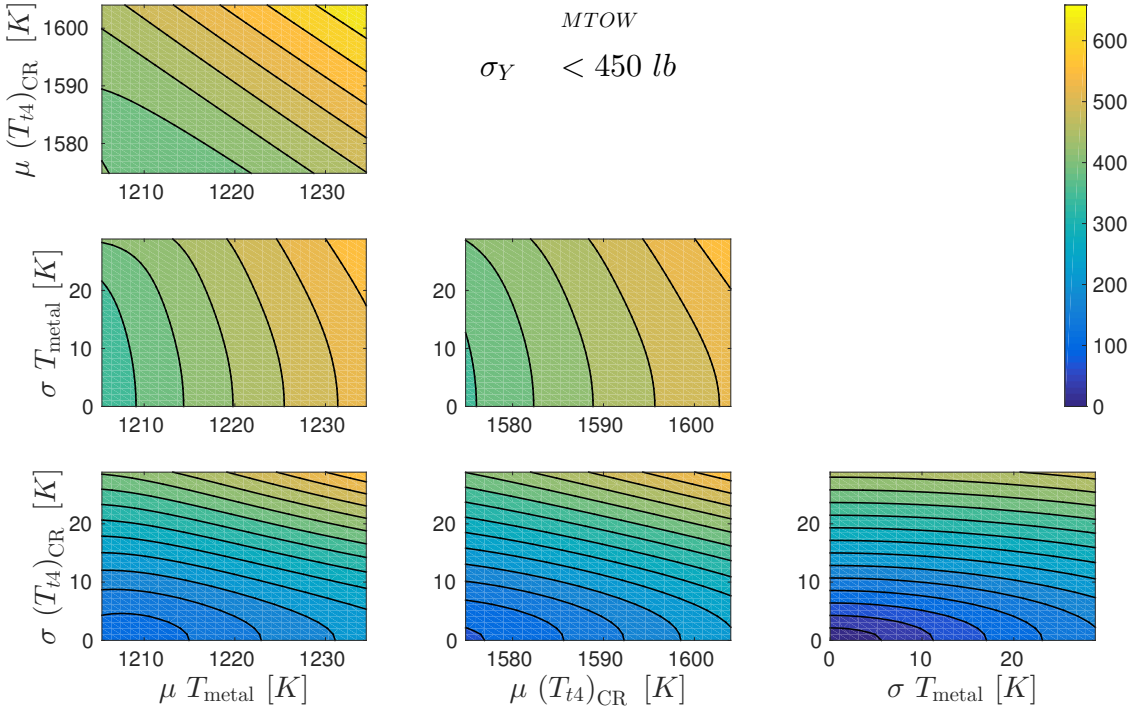

(b) Standard deviation (lb)

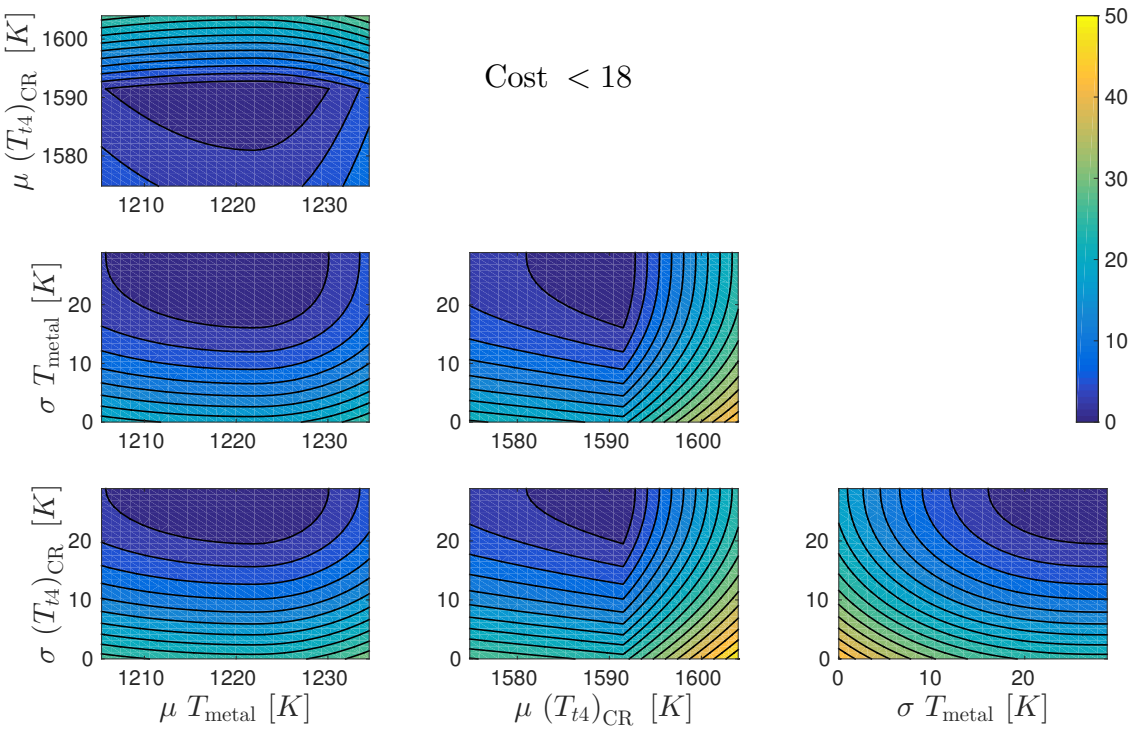

(c) Cost

Figure 5-10: *Pairwise contour plot of QoI risk, QoI standard deviation, and cost as a function of changes in input means and input standard deviations.*

Applying the budget constraints to the estimated surfaces of risk, standard deviation and cost defines a feasible region with respect to each budget constraint. Overlaying the results allows for visualizing the feasible design space, i.e., the range of input distribution changes for which all budget constraints are met. This is shown in Figure 5-11, where the darkest area indicates the feasible region. Other shaded areas correspond to region where only one or two of the three budget constraints are met. For this problem, it can be seen that the feasible region is mostly constrained by the cost and standard deviation budgets. This is consistent with the previous result that showed a large area of low-risk solutions.

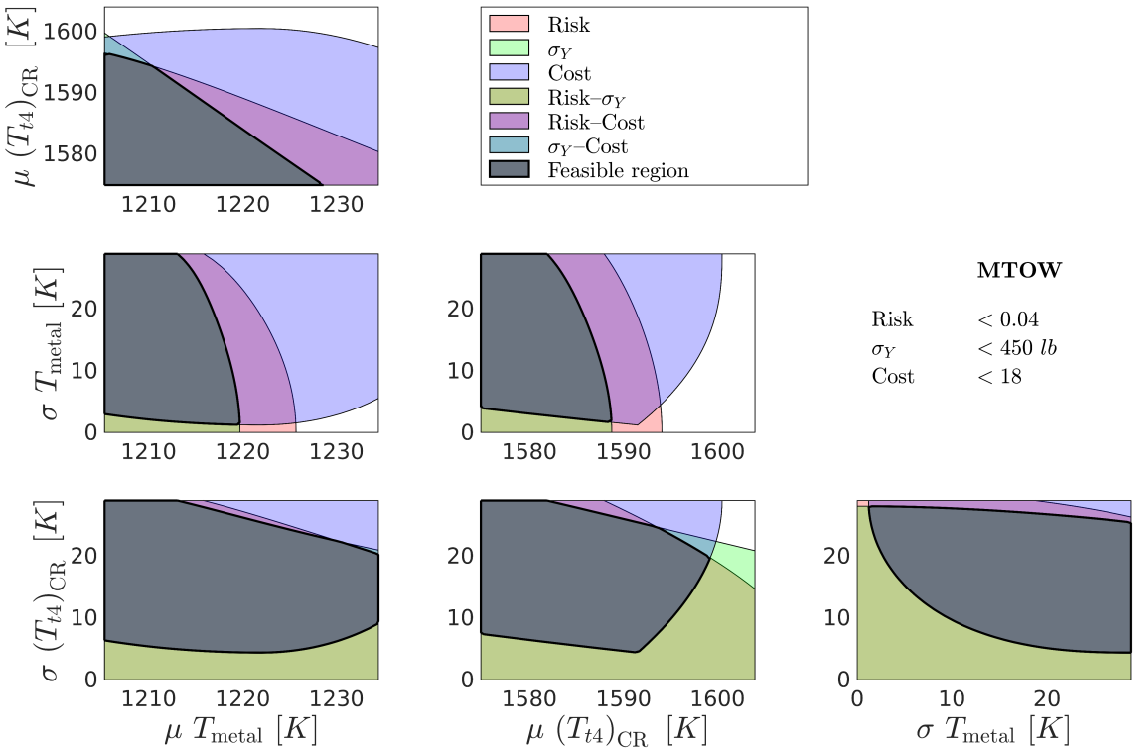

Figure 5-11: *Feasible area in the design space, satisfying risk, standard deviation and cost budgets. Also shown are the areas that satisfy one or two of the three budgets.*

5.3.3 Resource allocation optimization

The initial uncertainty distributions on T_{metal} and $(T_{t4})_{\mathrm{CR}}$ lead to the distribution of *MTOW* shown in Figure 5-12. The corresponding initial estimate of standard deviation is $\sigma_Y = 503.13$ lb and of risk is $\hat{p} = 5.49\%$. Both the standard deviation and the risk exceed the specified uncertainty budgets. We now solve the optimization problem (4.1) to determine redesign options that will reduce uncertainty to below the specified levels, while also satisfying the allowable cost budget.

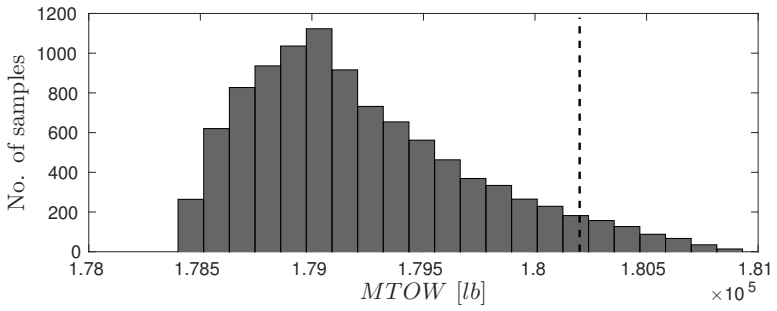

Figure 5-12: *Histogram of MTOW using 10,000 quasi Monte Carlo samples (dashed line indicates the not-exceed-value for risk).*

Figure 5-13 shows optimal solutions for four different objectives, for instance for minimum standard deviation ($\alpha = \gamma = 0,\ \beta = 1$), and equal weighting among risk, standard deviation and cost ($\alpha = \beta = \gamma = 1$). The radar plots indicate the relative changes in mean values and standard deviations from the baseline initial values for each design variable. We also consider multiple local optima as shown in Figure 5.13(a). For risk this is expected because as we saw in Figure 5.10(a), for a large part of the design space the risk is zero. It is therefore expected that there are multiple designs that yield a zero-valued objective function. The two designs shown in Figure 5.13(a) indicate one solution prefers less changes in the solution than the other. One of those designs is also the minimum-standard-deviation solution, because that one also has zero risk.

Figure 5.13(b) indicates that relatively large changes to the original input distributions are required to achieve the minimum-standard-deviation solution. This solution is achieved by a 32% standard deviation reduction for T_{metal} while shifting its mean to 1210 K, and a standard deviation reduction of 74% for $(T_{t4})_{\text{CR}}$ while shifting its mean to 1584 K. This results in 0% risk, a QoI standard deviation of 109 lb, and an associated cost of 18 cost units. In this case, the active cost constraint is preventing further reductions in QoI standard deviation. In this solution, the required standard deviation reduction for $(T_{t4})_{\text{CR}}$ is larger than for T_{metal}, which is consistent with the GSA results in Figure 5-9, although the cost models play an important role in determining the optimal uncertainty reduction balance across inputs.

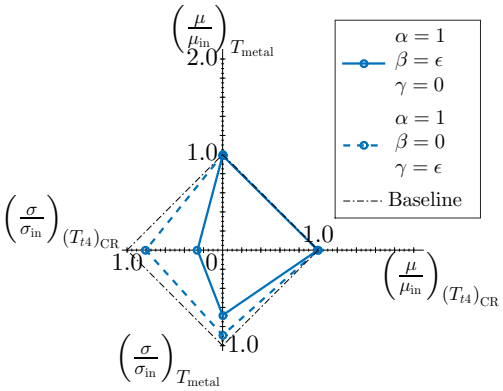

(a) Minimum risk ($\alpha = 1,\ \beta = \gamma = 0$)

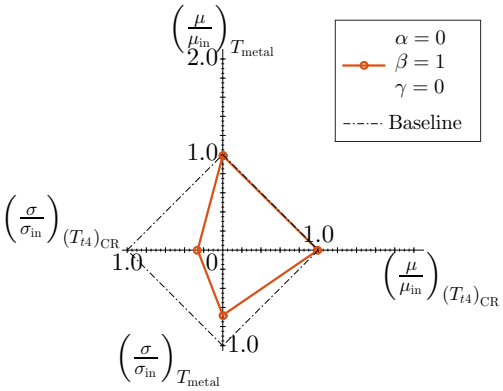

(b) Minimum output standard deviation ($\alpha = \gamma = 0,\ \beta = 1$)

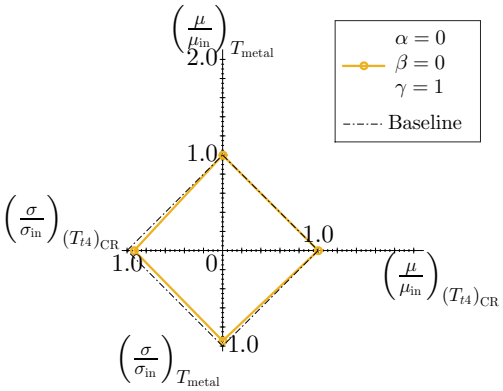

(c) Minimum cost ($\alpha = \beta = 0,\ \gamma = 1$)

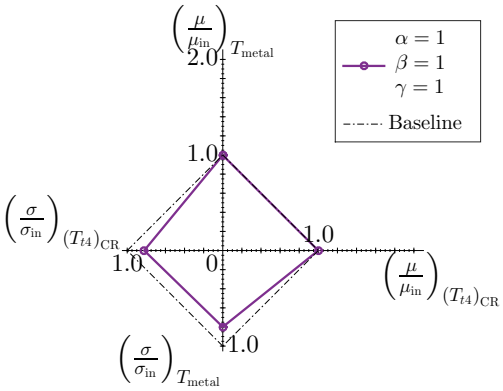

(d) Equally important ($\alpha = \beta = \gamma = 1$)

Figure 5-13: *Optimum resource allocation strategy for four different objective functions. Scales:* $0\ K < \mu_{T_{\text{metal}}} < 2444\ K$, $0\ K < \mu_{(T_{t4})_{\text{CR}}} < 3183\ K$, $0 < \sigma_{T_{\text{metal}}} < 28.87\ K$, $0 < \sigma_{(T_{t4})_{\text{CR}}} < 28.87\ K$.

The optimal solution for equal weighting among risk, standard deviation, and cost (Figure 5.13(d)) shows less dramatic changes in the input distributions than the solution for minimum standard deviation. For this problem, this result is due to cost now playing a role in the objective function. We can see, for instance, that the mean of $(T_{t4})_{\text{CR}}$ is barely changed, because it is expensive to do so (see Figure 5-6). The equally-weighted optimal solution is achieved by a standard deviation reduction of 15% for T_{metal} with its mean shifting to 1212 K, and a standard deviation reduction of 32% for $(T_{t4})_{\text{CR}}$ with its mean unaltered. These changes result in 0% risk, a QoI standard deviation of 306 lb, and an associated cost of 3.6 cost units.

Instead of looking at an individual optimization result for a single combination of

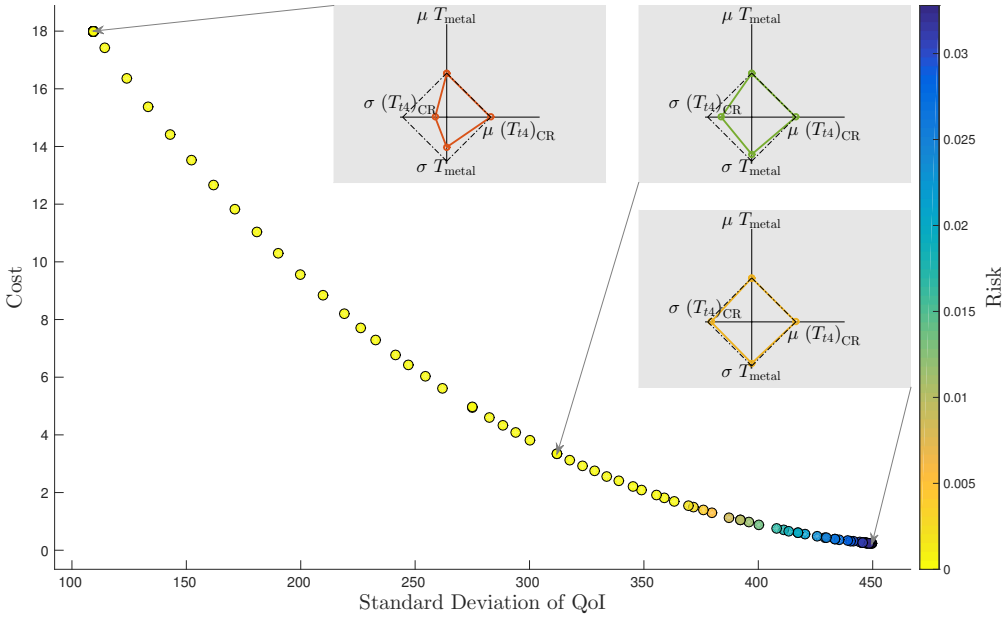

Figure 5-14: *Pareto front projected onto the cost – standard deviation plane of MTOW.*

α, β and γ, a Pareto front gives the designer more insight into the tradespace of uncertainty reduction options. We generate a Pareto front by running the optimization for different values of α, β and γ. In Figure 5-14, the Pareto front is projected onto the cost–standard deviation plane for *MTOW*, with the radar plots depicting the corresponding solution values for the optimization variables for three different points. The minimum-cost solution is that for which there are almost no changes in the input distribution and for which the requirements are just barely met (i.e., the standard deviation is exactly 450 lb and the risk is close to 4%). This minimum-cost solution requires only a small standard deviation reduction in T_{metal} of 6% while shifting its mean to 1219.4 K, and a standard deviation reduction in $(T_{t4})_{\text{CR}}$ of 7% with no change in its mean. These updated input distributions then result in a QoI standard deviation of 450 lb with a risk of 3.3% and an associated cost of 0.23 cost units. In contrast, the minimum-standard-deviation solution requires considerable changes in the input distribution and just barely meets the cost budget, as already explained and shown in Figure 5.13(b).

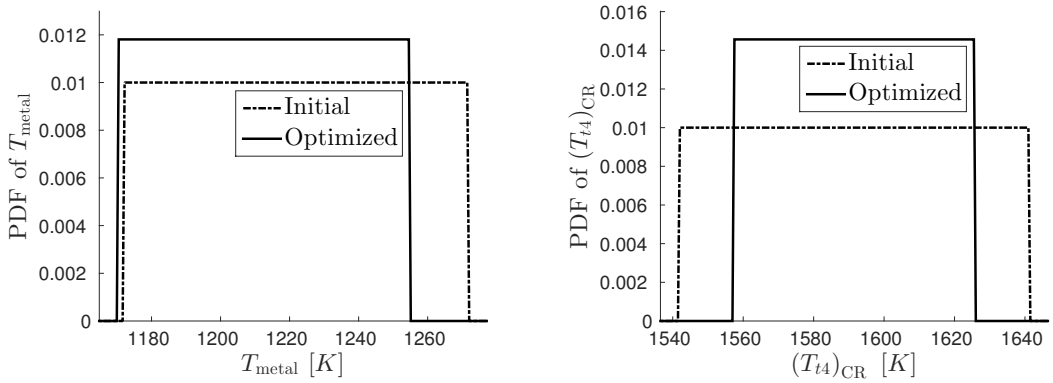

(a) T_{metal} (b) $(T_{t4})_{\text{CR}}$

Figure 5-15: *Initial PDFs for input variables T_{metal} and $(T_{t4})_{\text{CR}}$ compared to updated PDFs for the equally-weighted optimal solution ($\alpha = \beta = \gamma = 1$).*

Lastly, we plot the changes in distributions for some of the optimal solutions. Figure 5-15 shows the initial and updated input distributions that correspond to the equally-weighted optimized solution. Figure 5-16 compares the initial QoI PDF and the QoI PDF resulting from the optimal uncertainty reduction choices, for optimal input parameter distributions from Fig. 5-13. For the purposes of illustration, the QoI PDFs are estimated using kernel density estimation with 15,000 samples drawn from the surrogate. Figure 5-16 shows that the new risk is obviously zero for the minimum-risk solution. Similarly, the probability density function of the MTOW is very narrow for the minimum-standard-deviation solution, as expected. Figure 5-16 shows that the change in QoI distribution for the minimum-cost solution is small, but leads to a sufficient reduction in risk to satisfy the budget constraints. For the equally-weighted solution, the change is more significant; the standard deviation is considerably smaller and the risk approaches zero.

5.3.4 Assessment of optimization results

A final step in the methodology is to evaluate the most interesting (according to designer preferences) results from the optimization, using the original model in place of the surrogate. In our case, this assessment is performed by evaluating the uncertainty in TASOPT estimates of $MTOW$, using the updated distributions for T_{metal} and

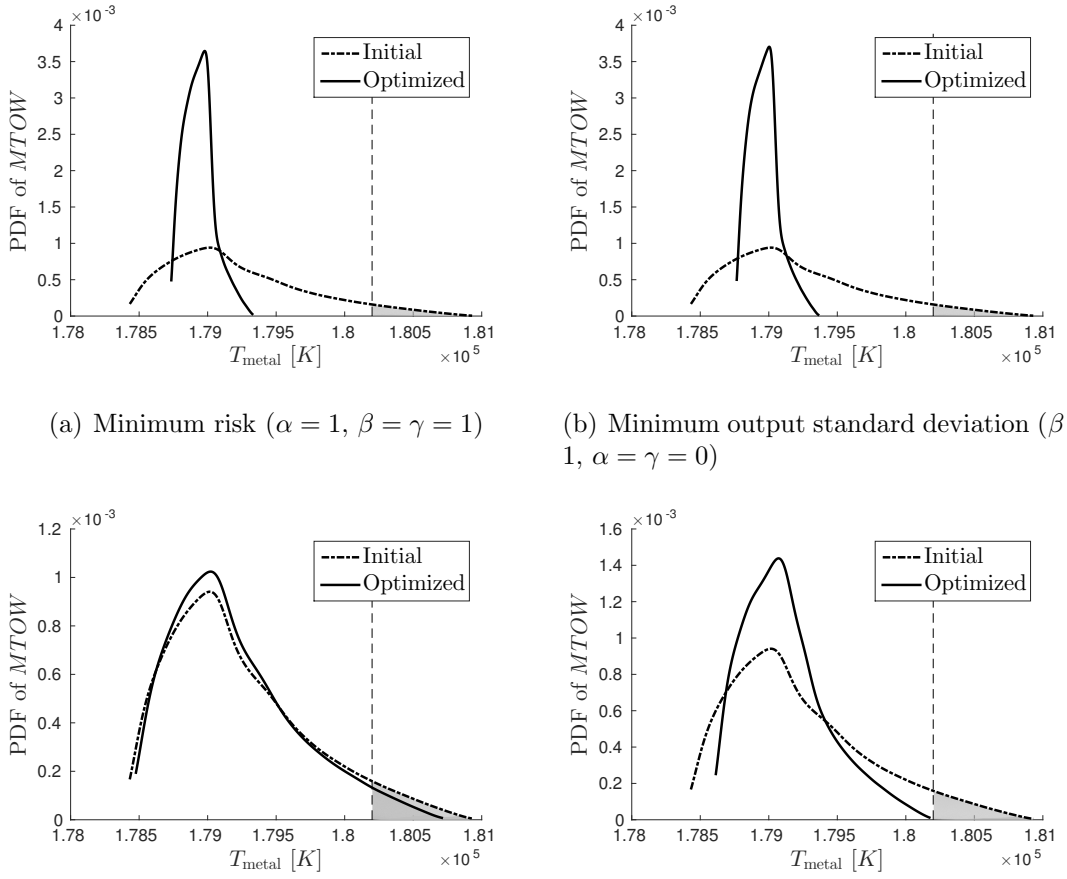

(a) Minimum risk ($\alpha = 1$, $\beta = \gamma = 1$)

(b) Minimum output standard deviation ($\beta = 1$, $\alpha = \gamma = 0$)

(c) Minimum cost ($\alpha = \beta = 0$, $\gamma = 1$)

(d) Equally important ($\alpha = \beta = \gamma = 1$)

Figure 5-16: *Initial MTOW QoI PDF compared to updated PDF for two different optimal solutions.*

$(T_{t4})_{\text{CR}}$. As an illustration, we execute this process for four different objectives: minimum risk, minimum standard deviation, minimum cost, and equal cost/risk/standard deviation weighting. In each case, we evaluate TASOPT at 15,000 input samples using quasi Monte Carlo sampling, and estimate the variance and risk of the *MTOW* QoI. Table 5-1 compares the results to those estimated using the surrogate model. The relative errors are all small (less than 2%), indicating that the surrogate modeling approach introduces little error. The error in the risk estimate is larger than that in the standard deviation estimate, due to the additional linearization approximation.

Table 5-1: *Risk and standard deviation estimates of optimal strategies; TASOPT estimates compared to surrogate model estimates.*

	Surrogate		TASOPT		Relative error	
Objective	Risk	σ_Y [lb]	Risk	σ_Y [lb]	Risk	σ_Y
Minimum Risk	0	109.477	0	109.522	0%	0.04%
Minimum σ_Y	0	109.435	0	109.459	0%	0.02%
Minimum Cost	0.0327	449.575	0.0332	449.708	1.57%	0.03%
Equally important	0	305.691	0	305.559	0%	0.04%

5.4 System-wide uncertainty

Now instead of looking only at two uncertain parameters confined to one particular discipline of the aircraft design, we look at more uncertain parameters in different disciplines throughout the aircraft. In order to choose which parameters are most interesting to look at, we first perform a global sensitivity analysis (GSA), following the approach outlined in Fig. 4-1. The results from the full GSA are shown in Fig. 5-3 for $MTOW$, $PFEI$ and L/D. We see that for all quantities of interest, T_{metal}, $(T_{t4})_{CR}$, OPR_D, $\sigma_{\text{fus,bend}}$, $\sigma_{\text{wt,cap}}$ and C_L contribute most to the uncertainty of the QoI's. Therefore, we only include these parameters in this system-wide optimization. Furthermore, the variation in L/D is rather small and its effects cascade through the design and show itself in $PFEI$. Therefore we place no requirements on or optimize for L/D and do not include this QoI in the resource allocation optimization.

The GSA results in Fig. 5-17 are obtained using $N_q = 7$ quadrature points in each dimension and fifth-order basis functions. This yields an acceptable error with only 735 TASOPT function evaluations. The sensitivity analysis results show that every parameter is important for either $MTOW$ or $PFEI$, but also that there are no significant interaction terms – the first-order sensitivity indices in Fig. 5-17 all add up to 1.

We now use the surrogate that we obtained as part of the GSA also in our resource allocation optimization. For that optimization, we place similar budgets on the design

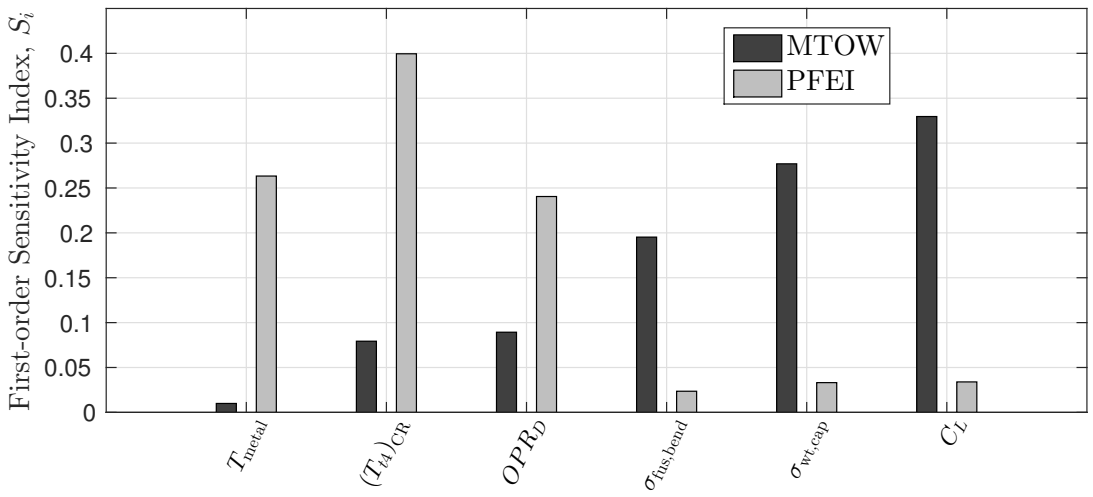

Figure 5-17: *Sensitivity indices of the chosen six uncertain design input parameters according to the distributions in Ref. 4.*

as in Section 5.3:

$$\mathbb{P}(MTOW > 1.810 \cdot 10^5\ lb) \leq 5\% = P_{b_1}, \quad \sigma_{Y_1} \leq 600\ lb = \sigma_{Y,b_1}, \quad C \leq 25 = C_b$$
$$\mathbb{P}(PFEI > 8.47\ KJ/kg \cdot km) \leq 4\% = P_{b_2}, \quad \sigma_{Y_2} \leq 0.16\ KJ/kg \cdot km = \sigma_{Y,b_2}.$$

However, we relax the budgets slightly because there is more uncertainty in the initial design and we place more constraints on the design. We again use a notional cost model for the parameters, as shown in Fig. 5-18. We retain the assumption that in general it is more difficult to increase the mean of a parameter than it is to reduce the mean.

We now consider multiple QoI's and therefore reformulate Eq. (4.1) into

$$\begin{aligned}
\underset{\boldsymbol{\mu},\boldsymbol{\sigma}}{\text{minimize}} \quad \mathcal{F}(\boldsymbol{\mu},\boldsymbol{\sigma}) &= \textstyle\sum_j \alpha_j \dfrac{P(\boldsymbol{\mu},\boldsymbol{\sigma})}{P_{b_j}} + \sum_j \beta_j \dfrac{\sigma_{Y_j}(\boldsymbol{\mu},\boldsymbol{\sigma})}{\sigma_{Y,b_j}} \\
&\quad + \gamma \dfrac{C(\boldsymbol{\mu},\boldsymbol{\sigma})}{C_b} + \textstyle\sum_j \theta_j \dfrac{\mu_j(\boldsymbol{\mu},\boldsymbol{\sigma})}{\mu_{\text{org}_j}} \\
\text{subject to} \quad \mathcal{G}_{P_j}(\boldsymbol{\mu},\boldsymbol{\sigma}) &= P_j(\boldsymbol{\mu},\boldsymbol{\sigma}) - P_{b_j} \leq 0 \\
\mathcal{G}_{\sigma_j}(\boldsymbol{\mu},\boldsymbol{\sigma}) &= \sigma_{Y_j}(\boldsymbol{\mu},\boldsymbol{\sigma}) - \sigma_{Y,b_j} \leq 0 \\
\mathcal{G}_C(\boldsymbol{\mu},\boldsymbol{\sigma}) &= C(\boldsymbol{\mu},\boldsymbol{\sigma}) - C_b \leq 0
\end{aligned} \tag{5.4}$$

while at the same time adding the expected value of the QoI to the objective function.

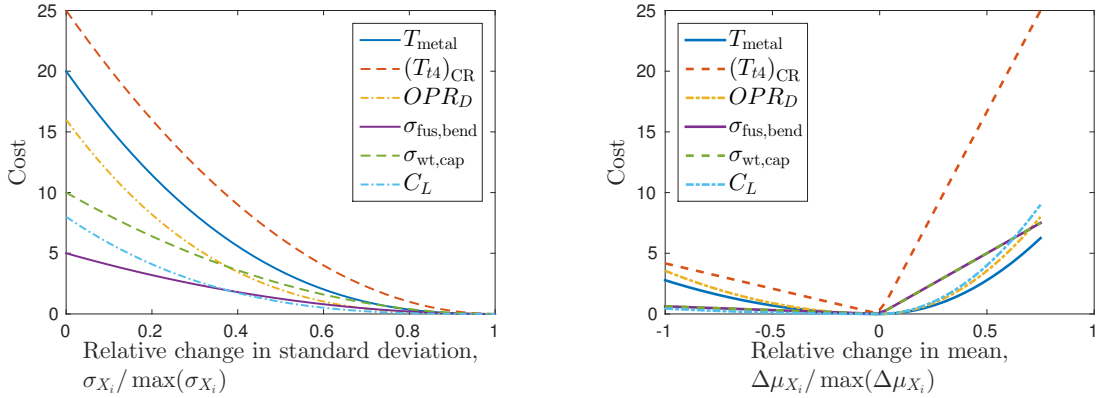

(a) for changes in the input standard deviation

(b) for changes in the input mean

Figure 5-18: *Notional cost model for the six system-wide uncertain input parameters.*

This allows for also focusing on direct performance measures of the design, rather than only from the design process.

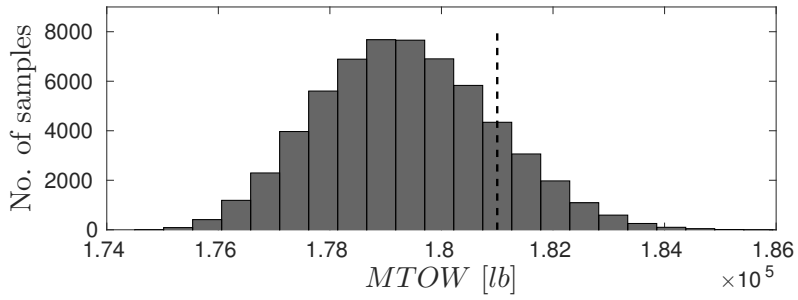

(a) $MTOW$

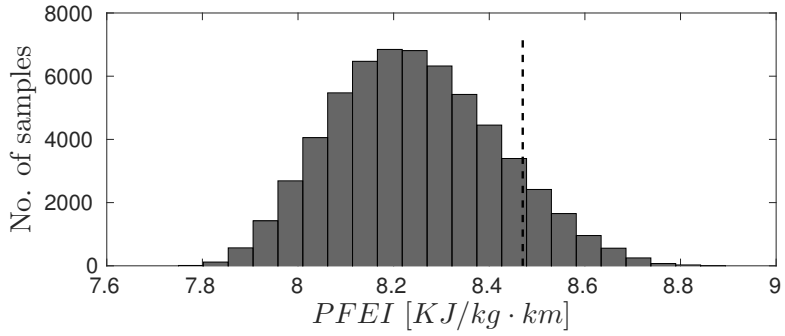

(b) $PFEI$

Figure 5-19: *Histograms of $MTOW$ and $PFEI$ using 60,000 quasi Monte Carlo samples (dashed line indicates the not-exceed-value for risk).*

For the initial input parameter distributions we find that the standard deviation of $MTOW$ is 1553 lb, while the standard deviation of $PFEI$ is 0.1715 $KJ/kg \cdot km$. These initial input parameter distributions lead to a distribution of $MTOW$ and $PFEI$ as in Fig. 5-19. From that Monte Carlo simulation we find that the initial risk for $MTOW$ is 15.3% and the risk for $PFEI$ is 10.6%.

Table 5-2: *Optimal mean and standard deviation for input parameters for system-wide uncertainty, together with values of risk, standard deviation and cost. Those values are also compared to a Monte Carlo simulation with 15,000 samples of TASOPT using the optimized standard deviations.*

	$\alpha_1 = 1$		$\gamma = 1$		$\beta_j = 1$		All	
Parameter	μ	σ	μ	σ	μ	σ	μ	σ
T_{metal}, $[K]$	1216.0	20.2	1216.0	23.0	1212.9	18.3	1213.5	19.6
$(T_{t4})_{CR}$, $[K]$	1568.1	20.1	1591.5	22.7	1591.5	15.6	1591.5	17.1
OPR_D, $[-]$	26.25	0.656	26.22	0.680	26.24	0.502	26.24	0.528
$\sigma_{\text{fus,bend}}$, $[Psi]$	3.020e4	344	2.989e4	233	3.000e4	135	2.986e4	152
$\sigma_{\text{wt,cap}}$, $[Psi]$	3.003e4	113	2.999e4	92	3.000e4	59.0	3.000e4	68.1
C_L, $[-]$	0.5778	1.96e-3	0.5772	1.50e-3	0.5772	1.03e-3	0.5772	1.16e-3
Parameter	HDMR	MC	HDMR	MC	HDMR	MC	HDMR	MC
Cost	24.9	–	13.7	–	25.0	–	22.2	–
Risk $MTOW$	0%	0%	0%	0.37%	0%	0%	0%	0%
Risk $PFEI$	0%	0%	1.1%	2.41%	0%	0.02%	0%	0.12%
σ_Y $MTOW$ [lb]	595	594	600	599	398	398	442	441
σ_Y $PFEI$ $\left[\frac{KJ}{kg \cdot km}\right]$	0.0997	0.0996	0.121	0.121	0.0885	0.0884	0.0956	0.0956
$\mathbb{E}[MTOW]$ [lb]	1.785e5	1.785e5	1.793e5	1.793e5	1.791e5	1.791e5	1.792e5	1.792e5
$\mathbb{E}[PFEI]$ $\left[\frac{KJ}{kg \cdot km}\right]$	8.118	8.118	8.221	8.220	8.203	8.202	8.208	8.208

Using those budgets and initial distributions, we perform the resource allocation optimization. Specifically, we show the results for four different objective functions: for minimum risk of $MTOW$, for minimum cost, for minimum standard deviation of $MTOW$ and $PFEI$ and for one where we considering everything to be equally important. Those results are shown in Fig. 5-20. Additionally, the optimization results for the different objective functions are listed in Table 5-2.

We see that indeed all budgets are satisfied in Table 5-2. For the minimum risk solution, we again see multiple minima. This is again due to the fact that in a large part of the design space, the risk is zero. Moreover, the general trend seems to be that there are mostly large uncertainty reductions in the structural parameters

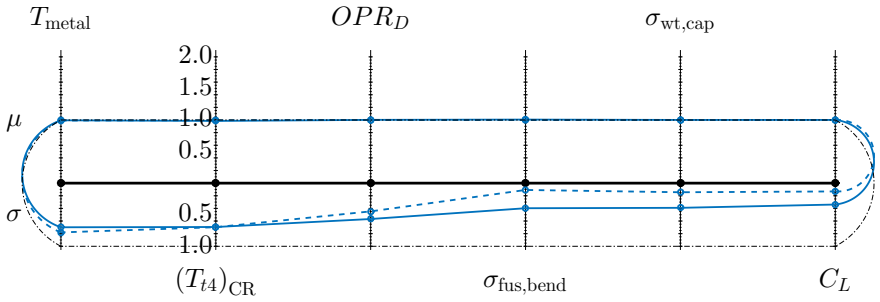

(a) Minimum risk for $MTOW$ ($\alpha_1 = 1$, $\alpha_2 = \beta_j = \gamma = \theta_j = 0$)

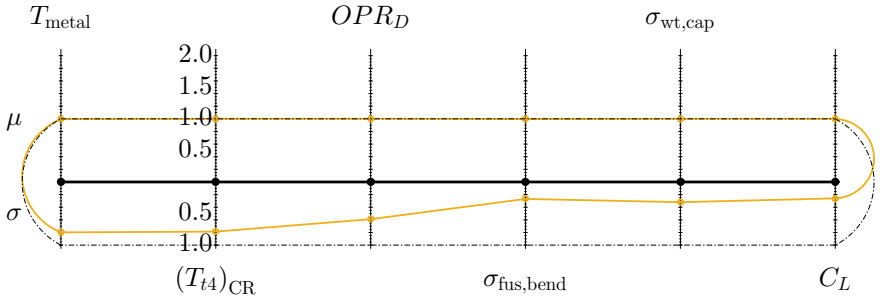

(b) Minimum cost ($\gamma = 1$, $\alpha_1 = \alpha_2 = \beta_j = \theta_j = 0$)

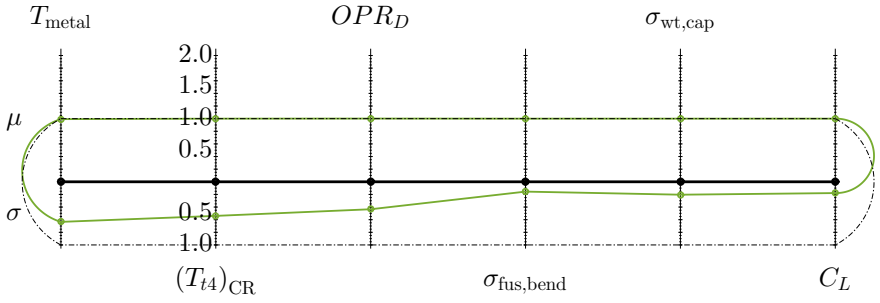

(c) Minimum combined standard deviation ($\beta_j = 1$, $\alpha_j = \gamma = \theta_j = 0$)

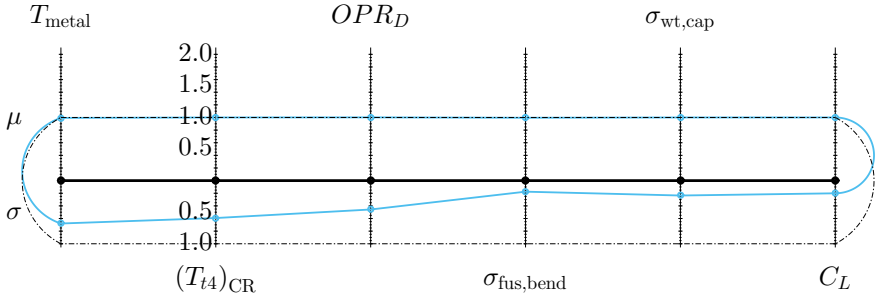

(d) All equally important ($\alpha_j = \beta_j = \gamma = \theta_j = 1$)

Figure 5-20: *Results for system-wide resource allocation optimization for four different objective functions.*

($\sigma_{\text{fus,bend}}$ and $\sigma_{\text{wt,cap}}$) and the aerodynamics parameter C_L. There are still uncertainty reductions in the engine parameters, because they have such a large influence on the uncertainty in the QoI's, as we have shown in Fig. 5-17. However, according to our cost model (Fig. 5-18), changes in those engine parameters are costly and are therefore kept to a minimum. This trend is also seen in the minimum cost solution, where the changes in the engine parameters are kept to a minimum.

Again, given our optimized input distributions we would like to know whether our approximations have been accurate. Therefore, we rerun the original model in place of the surrogate model given these new input distributions. This assessment is performed by running a (quasi) Monte Carlo simulation with 15,000 samples on TASOPT, from which we then compute the variance and risk of the QoI's. Those results are also shown in Table 5-2, labeled by "MC". The results from the optimization where we use the original ANOVA-HDMR expansion and the local sensitivity estimates are labeled "HDMR". We see that the standard deviation agrees well, which means the original ANOVA-HDMR expansion was sufficiently accurate. The differences in the risk estimates are however larger. In this problem we considered a larger initial risk, therefore the error further from that initial distribution is larger due to the linearization of the local sensitivity estimates. However, we see that the budgets are still satisfied and that the errors for objective functions with the risk included are lower. We could make the risk estimation more accurate by rerunning a Monte Carlo simulation every few optimization steps. This will be more expensive, but the results would be more accurate, because as we saw the initial surrogate model is sufficiently accurate.

Given these results with different disciplines, decision makers can more easily decide where to reduce uncertainty and where to change designs. Using such an methodology allows for instance Boeing to decide early on in the design process where they need to allocate more resources to meet their requirements. For these particular results, a decision could for instance be to focus efforts towards uncertainty reduction in the structural parameters ($\sigma_{\text{fus,bend}}$ and $\sigma_{\text{wt,cap}}$) and aerodynamics (C_L), and reduce the

uncertainty in the engine only slightly. The new input distributions would then be quantifiable targets for the uncertainty of the structures, aerodynamics and engine divisions.

This should most likely be an iterative process, wherein per stage of the design process a certain uncertainty and risk can be tolerated. Given those requirements, this uncertainty budgeting methodology provides each engineering division with a target for redesign and uncertainty reduction. Once they have met those goals, the uncertainty budgeting is repeated using the new input distributions (provided by the engineering divisions) and with the new uncertainty and risk targets for that design phase. This process would then be repeated until the end of the design phase, where the design parameters will have converged on (almost) deterministic values.

Chapter 6

Conclusions & Future Work

The final chapter of this thesis presents concluding remarks on the approach presented here, and on its value to the aerospace community. Additionally, potential avenues for future work are discussed.

6.1 Conclusions

The contributions presented in this thesis are twofold. Firstly, the distributional sensitivity analysis (DSA) methodology is extended to be more efficient and more widely applicable to different distributions. Secondly, an uncertainty budgeting approach for design decisions is developed.

Distributional sensitivity analysis offers a more realistic ranking of uncertain input parameters, based on their influence on the quantity of interest (QoI). Assuming that all uncertainty in an input parameter can be reduced, a key assumption in global sensitivity analysis (DSA), is relaxed by viewing sensitivity indices as functions of the uncertainty reduction of input parameters. This thesis extends that methodology by reducing the number of forward model evaluations using the ANOVA-HDMR framework, and by extending its use to different distributions. An example of the latter is the triangular distribution where a Monte Carlo-based acceptance-rejection methodology suffers from sample impoverishment towards the tail of the distribution, but where the presented methodology has no such problem.

Secondly, this thesis presents an uncertainty budgeting approach for supporting conceptual design decisions, and illustrates the approach on an example problem. An HDMR-based surrogate model allows for fast and accurate estimates of the QoI standard deviation and risk, evaluated as a function of changes in the distributions of uncertain inputs. The tradespace of re-design and uncertainty reduction decisions can then be evaluated and visualized; a multi-objective optimization problem can also be solved to determine a specific resource allocation strategy that balances cost and uncertainty reduction. This supports designers in deciding which areas require additional resources for maximum benefit. While the probabilistic analysis presented here may be somewhat costly to conduct, the decisions it is intended to support involve the allocation of significant resources (money, time, facilities and people).

The first illustrative example considers the influence of uncertainties in propulsion technology on the overall conceptual design of a commercial aircraft. The results highlight the kinds of useful conclusions that may be drawn from the analysis. In the case considered, the uncertainties in engine technology are represented by T_{metal} – the maximum allowable temperature of the metal in the turbine – and $(T_{t4})_{\text{CR}}$ – the total temperature at the inlet of the turbine. For the specific analysis case studied, $(T_{t4})_{\text{CR}}$ has the largest influence on the uncertainty in the Maximum Take-off Weight ($MTOW$) of the aircraft, while the interaction between T_{metal} and $(T_{t4})_{\text{CR}}$ is also responsible for a substantial part of the uncertainty in $MTOW$. The resource allocation optimization leads to solutions for which the standard deviation of $(T_{t4})_{\text{CR}}$ is reduced more than the standard deviation of T_{metal}, reflecting this higher sensitivity.

A second example considers the influence of system-wide uncertainties – in propulsion technology, material properties and aerodynamic performance parameters – on the overall conceptual design of the same commercial aircraft. The propulsion technology is represented by T_{metal}, $(T_{t4})_{\text{CR}}$, and OPR_D – the overall pressure ratio of the engine. The material properties considered are $\sigma_{\text{fus,bend}}$ and $\sigma_{\text{wt,cap}}$ – the maximum allowable stress in the fuselage skin and wing and tail spar caps, respectively. Finally, the aerodynamic uncertainty pertains to the value of C_L, the overall lift coef-

ficient. The resource allocation optimization then shows that it makes more sense to look at a large uncertainty reduction in the material properties and the aerodynamic performance, and only a small uncertainty reduction in the propulsion technology. This result then allows a company like Boeing to give each engineering division, e.g., the propulsion group, materials group and aerodynamic design group, targets for redesign, i.e., mean changes, and uncertainty reduction. Such an approach would then be iterated until the end of the design phase, where the design parameters have converged on (almost) deterministic values.

In both cases, the optimization yields strategies for which the changes in mean value are much smaller (relatively speaking) than the changes in input standard deviation. While the solutions found here reflect our particular problem set up and our chosen notional cost model, which places a large penalty on changes in the mean design point, this general result is consistent with many conceptual design problems where the cost of design changes are large. This thesis aims not to recommend a specific aircraft design choice, but rather to provide a general methodology by which the designer can systematically explore these tradeoffs between design modifications and uncertainty reduction. We note that the bulk of multidisciplinary design optimization methods focus on finding a single "optimal design"—even if uncertainty is included, the problem is still usually formulated as finding a single optimal design that minimizes some statistic of the QoI. However, the analysis enabled by our methodology suggests that focusing on uncertainty reduction rather than just design changes may be a more productive approach.

6.2 Future work

This thesis has introduced the idea of uncertainty budgets and applied it to an aircraft design problem. This section describes a few potential avenues for further development of this work.

Extension to more families of distributions with dependent random variables

As for the method itself, we have presented the distributional sensitivity analysis method for uniform, triangular, normal (and exponential) distributions, but have only shown the uncertainty budgeting methodology for uniform distributions. The methods can however be readily extended to other distributions. For distributional sensitivity analysis one has to use an appropriate surrogate model for a new distribution and come up with a sampling strategy for new distributions, which depends on the number of parameters in the distribution.

Furthermore, we took all our design variables to be independent random variables. More realistic would be to treat some design parameters to be correlated to one another. One example would be the maximum yield stress of a material with the density of the material. If we need to change maximum yield stress of that material, that may also change other material properties of that material, such as the density.

When we start introducing dependent random variables, we need to use a surrogate model that can account for that. Rahman[58] introduced the generalized ANOVA-HDMR with dependent random variables. Or we can step away from the ANOVA-HDMR approach and instead use a Polynomial Chaos Expansion (PCE)[59] with sparse quadrature techniques.[60] For our uncertainty budgeting methodology, working with dependent random variables implies we get more design variables: besides the parameters of the distribution of each design variable, we also get the correlation between those random variables. Future work should assess whether it would actually make sense to optimize over the correlation, given that may be hard to control in practice.

Increased computational efficiency

In this work we have already shown an increased computational efficiency with respect to for instance the sensitivity analysis method of Ref. 37, which relied heavily on Monte Carlo simulation and required thousands of forward model evaluations already for a small problem. This work therefore built up a surrogate of the forward model

and then used that in the optimization, drastically reducing the number of original forward model evaluations.

However, in building up the cut-HDMR, as explained in Section 4.3.2, we choose the order of the basis functions and the number of quadrature points to use. We can then evaluate the error *a priori* using a higher-order quadrature scheme or a Monte Carlo simulation. This approach also means that the number of quadrature and order of basis function is the same in each dimension. This is potentially a waste of computational effort, because we could for instance have a linear function in the first dimension, but a cubic function in the third dimension. Therefore, it would make sense to look at an adaptive algorithm, either for the ANOVA-HDMR or to use an adaptive sparse-quadrature algorithm.[60]

Application as intrusive method

Throughout this work we have only considered blackbox functions, requiring surrogate models to treat them efficiently. A recent development in multidisciplinary design optimization within the aerospace community is the application of geometric programming to aircraft design. Geometric programming requires models to be written in terms of monomials and posynomials, and if that is possible, yields a globally optimal solution with very low computational effort.[61] Hoburg and Abbeel[62] showed that many models in aircraft design can be written in such a form, and succesfully applied geometric programming to aircraft design. It would be interesting to see if this uncertainty budgeting method can be cast into such a formulation in order to speed up the optimization considerably and without the need for using surrogate models.

Trade off between design uncertainty with numerical uncertainty

Finally, another interesting application of this framework would be to investigate how one should trade off design uncertainty with numerical uncertainty. In the aircraft conceptual design or early preliminary design, some research is focused on driving down numerical uncertainty as early as possible. The reason for that is that lower

fidelity models sometimes yield such different results that they are useless, an example being using an Euler solver for the optimization of a commericial transport aircraft wing in transonic flow.[63] However, the question then becomes: Does it make sense to drive down *all* numerical uncertainty when there is still uncertainty in the design variables?

Our framework would be able to answer that question; it would however need to be able to quantify how "wrong" a model is through a model error assumption, using for instance the Kennedy & O'Hagan approach.[64] Furthermore, if we intend to use a coupled PDE-based system as our black-box function – such as an aerostructural system[65] – we need to be able to quantify the error in the coupled output functionals, e.g., total lift, as a function of the model error of both systems. It remains an open question for how to do this efficiently.

Appendix A

Gradient Evaluation for Resource Allocation Optimization

Here we derive analytical expression for the integral of a function with respect to the parameters of its probability density function. We start with the derivation in a one-dimensional example in Section A.1, followed by an extension to higher dimensions in Section A.2. Finally, we apply those results to the objective and constraint functions used in Chapter 4.

A.1 Derivation for generic function

We need to evaluate the gradient of an integral of a generic function $h(\mathbf{x})$ with a joint probability density function $f(\mathbf{x}, \boldsymbol{\nu}_1, \ldots, \boldsymbol{\nu}_m)$ of a distribution with m parameters, e.g.

$$I(\boldsymbol{\nu}_1, \ldots, \boldsymbol{\nu}_m) = \int h(\mathbf{x}) f_{\mathbf{x}}(\mathbf{x}, \boldsymbol{\nu}_1, \ldots, \boldsymbol{\nu}_m) \, \mathrm{d}\mathbf{x}$$

where $\mathbf{x} = [x_1, x_2, \ldots, x_n]^\top$, and $\mathrm{d}\mathbf{x} = \mathrm{d}x_1 \mathrm{d}x_2 \ldots \mathrm{d}x_n$. $\boldsymbol{\nu}_1$ is a vector containing the first parameter of the distribution for every input parameter, i.e. $\boldsymbol{\nu}_1 = [\nu_{1,1}, \nu_{2,1}, \ldots, \nu_{n,1}]^\top$. Note that we consider every parameter to be independent, i.e. $f_{\mathbf{x}}(\mathbf{x}) = f_1(x_1) f_2(x_2) \ldots f_n(x_n)$.

Let $\nu_{i,j}$ be the jth parameter of the distribution of the ith input variable and say we wish to evaluate $\partial I / \partial \nu_{i,j}$. The function $h(\mathbf{x})$ does not depend on the parameters

of the distribution, which allows for evaluating the gradient as

$$\frac{\partial I\left(\boldsymbol{\nu}_1,\ldots,\boldsymbol{\nu}_m\right)}{\partial \nu} = \int h\left(\mathbf{x}\right) \frac{\partial f_{\mathbf{x}}\left(\mathbf{x},\boldsymbol{\nu}_1,\ldots,\boldsymbol{\nu}_m\right)}{\partial \nu}\,\mathrm{d}\mathbf{x}.$$

Normal distribution

As an example, consider all input variables to be normally distributed and we wish to evaluate the gradient of the integral with respect to the mean of ith input variable, i.e.

$$\frac{\partial I\left(\boldsymbol{\mu},\boldsymbol{\sigma}\right)}{\partial \mu_i} = \int h\left(\mathbf{x}\right) \frac{\partial f_{\mathbf{x}}\left(\mathbf{x},\boldsymbol{\mu},\boldsymbol{\sigma}\right)}{\partial \mu_i}\,\mathrm{d}\mathbf{x}.$$

The probability density function of the ith input variable is

$$f\left(x_i,\mu_i,\sigma_i\right) = \int_{-\infty}^{\infty} \frac{1}{\sqrt{2\pi}\sigma_i} e^{-\left(x_i-\mu_i\right)^2/2\sigma_i^2}.$$

Thus,

$$\frac{\partial f\left(x_i,\mu_i,\sigma_i\right)}{\partial \mu_i} = \frac{1}{\sqrt{2\pi}\sigma_i} e^{-\left(x_i-\mu_i\right)^2/2\sigma_i^2} \frac{x_i-\mu_i}{\sigma_i^2}$$

and, provided the input parameters are independent,

$$\begin{aligned}\frac{\partial f_{\mathbf{x}}\left(\mathbf{x},\boldsymbol{\mu},\boldsymbol{\sigma}\right)}{\partial \mu_i} &= f\left(x_1,\mu_1,\sigma_1\right)\ldots f\left(x_{i-1},\mu_{i-1},\sigma_{i-1}\right)\ldots \\ &\quad \frac{\partial f\left(x_i,\mu_i,\sigma_i\right)}{\partial \mu_i} f\left(x_{i+1},\mu_{i+1},\sigma_{i+1}\right)\ldots f\left(x_n,\mu_n,\sigma_n\right) \\ &\quad = \frac{x_i-\mu_i}{\sigma_i^2} f_{\mathbf{x}}\left(\mathbf{x},\boldsymbol{\mu},\boldsymbol{\sigma}\right).\end{aligned}$$

Therefore,

$$\frac{\partial I\left(\boldsymbol{\mu},\boldsymbol{\sigma}\right)}{\partial \mu_i} = \int h\left(\mathbf{x}\right) \frac{x_i-\mu_i}{\sigma_i^2} f_{\mathbf{x}}\left(\mathbf{x},\boldsymbol{\mu},\boldsymbol{\sigma}\right)\,\mathrm{d}\mathbf{x}. \tag{A.1}$$

Similarly, the gradient of the integral I with respect to the standard deviation of

the ith input variable is found as

$$\frac{\partial I\left(\boldsymbol{\mu},\boldsymbol{\sigma}\right)}{\partial\sigma_i}=\int h\left(\mathbf{x}\right)\left(-\frac{1}{\sigma_i}+\frac{\left(x_i-\mu_i\right)^2}{\sigma_i^3}\right)f_{\mathbf{x}}\left(\mathbf{x},\boldsymbol{\mu},\boldsymbol{\sigma}\right)\,\mathrm{d}\mathbf{x}. \tag{A.2}$$

Equations (A.2) and (A.2) reveal that $f_{\mathbf{x}}\left(\mathbf{x},\boldsymbol{\mu},\boldsymbol{\sigma}\right)$ still shows up in the gradient evaluation. We could therefore use the same samples as we originally used for computing I to also compute the gradient of I, provided that any quadrature rule is still accurate with the higher order integrand.

Uniform distribution

For the uniform distribution we need to be careful in evaluating $\partial f\left(x_i,\mu_i,\sigma_i\right)/\partial\nu_{i,j}$ because the bounds of integral change. As an example consider a one-dimensional problem, with $x\sim\mathcal{U}\left[a,b\right]$, such that

$$I=\int_a^b h(x)\frac{1}{b-a}\,\mathrm{d}x.$$

When we wish to evaluate $\partial I/\partial\mu$, $1/(b-a)$ does not change, but the bounds of the domain do. For the uniform distribution $\sigma=1/\sqrt{12}\left(b-a\right)$ and $\mu=\left(a+b\right)/2$. Hence, we can rewrite I as

$$I=\int_{\mu-\frac{1}{2}\sqrt{12}\sigma}^{\mu+\frac{1}{2}\sqrt{12}\sigma} h(x)\frac{1}{\sqrt{12}\sigma}\,\mathrm{d}x.$$

Consider an infinitesimal change $\mathrm{d}\mu$ in the mean of x, the change in integral is then

$$\begin{aligned}\mathrm{d}I&=\int_{\mu+\mathrm{d}\mu-\frac{1}{2}\sqrt{12}\sigma}^{\mu+\mathrm{d}\mu+\frac{1}{2}\sqrt{12}\sigma} h(x)\frac{1}{\sqrt{12}\sigma}\mathrm{d}x-\int_{\mu-\frac{1}{2}\sqrt{12}\sigma}^{\mu+\frac{1}{2}\sqrt{12}\sigma} h(x)\frac{1}{\sqrt{12}\sigma}\,\mathrm{d}x\\&=\int_{\mu+\frac{1}{2}\sqrt{12}\sigma}^{\mu+\mathrm{d}\mu+\frac{1}{2}\sqrt{12}\sigma} h(x)\frac{1}{\sqrt{12}\sigma}\mathrm{d}x-\int_{\mu-\frac{1}{2}\sqrt{12}\sigma}^{\mu+\mathrm{d}\mu-\frac{1}{2}\sqrt{12}\sigma} h(x)\frac{1}{\sqrt{12}\sigma}\,\mathrm{d}x.\end{aligned} \tag{A.3}$$

A Taylor expansion of $h(x)$ allows for approximating the integrals in Eq. (A.3). The Taylor expansion of $h(x)$ at $x = a$ is

$$h\left(a + \Delta x\right) = h(a) + \frac{\mathrm{d}h(a)}{\mathrm{d}x}\Delta x + \frac{1}{2}\frac{\mathrm{d}^2 h(a)}{\mathrm{d}x^2}\Delta x^2 + \mathcal{O}\left(\Delta x^3\right).$$

Therefore, we can approximate the integral in Eq. (A.3) as

$$\int_{\mu+\frac{1}{2}\sqrt{12}\sigma}^{\mu+\mathrm{d}\mu+\frac{1}{2}\sqrt{12}\sigma} h(x)\frac{1}{\sqrt{12}\sigma}\mathrm{d}x = \frac{1}{\sqrt{12}\sigma}\left[h\left(\mu + 1/2\sqrt{12}\sigma\right)\mathrm{d}\mu + \ldots \right.$$
$$\left. \frac{\mathrm{d}h(\mu + 1/2\sqrt{12}\sigma)}{\mathrm{d}x}\mathrm{d}\mu^2\right] + \mathcal{O}\left(\mathrm{d}\mu^3\right).$$

That allows us to evaluate $\partial I/\partial\mu$ as

$$\frac{\partial I}{\partial \mu} = \lim_{\mathrm{d}\mu\to 0}\frac{\mathrm{d}I}{\mathrm{d}\mu} = \frac{1}{\sqrt{12}\sigma}\left[h\left(b\right) - h\left(a\right)\right]. \tag{A.4}$$

For the gradient with respect to the standard deviation we follow a similar approach. Consider an infinitesimal change in standard deviation $\mathrm{d}\sigma$, yielding a change in the integral as

$$\begin{aligned}\mathrm{d}I &= \int_{\mu-\frac{1}{2}\sqrt{12}(\sigma+\mathrm{d}\sigma)}^{\mu+\frac{1}{2}\sqrt{12}(\sigma+\mathrm{d}\sigma)} h(x)\left[\frac{1}{\sqrt{12}\sigma} - \frac{1}{\sqrt{12}\sigma^2}\mathrm{d}\sigma\right]\mathrm{d}x - \int_{\mu-\frac{1}{2}\sqrt{12}\sigma}^{\mu+\frac{1}{2}\sqrt{12}\sigma} h(x)\frac{1}{\sqrt{12}\sigma}\,\mathrm{d}x \\ &= -\mathrm{d}\sigma\int_{\mu-\frac{1}{2}\sqrt{12}\sigma}^{\mu+\frac{1}{2}\sqrt{12}\sigma} h(x)\frac{1}{\sqrt{12}\sigma^2}\,\mathrm{d}x + \ldots \\ &\quad \left[\frac{1}{\sqrt{12}\sigma} - \frac{1}{\sqrt{12}\sigma^2}\mathrm{d}\sigma\right]\left[\int_{\mu+\frac{1}{2}\sqrt{12}\sigma}^{\mu+\frac{1}{2}\sqrt{12}(\sigma+\mathrm{d}\sigma)} h(x)\,\mathrm{d}x - \int_{\mu-\frac{1}{2}\sqrt{12}\sigma}^{\mu-\frac{1}{2}\sqrt{12}(\sigma+\mathrm{d}\sigma)} h(x)\,\mathrm{d}x\right]\end{aligned}$$

Using the Taylor expansion of $h(x)$ at $x = a$, allows us to rewrite the second integral as

$$\int_{\mu+\frac{1}{2}\sqrt{12}\sigma}^{\mu+\frac{1}{2}\sqrt{12}(\sigma+\mathrm{d}\sigma)} h(x)\,\mathrm{d}x = h\left(\mu + 1/2\sqrt{12}\sigma\right)\frac{1}{2}\sqrt{12}\mathrm{d}\sigma + \ldots$$
$$\frac{\mathrm{d}h(\mu + 1/2\sqrt{12}\sigma)}{\mathrm{d}x}\left(\frac{1}{2}\sqrt{12}\mathrm{d}\sigma\right)^2 + \mathcal{O}\left(\mathrm{d}\sigma^3\right).$$

Those Taylor expressions allow us to find the gradient of I with respect to σ as

$$\frac{\partial I}{\partial \sigma} = \lim_{\mathrm{d}\sigma \to 0} \frac{\mathrm{d}I}{\mathrm{d}\sigma} = -\frac{I}{\sigma} + \frac{1}{2\sigma}\left[h\left(b\right) + h\left(a\right)\right]. \tag{A.5}$$

The conclusions from the one dimensional example extend readily to higher dimensions: the dimension for the gradient of the integral is one lower than the dimension of the integral itself. The gradient of an n-dimensional integral I with respect to the mean of the ith input variable, μ_i, is found to be

$$\frac{\partial I}{\partial \mu_i} = \int h\left(\mathbf{x}^+\right) f\left(\mathbf{x}^+\right)\, \mathrm{d}\mathbf{x}^i - \int h\left(\mathbf{x}^-\right) f\left(\mathbf{x}^-\right)\, \mathrm{d}\mathbf{x}^i \tag{A.6}$$

$$\text{where} \quad \mathbf{x}^+ = \left[x_1, \ldots, x_{i-1}, \mu_i + \frac{1}{2}\sqrt{12}\sigma_i, x_{i+1}, \ldots, x_n\right]^\top$$

$$\mathbf{x}^- = \left[x_1, \ldots, x_{i-1}, \mu_i - \frac{1}{2}\sqrt{12}\sigma_i, x_{i+1}, \ldots, x_n\right]^\top,$$

and $\mathrm{d}\mathbf{x}^i = \mathrm{d}x_1 \ldots \mathrm{d}x_{i-1}\mathrm{d}x_{i+1} \ldots \mathrm{d}x_n$.

Similarly, the gradient of an n-dimensional integral I with respect to the standard deviation of the ith input variable, σ_i can be expressed as

$$\frac{\partial I}{\partial \sigma_i} = -\frac{I}{\sigma_i} + \frac{1}{2\sigma_i}\left[\int h\left(\mathbf{x}^+\right) f\left(\mathbf{x}^+\right)\, \mathrm{d}\mathbf{x}^i + \int h\left(\mathbf{x}^-\right) f\left(\mathbf{x}^-\right)\, \mathrm{d}\mathbf{x}^i\right]. \tag{A.7}$$

Gradient evaluation for $\sigma \to 0$

The expressions in Equations (A.6) and (A.7) are derived assuming $\sigma > 0$. When $\sigma = 0$, $\partial I/\partial \sigma_i = 0$ by taking the limit of Eq. (A.7), and going through the derivation by taking the limit $\sigma_i \to 0$ yields the same result. Due to round-off errors this might need to be enforced explicitly. On the other hand, Eq. (A.6) also tells us that $\partial I/\partial \mu_i = 0$, which is not true. Instead it should be,

$$\frac{\partial I}{\partial \mu_i} = \int \frac{\partial h\left(\mathbf{x}^+\right)}{\partial \mu_i} f\left(\mathbf{x}^+\right)\, \mathrm{d}\mathbf{x}^i, \tag{A.8}$$

which is seen by setting $I = h(x)$ in the one dimensional case and differentiating with respect to x, which is now equal to the mean.

In general we do not have access to the derivative of $h(\mathbf{x})$.One approach is to solve for the gradient using *finite differencing*. For example if we are interested in the gradient of the objective function with respect to the mean of the jth input parameter, we can derive the gradient from a Taylor expansion as,

$$\frac{\partial \mathcal{F}(\boldsymbol{\mu}, \boldsymbol{\sigma})}{\partial \mu_j} = \frac{\mathcal{F}(\boldsymbol{\mu} + \mathbf{e}_j h, \boldsymbol{\sigma}) - \mathcal{F}(\boldsymbol{\mu}, \boldsymbol{\sigma})}{h} + \mathcal{O}(h) \tag{A.9}$$

where $\boldsymbol{\mu} = [\mu_1, \ldots, \mu_n]$ and $\boldsymbol{\sigma} = [\sigma_1, \ldots, \sigma_n]$ and h is the size of the finite difference step. For large h the error in the gradient is large due to the neglected higher order terms. However, when h approaches machine precision, the error becomes large as well due to round-off errors related to the subtraction in Eq. (A.9).

Instead of taking a real valued step, we can also take an imaginary step. This *complex-step method* is also derived from a Taylor expansion, only now with an imaginary step.[66] We then arrive at

$$\frac{\partial \mathcal{F}(\boldsymbol{\mu}, \boldsymbol{\sigma})}{\partial \mu_j} = \frac{\mathrm{Im}\left[\mathcal{F}(\boldsymbol{\mu} + ih\mathbf{e}_j, \boldsymbol{\sigma})\right]}{h} + \mathcal{O}(h^2). \tag{A.10}$$

This method does not suffer from the round-off errors of finite differencing, because there is no subtraction. Martins et al.[67] showed that this method is generally applicable to any algorithm.

These methods are easy to implement and give a reasonable approximation of the gradient. For our particular case, we use finite differencing, because TASOPT does not handle complex arithmetic.

A.2 Application to resource allocation optimization

To find the gradient of the objective function and constraint functions from Section 4.2, we need to evaluate the gradient of the standard deviation of the QoI, σ_Y, with respect to the mean and standard deviation of every input parameter. We

evaluate the standard deviation of the QoI as

$$\sigma_Y^2 = \int \left(g(\mathbf{x}) - g_0\right)^2 f\left(\mathbf{x}\right)\, \mathrm{d}\mathbf{x}. \tag{A.11}$$

For uniform distributions, following Eq. (A.6), we can evaluate the variance of Y with respect to μ_i as

$$\frac{\partial \mathrm{var}_Y}{\partial \mu_i} = \int \left(g\left(\mathbf{x}^+\right) - g_0\right)^2 f\left(\mathbf{x}^+\right)\, \mathrm{d}\mathbf{x}^i - \int \left(g\left(\mathbf{x}^-\right) - g_0\right)^2 f\left(\mathbf{x}^-\right)\, \mathrm{d}\mathbf{x}^i \tag{A.12}$$

and with respect to σ_i as

$$\frac{\partial \mathrm{var}_Y}{\partial \sigma_i} = -\frac{\mathrm{var}_Y}{\sigma_i} + \frac{1}{2\sigma_i}\left[\int \left(g\left(\mathbf{x}^+\right) - g_0\right)^2 f\left(\mathbf{x}^+\right)\, \mathrm{d}\mathbf{x}^i + \ldots \right.$$
$$\left. \int \left(g\left(\mathbf{x}^-\right) - g_0\right)^2 f\left(\mathbf{x}^-\right)\, \mathrm{d}\mathbf{x}^i\right]. \tag{A.13}$$

After applying the chain rule we find the gradient of σ_Y with respect to distribution parameter ν as

$$\frac{\partial \sigma_Y}{\partial \nu} = \frac{1}{2\sqrt{\sigma_Y}} \frac{\partial \mathrm{var}_Y}{\partial \nu}. \tag{A.14}$$

For the risk gradient evaluation we use the local sensitivity estimates as defined in Ref. 37. Employing the chain rule, the gradient of the risk is expressed as

$$\frac{\partial P(Y < r)}{\partial \sigma_i} = -f_Y(r)\frac{\partial \mu_Y}{\partial \sigma_i} + \frac{\mu_Y - r}{\sigma_Y} f_Y(r) \frac{\partial \sigma_Y}{\partial \sigma_i} \tag{A.15}$$

$$\frac{\partial P(Y < r)}{\partial \mu_i} = -f_Y(r)\frac{\partial \mu_Y}{\partial \mu_i} + \frac{\mu_Y - r}{\sigma_Y} f_Y(r) \frac{\partial \sigma_Y}{\partial \mu_i}, \tag{A.16}$$

where $\partial \mu_Y / \partial \sigma_i$ and $\partial \mu_Y / \partial \mu_i$ are obtained from evaluating Equation (A.6) or (A.7).

Appendix B

Distributions for the Aircraft Design Problem

This appendix holds the distribution parameters for the uncertain design parameters used throughout this thesis. Table B-1 holds the uniform distribution parameters of the uncertain design variables[a] considered for the Boeing 737-800 from Ref. 4.

[a]Note that we did change the distribution of $\sigma_{\text{wt,cap}}$ from $\mathcal{U}[28500, 31500]$ Psi to $\mathcal{U}[29500, 30500]$ Psi, otherwise the sensitivity index for that parameter for $MTOW$ was $> 80\%$. This was deemed unrealistic.

Table B-1: *Uniform distribution parameters ($\mathcal{U}[a, b]$) of the uncertain design variables considered for the Boeing 737-800 from Ref. 4.*

Parameter	Units	Lower bound	Upper bound
St_h	$-$	0.094	0.096
t_{film}	$-$	0.315	0.325
$\eta_{\text{pol}_{lc}}$	$-$	0.936	0.937
$\eta_{\text{pol}_{hc}}$	$-$	0.903	0.905
$\eta_{\text{pol}_{lt}}$	$-$	0.875	0.877
$\eta_{\text{pol}_{ht}}$	$-$	0.870	0.872
T_{metal}	K	1,172	1,272
$(T_{t4})_{\text{TO}}$	K	1,783	1,883
$(T_{t4})_{\text{CR}}$	K	1,541.5	1,641.5
OPR_D	$-$	24.2	28.2
π_{f_D}	$-$	1.609	1.611
$\sigma_{\text{fus,skin}}$	Psi	14,250	15,750
$\sigma_{\text{fus,bend}}$	Psi	28,500	31,500
$\sigma_{\text{wt,cap}}$	Psi	29,500	30,500
$\tau_{\text{wt,web}}$	Psi	19,000	21,000
$E_{\text{wt,cap}}$	Psi	$9.50 \cdot 10^6$	$10.5 \cdot 10^6$
$\rho_{\text{fus,skin}}$	kg/m^3	2,672	2,726
$\rho_{\text{fus,bend}}$	kg/m^3	2,672	2,726
$\rho_{\text{wt,cap}}$	kg/m^3	2,672	2,726
$\rho_{\text{wt,web}}$	kg/m^3	2,672	2,726
h_{CR}	ft	34,000	36,000
$C_{L_{\perp,\max}}$	$-$	2.2	2.3
C_L	$-$	0.56714	0.58714
M	$-$	0.77	0.79

Bibliography

[1] The Boeing Company, "787 Dreamliner Timeline," `http://www.boeing.com/commercial/787/timeline/`, 2015, Accessed: 2015/08/24.

[2] He, Q., *Uncertainty and Sensitivity Analysis Methods for Improving Design Robustness and Reliability*, Ph.D. thesis, Massachusetts Institute of Technology, June 2014.

[3] Rabitz, H., Aliş, Ö. F., Shorter, J., and Shim, K., "Efficient input-output model representations," *Computer Physics Communications*, Vol. 117, No. 1, 1999, pp. 11–20.

[4] Amaral, S., *A Decomposition-Based approach to Uncertainty Quantification of Multicomponent Systems*, Ph.D. thesis, Massachusetts Institute of Technology, June 2015.

[5] Haldar, A. and Mahadevan, S., *Probability, Reliability and Statistical Methods in Engineering Design*, John Wiley & Sons, Inc., New York, NY, 2000.

[6] Roy, C. J. and Oberkampf, W. L., "A Comprehensive Framework for Verification, Validation, and Uncertainty Quantification in Scientific Computing," *Computer Methods in Applied Mechanics and Engineering*, Vol. 200, 2011, pp. 2131–2144.

[7] Mavris, D. N., Bandte, O., and DeLaurentis, D. A., "Robust Design Simulation: A Probabilistic Approach to Multidisciplinary Design," *Journal of Aircraft*, Vol. 36, No. 1, 1999, pp. 298–307.

[8] Smith, R., *Uncertainty Quantification: Theory, Implementation, and Applications*, SIAM, Philadelphia, 2014.

[9] Oberkampf, W. L., DeLand, S. M., Rutherford, B. M., Diegert, K. V., and Alvin, K. F., "Error and Uncertainty in Modeling and Simulation," *Reliability Engineering and System Safety*, Vol. 75, 2002, pp. 333–357.

[10] Ang, A. H.-S. and Tang, W. H., *Probability Concepts in Engineering: Emphasis on Applications to Civil and Environmental Engineering*, John Wiley & Sons, Inc., Hoboken, NJ, 2nd ed., 2007.

[11] Kennedy, M. C. and O'Hagan, A., "Bayesian Calibration of Computer Models," *Journal of the Royal Statistical Society, Series B*, Vol. 63, No. 3, 2001, pp. 425–464.

[12] Cacuci, D., Ionescu-Bujor, M., and Navon, I., *Sensitivity And Uncertainty Analysis: Applications to Large-Scale Systems (Volume II)*, Chapman & Hall, 2005.

[13] Agarwal, H., Renaud, J. E., Preston, E. L., and Padmanabhan, D., "Uncertainty Quantification Using Evidence Theory in Multidisciplinary Design Optimization," *Reliability Engineering and System Safety*, Vol. 85, 2004, pp. 281–294.

[14] Helton, J. C., Johnson, J. D., Sallaberry, C. J., and Storlie, C. B., "Survey of Sampling-Based Methods for Uncertainty and Sensitivity Analysis," *Reliability Engineering and System Safety*, Vol. 91, 2006, pp. 1175–1209.

[15] Aughenbaugh, J. M. and Paredis, C. J., "The Value of Using Imprecise Probabilities in Engineering Design," *Journal of Mechanical Design*, Vol. 128, No. 4, 2006, pp. 969–979.

[16] Venter, G., Haftka, R. T., and Starnes, J. H., "Construction of Response Surface Approximations for Design Optimization," *AIAA Journal*, Vol. 36, No. 12, 1998, pp. 2242–2249.

[17] Eldred, M. S., Giunta, A. A., and Collis, S. S., "Second-Order Corrections for Surrogate-Based Optimization with Model Hierarchies," *10th AIAA/ISSMO Multidisciplinary Analysis and Optimization Conference, AIAA Paper 2004-4457*, Albany, NY, 2004.

[18] Simpson, T. W., Peplinski, J. D., Koch, P. N., and Allen, J. K., "Metamodels for Computer-Based Engineering Design: Survey and Recommendations," *Engineering with Computers*, Vol. 17, No. 2, 2001, pp. 129–150.

[19] Alexandrov, N. M., Lewis, R. M., Gumbert, C. R., Green, L. L., and Newman, P. A., "Approximation and Model Management in Aerodynamic Optimization with Variable-Fidelity Models," *Journal of Aircraft*, Vol. 38, No. 6, 2001, pp. 1093–1101.

[20] Queipo, N. V., Haftka, R. T., Shyy, W., Goel, T., Vaidyanathan, R., and Tucker, P. K., "Surrogate-based Analysis and Optimization," *Progress in Aerospace Sciences*, Vol. 41, No. 1, 2005, pp. 1–28.

[21] Lee, S. H. and Chen, W., "A Comparative Study of Uncertainty Propagation Methods for Black-box-type Problems," *Structural and Multidisciplinary Optimization*, Vol. 37, No. 3, 2009, pp. 239–253.

[22] Saltelli, A., Chan, K., and Scott, E. M., *Sensitivity Analysis*, John Wiley & Sons, Inc., New York, NY, 2000.

[23] Homma, T. and Saltelli, A., "Importance Measures in Global Sensitivity Analysis of Nonlinear Models," *Reliability Engineering & System Safety*, Vol. 52, No. 1, 1996, pp. 1–17.

[24] Sobol', I. M., "Sensitivity Estimates for Nonlinear Mathematical Models," *Mathematical Modeling and Computational Experiment*, Vol. 1, No. 4, 1993, pp. 407–414.

[25] Sobol, I. M., "Theorems and examples on high dimensional model representation," *Reliability Engineering & System Safety*, Vol. 79, No. 2, 2003, pp. 187–193.

[26] Chan, K., Saltelli, A., and Tarantola, S., "Sensitivity Analysis of Model Output: Variance-Based Methods Make the Difference," Proceedings of the 1997 Winter Simulation Conference, 1997.

[27] Saltelli, A. and Bolado, R., "An Alternative Way to Compute Fourier Amplitude Sensitivity Test (FAST)," *Computational Statistics and Data Analysis*, Vol. 26, 1998, pp. 445–460.

[28] Liu, H., Chen, W., and Sudjianto, A., "Relative Entropy Based Method for Probabilistic Sensitivity Analysis in Engineering Design," *Journal of Mechanical Design*, Vol. 128, No. 2, 2006, pp. 326–336.

[29] Knoll, F. and Vogel, T., *Design for Robustness*, IABSE (International Association for Bridge and Structural Engineering), Zurich, Switzerland, 2009.

[30] Taguchi, G., *The System of Experimental Design: Engineering Methods to Optimize Quality and Minimize Costs (2 vols.)*, UNIPUB/Kraus International Publications and American Supplier Institute, White Plains, NY and Dearborn, MI, 1987.

[31] Phadke, M. S., *Quality Engineering Using Robust Design*, Prentice Hall, Englewood Cliffs, NJ, 1989.

[32] Chen, W., Allen, J. K., Tsui, K.-L., and Mistree, F., "Procedure for Robust Design: Minimizing Variations caused by Noise Factors and Control Factors," *Journal of Mechanical Design*, Vol. 118, No. 4, 1996, pp. 478–485.

[33] Du, X., Sudjianto, A., and Chen, W., "An integrated framework for optimization under uncertainty using inverse reliability strategy," *Journal of Mechanical Design*, Vol. 126, No. 4, 2004, pp. 562–570.

[34] Kim, H. M., Michelena, N. F., Papalambros, P. Y., and Jiang, T., "Target Cascading in Optimal System Design," *Journal of Mechanical Design*, Vol. 125, No. 3, 2003, pp. 474–480.

[35] Kokkolaras, M., Mourelatos, Z. P., and Papalambros, P. Y., "Design optimization of hierarchically decomposed multilevel systems under uncertainty," *Journal of mechanical design*, Vol. 128, No. 2, 2006, pp. 503–508.

[36] Kokkolaras, M., "Reliability Allocation in Probabilistic Design Optimization of Decomposed Systems using Analytical Target Cascading," *12th AIAA/ISSMO Multidisciplinary Analysis and Optimization Conference, Victoria, British Columbia, Canada, Paper No. AIAA-2008-6040*, September 10–12 2008.

[37] Curran, C. and Willcox, K. E., "Sensitivity Analysis Methods for Mitigating Uncertainty in Engineering System Design," *56th AIAA/ASCE/AHS/ASC Structures, Structural Dynamics, and Materials Conference, Kissimee, FL, Paper No. AIAA-2015-0899*, January 5–9 2015.

[38] Opgenoord, M. M. J. and Willcox, K. E., "Sensitivity Analysis Methods for Uncertainty Budgeting in System Design," *57th AIAA/ASCE/AHS/ASC Structures, Structural Dynamics, and Materials Conference, San Diego, CA, Paper No. AIAA-2016-1423*, January 4–8 2016.

[39] Torenbeek, E., *Synthesis of subsonic airplane design : an introduction to the preliminary design, of subsonic general aviation and transport aircraft, with emphasis on layout, aerodynamic design, propulsion, and performance*, Delft University Press Nijhoff Sold and distributed in the U.S. and Canada by Kluwer Boston, Delft The Hague Hingham, MA, 1982.

[40] Rabitz, H. and Aliş, Ö. F., "General foundations of high-dimensional model representations," *Journal of Mathematical Chemistry*, Vol. 25, No. 2-3, 1999, pp. 197–233.

[41] Alış, Ö. F. and Rabitz, H., "Efficient implementation of high dimensional model representations," *Journal of Mathematical Chemistry*, Vol. 29, No. 2, 2001, pp. 127–142.

[42] Wang, S.-W., Georgopoulos, P. G., Li, G., and Rabitz, H., "Random sampling-high dimensional model representation (RS-HDMR) with nonuniformly distributed variables: application to an integrated multimedia/multipathway exposure and dose model for trichloroethylene," *The Journal of Physical Chemistry A*, Vol. 107, No. 23, 2003, pp. 4707–4716.

[43] Li, G. and Rabitz, H., "General formulation of HDMR component functions with independent and correlated variables," *Journal of Mathematical Chemistry*, Vol. 50, No. 1, 2012, pp. 99–130.

[44] Li, G., Wang, S.-W., and Rabitz, H., "Practical approaches to construct RS-HDMR component functions," *The Journal of Physical Chemistry A*, Vol. 106, No. 37, 2002, pp. 8721–8733.

[45] Saltelli, A., *Global sensitivity analysis : the primer*, John Wiley, Chichester, England Hoboken, NJ, 2008.

[46] Sobol, I. M., "Global sensitivity indices for nonlinear mathematical models and their Monte Carlo estimates," *Mathematics and computers in simulation*, Vol. 55, No. 1-3, 2001, pp. 271–280.

[47] Oakley, J. E. and O'Hagan, A., "Probabilistic sensitivity analysis of complex models: a Bayesian approach," *Journal of the Royal Statistical Society: Series B (Statistical Methodology)*, Vol. 66, No. 3, 2004, pp. 751–769.

[48] Allaire, D. L. and Willcox, K. E., "A variance-based sensitivity index function for factor prioritization," *Reliability Engineering & System Safety*, Vol. 107, 2012, pp. 107–114.

[49] Allaire, D. L., *Uncertainty assessment of complex models with application to aviation environmental systems*, Ph.D. thesis, Massachusetts Institute of Technology, June 2009.

[50] Ratto, M., Pagano, A., and Young, P. C., "Non-parametric estimation of conditional moments for sensitivity analysis," *Reliability Engineering & System Safety*, Vol. 94, No. 2, 2009, pp. 237–243.

[51] Liu, J., *Monte Carlo strategies in scientific computing*, Springer, New York, 2008.

[52] Johnsson, S. G., "The NLopt nonlinear-optimization package," http://ab-initio.mit.edu/nlopt.

[53] Svanberg, K., "A class of globally convergent optimization methods based on conservative convex separable approximations," *SIAM journal on optimization*, Vol. 12, No. 2, 2002, pp. 555–573.

[54] Li, G., Hu, J., Wang, S.-W., Georgopoulos, P. G., Schoendorf, J., and Rabitz, H., "Random sampling-high dimensional model representation (RS-HDMR) and orthogonality of its different order component functions," *The Journal of Physical Chemistry A*, Vol. 110, No. 7, 2006, pp. 2474–2485.

[55] Gao, Z. and Hesthaven, J. S., "On ANOVA expansions and strategies for choosing the anchor point," *Applied Mathematics and Computation*, Vol. 217, No. 7, 2010, pp. 3274–3285.

[56] Drela, M., "N3 Aircraft Concept Designs and Trade Studies – Appendix," Tech. Rep. NASA CR-2010-216794/VOL2, 2010.

[57] Drela, M., "TASOPT 2.08 – Transport Aircraft System OPTimization," Tech. rep., Massachusetts Institute of Technology, February 2011.

[58] Rahman, S., "A Generalized ANOVA Dimensional Decomposition for Dependent Probability Measures," *SIAM/ASA Journal on Uncertainty Quantification*, Vol. 2, No. 1, 2014, pp. 670–697.

[59] Ghanem, R. G. and Spanos, P. D., *Stochastic finite elements: a spectral approach*, Courier Corporation, 2003.

[60] Xiu, D. and Hesthaven, J. S., "High-order collocation methods for differential equations with random inputs," *SIAM Journal on Scientific Computing*, Vol. 27, No. 3, 2005, pp. 1118–1139.

[61] Boyd, S., Kim, S.-J., Vandenberghe, L., and Hassibi, A., "A tutorial on geometric programming," *Optimization and engineering*, Vol. 8, No. 1, 2007, pp. 67–127.

[62] Hoburg, W. and Abbeel, P., "Geometric programming for aircraft design optimization," *AIAA Journal*, Vol. 52, No. 11, 2014, pp. 2414–2426.

[63] Lyu, Z., Kenway, G. K., Paige, C., and Martins, J., "Automatic Differentiation Adjoint of the Reynolds-Averaged Navier–Stokes Equations with a Turbulence Model," *43rd AIAA Fluid Dynamics Conference and Exhibit, San Diego, CA, Paper No. AIAA 2013-2581*, June 24–27 2013.

[64] Kennedy, M. C. and O'Hagan, A., "Bayesian calibration of computer models," *Journal of the Royal Statistical Society. Series B, Statistical Methodology*, 2001, pp. 425–464.

[65] Kenway, G. K. and Martins, J. R., "Multipoint High-Fidelity Aerostructural Optimization of a Transport Aircraft Configuration," *Journal of Aircraft*, Vol. 51, No. 1, 2014, pp. 144–160.

[66] Squire, W. and Trapp, G., "Using complex variables to estimate derivatives of real functions," *Siam Review*, Vol. 40, No. 1, 1998, pp. 110–112.

[67] Martins, J. R., Sturdza, P., and Alonso, J. J., "The complex-step derivative approximation," *ACM Transactions on Mathematical Software (TOMS)*, Vol. 29, No. 3, 2003, pp. 245–262.